[redacted]

CENTRAL RESEARCH LIBRARY
DOCUMENT COLLECTION

MARTIN MARIETTA ENERGY SYSTEMS LIBRARIES
3 4456 0353319 3

ORNL-1509

Reactors - Research and Power

17A

CLASSIFICATION CHANGED TO:
BY AUTHORITY OF: AEC 5-28-69
BY: G. Lackenmeier 10-28-69

AEC RESEARCH AND DEVELOPMENT REPORT

PRELIMINARY DESIGN AND PERFORMANCE STUDIES OF SODIUM-TO-AIR RADIATORS

LABORATORY RECORDS
1954

W. S. Farmer
A. P. Fraas
H. J. Stumpf
G. D. Whitman

CENTRAL RESEARCH LIBRARY
DOCUMENT COLLECTION

LIBRARY LOAN COPY

DO NOT TRANSFER TO ANOTHER PERSON

If you wish someone else to see this document, send in name with document and the library will arrange a loan.

OAK RIDGE NATIONAL LABORATORY
OPERATED BY
CARBIDE AND CARBON CHEMICALS COMPANY
A DIVISION OF UNION CARBIDE AND CARBON CORPORATION
UCC
POST OFFICE BOX P
OAK RIDGE, TENNESSEE

[redacted]

[redacted]

ORNL-1509

This document consists of 125 pages.
Copy 17 of 175 copies. Series A.

Contract No. W-7405-Eng-26

AIRCRAFT NUCLEAR PROPULSION PROJECT

Preliminary Design and Performance Studies of Sodium-To-Air Radiators

W. S. Farmer
A. P. Fraas
H. J. Stumpf
G. D. Whitman

Date Issued [redacted] 3 1953

OAK RIDGE NATIONAL LABORATORY
Operated by

CARBIDE AND CARBON CHEMICALS COMPANY
A Division of Union Carbide and Carbon Corporation
Post Office Box P
Oak Ridge, Tennessee

[redacted]

MARTIN MARIETTA ENERGY SYSTEMS LIBRARIES
3 4456 0353319 3

[redacted]

INTERNAL DISTRIBUTION

1. C. E. Center
2. Biology Library
3. Health Physics Library
4. Reactor Experimental Engineering Library
5-10. ANP Library
11-16. Central Files
17-18. Central Research Library
19. C. E. Larson
20. W. B. Humes (K-25)
21. L. B. Emlet (Y-12)
22. A. M. Weinberg
23. E. H. Taylor
24. E. D. Shipley
25. R. C. Briant
26. F. C. VonderLage
27. R. S. Livingston
28. J. H. Frye, Jr.
29. C. P. Keim
30. J. A. Swartout
31. S. C. Lind
32. F. L. Culler
33. A. H. Snell
34. A. Hollaender
35. M. T. Kelley
36. G. H. Clewett
37. K. L. Morgan
38. [illegible] S. Felton
39. [illegible] S. Householder
40. C. S. Harrill
41. C. E. Winters
42. D. W. Cardwell
43. A. J. Miller
44. D. D. Cowen
45. R. A. Charpie
46. F. H. Abernathy
47. E. S. Bettis
48. R. W. Bussard
49. W. S. Farmer
50. A. P. Fraas
51. M. E. LaVerne
52. R. N. Lyon
53. W. D. Manly
54. P. Patriarca
55. G. Petersen
56. H. F. Poppendiek
57. R. L. Potter
58. H. W. Savage
59. M. Slaughter
60. H. J. Stumpf
61. G. D. Whitman
62. E. M. King

EXTERNAL DISTRIBUTION

63. AF Plant Representative, Burbank
64. AF Plant Representative, Seattle
65. ANP Project Office, Fort Worth
66-76. Argonne National Laboratory
77. Armed Forces Special Weapons Project (Sandia)
78-82. Atomic Energy Commission, Washington
83. Battelle Memorial Institute
84. Bechtel Corporation
85-87. Brookhaven National Laboratory
88. Bureau of Ships
89-90. California Research and Development Company
91-96. Carbide and Carbon Chemicals Company (Y-12 Plant)
97. Chicago Patent Group
98. Chief of Naval Research
99. Commonwealth Edison Company
100. Department of the Navy - Op-362

[redacted]

[redacted]

[redacted]

101. Detroit Edison Company
102-105. duPont Company, Augusta
106. duPont Company, Wilmington
107. Foster Wheeler Corporation
108-110. General Electric Company (ANPP)
111-114. General Electric Company, Richland
115. Hanford Operations Office
116-122. Idaho Operations Office
123. Iowa State College
124-127. Knolls Atomic Power Laboratory
128-129. Los Alamos Scientific Laboratory
130. Massachusetts Institute of Technology (Kaufmann)
131. Monsanto Chemical Company
132. Mound Laboratory
133. National Advisory Committee for Aeronautics, Cleveland
134. National Advisory Committee for Aeronautics, Washington
135. Naval Research Laboratory
136-137. New York Operations Office
138-139. North American Aviation, Inc.
140. Nuclear Development Associates, Inc.
141. Patent Branch, Washington
142. Pioneer Service and Engineering Company
143. Powerplant Laboratory (WADC)
144. Rand Corporation
145. San Francisco Operations Office
146. Savannah River Operations Office, Augusta
147. USAF Resident, East Hartford
148. U. S. Naval Radiological Defense Laboratory
149-150. University of California Radiation Laboratory, Berkeley
151-152. University of California Radiation Laboratory, Livermore
153. Vitro Corporation of America
154. Walter Kidde Nuclear Laboratories, Inc.
155-160. Westinghouse Electric Corporation
161-175. Technical Information Service, Oak Ridge

[redacted]

[redacted]

CONTENTS

Section	Page
INTRODUCTION	16
SUMMARY	16
RECOMMENDATIONS	18
PRELIMINARY DESIGN AND ANALYSIS	18
HIGH TEMPERATURE BRAZING ALLOYS AND BRAZING TECHNIQUES	28
HEAT TRANSFER ANALYSIS	34
DESCRIPTION OF RADIATOR CORE ELEMENTS TESTED	39
Radiator Core Element No. 1	39
Radiator Core Element No. 2	39
Radiator Core Element No. 3	39
Radiator Core Element No. 4	39
DESCRIPTION OF TEST LOOP	46
RADIATOR TEST DATA	50
CHARTS FOR THE ANALYSIS OF TEST DATA	63
ENGINE PERFORMANCE STUDIES	69
Turbojet Engine Performance	69
Ram-jet Engine Performance	77
LIST OF ILLUSTRATIONS	5
LIST OF TABLES	10
LIST OF APPENDICES	11
REFERENCES	124
SYMBOLS	12

[redacted]

List of Illustrations

Figure No.	Title	Page No.
1	Radiator Installation Arrangement for a Turbojet Engine	19
2	Computed Characteristics of Round Tube and Plain Continuous Fin Stainless Steel Radiator Cores for Fins Spaced 10 Per Inch	21
	A. Tube Diameter = 0.12 in.	21
	B. Tube Diameter = 0.18 in.	22
	C. Tube Diameter = 0.24 in.	23
3	Type of Radiator to be Used in Boeing Turbojet Engine Test	27
4	Comparison of Experimental and Predicted Heat Transfer Coefficients (Radiator No. 2)	37
5	Computed Characteristics of Round Tube and Plain Continuous Stainless Steel Fin Radiator Cores. (Relative Weight Against Fins per inch for Various Tube Diameters)	38
6	Second Radiator Core Element Tested	41
7	Fourth Radiator Core Element Tested	42
8	Disc Fin Type Radiator Core Element Proposed for Testing (Type G and H)	44
9	Disc Fin Type Radiator Core Element Proposed for Testing (Type I and J)	45
10	Radiator Core Element Test Rig	47
11	Heating Coils of Radiator Core Element Test Rig	48
12	View of Air Outlet Duct of Radiator Core Element Test Rig	49

[redacted]

List of Illustrations (Continued)

Figure No.	Title	Page No.
13	Sodium-to-Air Radiator Core Element Heat Transfer Performance (h vs. Air Flow)	51
	A. Radiator Core Element No. 1 (Plain Fin, 10.5 Fins/in.)	51
	Fins: Type 347 Stainless Steel, 0.010" Thick	
	Tubes: 3/16" O.D., 2/3" ℄ - ℄ Square Spacing	
	B. Radiator Core Element No. 2 (Plain Fin, 15 Fins/in.)	52
	Fins: Type 347 Stainless Steel, 0.010" Thick	
	Tubes: 3/16" O.D., 2/3" ℄ - ℄ Square Spacing	
	C. Radiator Core Element No. 3 (Interrupted Fin, 15 Fins/in.)	53
	Fins: Type 304 Stainless Steel, 0.010" Thick	
	Tubes: 3/16" O.D., 2/3" ℄ - ℄ Square Spacing	
14	Sodium-to-Air Radiator Core Element Heat Transfer Performance (h vs. R_e)	54
	A. Radiator Core Element No. 1 (Plain Fin, 10.5 Fins/in.)	54
	Fins: Type 347 Stainless Steel, 0.010" Thick	
	Tubes: 3/16" O.D., 2/3" ℄ - ℄ Square Spacing	
	B. Radiator Core Element No. 2 (Plain Fin, 15 Fins/in.)	55
	Fins: Type 347 Stainless Steel, 0.010" Thick	
	Tubes: 3/16" O.D., 2/3" ℄ - ℄ Square Spacing	
	C. Radiator Core Element No. 3 (Interrupted Fin, 15 Fins/in.)	56
	Fins: Type 304 Stainless Steel, 0.010" Thick	
	Tubes: 3/16" O.D., 2/3" ℄ - ℄ Square Spacing	

[redacted]

List of Illustrations (Continued)

Figure No.	Title	Page No.
15	Air Radiator Core Element Performance ($\sigma\Delta P$ vs. Air Flow)	57
	A. Radiator Core Element No. 1 (Plain Fin, 10.5 Fins/in)	
	Fins: Type 347 Stainless Steel, 0.010" Thick	
	Tubes: 3/16" O.D., 2/3" ℄ - ℄ Square Spacing	
	B. Radiator Core Element No. 2 (Plain Fin, 15 Fins/in)	58
	Fins: Type 347 Stainless Steel, 0.010" Thick	
	Tubes: 3/16" O.D., 2/3" ℄ - ℄ Square Spacing	
	C. Radiator Core Element No. 3 (Interrupted Fin, 15 Fins/in)	59
	Fins: Type 304 Stainless Steel, 0.010" Thick	
	Tubes: 3/16" O.D., 2/3" ℄ - ℄ Square Spacing	
16	Air Pressure Drop Vs. Air Flow for Radiator Core Element	60
17	Heat Transfer Performance (Nu vs. R_e)	61
18	Logarithmic Mean Temperature Difference Vs. Least Temperature Difference for Various Values of Greatest Temperature Difference	64
19	Logarithmic Mean Temperature Difference Against Cooling Effectiveness for Various Ratios of Primary Fluid Temperature Change to Inlet Temperature Difference	65
20	Local Vs. Over-all Heat Transfer Coefficients for .667" O.D. Disc Fins of 18-8 Stainless Steel, 010" Thick on .1875 O.D. Tubes	66
21	Fin Efficiency Vs. Heat Transfer Coefficient for Various Thermal Conductivities	67
22	Air Radiator Performance (Heating Effectiveness Vs. Air Passage Length for Various Air Flows)	68

[redacted]

List of Illustrations (Continued)

Figure No.	Title	Page No.
23	Weight Studies of a Modified Sapphire Engine	71
	A. Mach Number = 0 Altitude - Sea Level	71
	B. Mach Number = 1.5 Altitude - 35,000 ft	72
	C. Mach Number = 1.5 Altitude - 45,000 ft	73
24	Effect of Pipe Size on Pump and Line Weights for a Typical Radiator Installation in a Turbojet Engine	74
25	Estimated Performance of a Modified Sapphire Engine	75
26	Estimated Performance of a Modified Wright Turbojet Engine	76
27	Weight Studies of a Ram-jet Engine	79
	A. Mach Number = 2.5 Altitude - 65,000 ft	79
	B. Mach Number = 3.5 Altitude - 65,000 ft	80
	(The following figures appear in Appendix F)	
F-1	Heat Exchanger	113
F-2	Heat Exchanger	113
F-3	Radiator Section (bottom view)	113
F-4	Tube-to-Header Section	114
F-5	Tube-to-Header Section	114
F-6	Manifold-Header Tank Braze	115
F-7	Tube-to-Header Braze	115
F-8	Tube-to-Header Braze	116
F-9	Tube-to-Header Braze	116
F-10	Tube-to-Header Braze	117

[redacted]

List of Illustrations (Continued)

Figure No.	Title	Page No.
F-11	Tube-to-Fin Braze	117
F-12	Tube-to-Fin Braze	117
F-13	Tube-to-Fin Braze	118
F-14	304 Stainless Steel Tubes	118
F-15	Heat Exchanger Following Test	119
F-16	Leak in Tube	120
F-17	Tube-to-Header Braze Where Leak Occurred	120
F-18	Nicrobrazed Tube-to-Header	121
F-19	Nicrobrazed Tube-to-Header	121
F-20	Nicrobrazed Tube-to-Header	122
F-21	Inside Surface of 304 Stainless Tube from Hot Section	122
F-22	Inside Surface of 304 Stainless Tube from Cold Section	123
F-23	Inside Surface of Manifold (Unetched)	123

[redacted]

List of Tables

Table No.	Title	Page No.
I	Data on Proposed Air Radiator Cores	25
II	Types of Tube and Fin Radiator Core Elements Proposed For Development Testing	43
III	Design Details of Air Radiators	62

List of Appendices

Appendix	Title	Page No.
A	Radiator Core Element Test Instrumentation and Computation	81
B	Example of the Use of Figure 19 (Logarithmic Mean Temperature Difference Against Cooling Effectiveness for Various Ratios of Primary Fluid Temperature Change to Inlet Temperature Difference)	90
C	Pump and Line Weight Study for a Full-Scale Turbojet NaK System (Sample Calculation)	93
D	Performance Calculations for a Modified Sapphire Turbojet Engine	98
E	Performance Calculations for a Nuclear Powered Ram-jet Engine	104
F	Metallographic Examination of Nicrobrazed Stainless Steel Sodium-Air Heat Exchangers Following Failure During Test	110

SYMBOLS

A - area (ft^2)

A_f - face area (ft^2)

A_{fr} - free flow area (ft^2)

a - acoustic velocity (ft/sec) = $\sqrt{\gamma gRT}$

c_p - specific heat at constant pressure (Btu/lb-^oF)

c_v - specific heat at constant volume (Btu/lb-^oF)

C_s - specific heat consumption (Btu/lb thrust-sec)

C_t - total heat consumption (kw)

D_h - hydraulic diameter (ft) = $\frac{4A_f}{P_w}$

D_d - duct diameter (ft)

D - drag (lb)

E - fin efficiency (dimensionless) = $\frac{U}{h}$

e - efficiency (dimensionless)

f - friction factor (dimensionless)

F - flow rate (lb/sec)

g - gravitational constant (ft/sec^2) = 32.17 ft/sec^2

G - flow rate (lb/sec-ft^2)

h - local heat transfer coefficient (Btu/ft^2-hr-^oF)

H - altitude (ft)

ITD - initial temperature difference (^{o}F)

I - specific thrust or specific impulse (lb thrust/lb air/sec)

I_d - nacelle drag (lb drag/lb air/sec)

I_n - net specific thrust (lb thrust/lb air/sec)

J - mechanical equivalent of heat (ft-lbs/Btu) = 778.16 ft-lb/Btu

K - thermal conductivity (Btu/hr-^{o}F)

LMTD - logarithmic mean temperature difference (^{o}F) = $\frac{ITD - OTD}{\log_e \frac{(ITD)}{(OTD)}}$

L - length of flow passage (ft)

M - Mach number (dimensionless) = $\frac{V}{a}$

N_u - Nusselt's number (dimensionless) = $\frac{hD_h}{K}$

OTD - outlet temperature difference (^{o}F)

P_w - wetted perimeter (ft)

P - pressure (lb/ft^2)

p - pressure (lb/in^2)

P_r - this designation is the same as is used in "Gas Tables" by Keenan and Kaye. It is the ratio of pressures P_a and P_b corresponding to temperatures T_a and T_b along a given isentropic. (dimensionless)

Q - heat flow (Btu/hr)

R - gas constant (ft-lb/^{o}R-lb)

R_e - Reynolds number (dimensionless) = $\frac{VD_h\rho}{\mu}$

T - temperature in degrees Rankine (^{o}R)

t - temperature in degrees Fahrenheit (^{o}F)

U - overall heat transfer coefficient (Btu/ft^2-hr-^{o}F)

V - velocity (ft/sec)

W - weight (lb)

Z - compression ratio (dimensionless)

γ - ratio of specific heats (dimensionless) = $\frac{C_p}{C_v}$

Δ - change in or change of (dimensionless)

η - heating effectiveness or cooling effectiveness (dimensionless)

μ - viscosity (lb/sec-ft)

ρ - mass density ($slugs/ft^3$)

σ - density ratio (dimensionless)

τ - total thrust (lb)

ϕ - enthalpy (Btu/lb)

w - specific weight (lb/ft^3)

Subscripts

av	-	average
c	-	compressor or compression
D	-	diffuser
d	-	duct
e	-	engine
ex	-	expansion
i	-	inlet
is	-	isentropic
j	-	jet or nozzle
P	-	pump and line
R	-	radiator
r	-	ram
rj	-	ram-jet
SL	-	sea level conditions
T	-	total or overall
$^{o}/o$	-	percent
o	-	ambient or altitude conditions
1	-	conditions after ram compression or conditions at compressor inlet
2	-	conditions at compressor outlet or conditions at radiator inlet
3	-	conditions at radiator outlet or conditions at nozzle inlet
4	-	conditions at nozzle exit

[redacted]

INTRODUCTION

The development of a nuclear aircraft power plant employing a high temperature liquid as the heat transfer medium depends upon the construction of a satisfactory air radiator. NEPA designs for the sodium-lithium cycle employed a very clever plate and fin type of structure that proved difficult to fabricate -- so difficult in fact, that after 3 years of effort it has not been possible to build any unit suitable for testing. Since the development of a satisfactory radiator was considered vital to the circulating fuel program at ORNL, it was decided that an attempt should be made to design a unit that would not be too difficult to build and yet would have sufficiently high performance to be acceptable for a tactical nuclear aircraft.

It was felt that a tube and fin design employing round tubes would greatly simplify fabrication and give a rugged, simple, and dependable structure that would be as unlikely to develop leaks as any that might be devised. This report covers the analytical and design work, the heat transfer tests, and the endurance tests that have been carried out on this basic type of construction.

SUMMARY

The analytical work indicates that a tube and fin design yields an aircraft type of radiator having a higher performance and a lower weight than the plate and fin unit. The former has the added advantage of requiring less than one-one thousandth of the number of lineal feet of seam that must be made leak-tight than that of a comparable plate and fin type radiator.

In any radiator of this type suited to a nuclear aircraft power plant one must contend with large variations in the physical properties of the air since the temperature rise through the radiator is approximately 1000°F. These variations in the physical properties of the air cause the heat transfer coefficient to be a sensitive function of the detail geometry of the heat transfer surfaces. It was surprising to find that for the plain fin type of construction the heat transfer coefficient decreased rather rapidly with an increase in metal temperature, whereas with interrupted fins the heat transfer coefficient was found to increase slightly with increasing metal temperature. It would appear that in the former case increased air viscosity at higher temperatures caused a thickening of the boundary layer resulting in reduced heat transfer. This factor apparently more than offsets the effects of the

[redacted]

increase in thermal conductivity of the air with increasing temperature. Interruption of the fins reduced the tendency toward boundary layer thickening so that with the greater turbulence the increase in the thermal conductivity of the air more than offsets the boundary layer thickening resulting from increased air viscosity.

The technique of making sound, brazed joints with brazing alloys having remelt temperatures above 2000°F is difficult. The first unit to be tested was nicrobrazed by the Wall-Colomonoy Corporation of Detroit while the second unit was nicrobrazed at Y-12. The first unit was operated for 330 hr and the second unit for 200 hr, each time the test being terminated when a leak developed at one of the brazed joints. The third unit tested was nicrobrazed at X-10 and was operated for 1212 hr before a leak developed, again at a brazed joint. The fourth unit tested was nicrobrazed at X-10 and was operated for 200 hr but, since the heat transfer performance was poor, the test was terminated without running to failure. Each of the first two units was operated at sodium inlet temperatures of 1500 - 1600°F for about 130 hr, while the third unit was operated for 655 hr at 1500°F, 336 hr at 1600°F, and 43 hr at 1700°F.

All three failures were disappointingly unspectacular, the first indication of trouble in each instance being the appearance of smoke. In one case a small fire also occurred but it was easily extinguished. This seems to indicate that the fundamental philosophy of design was sound, that is, the radiator structure was designed so that it would be relatively free of redundant stresses from differential thermal expansion while pressure stresses were kept to less than 1000 psi so that a burst type failure should not occur. The most likely type of failure therefore would be the development of a small leak at a fatigue crack or at a point of localized corrosion caused by imperfections such as a flaw in the material or a poorly brazed joint.

Heat transfer data from the above tests were used to construct performance charts for full-scale aircraft type radiators to facilitate turbojet and ramjet performance analyses. The performance characteristics of two hypothetical turbojet engines were estimated from the above charts. The first engine was assumed to have the same weight but a lower compression ratio than that of the Sapphire. The second was a modification of a Wright engine under development. Curves for these engines are included in Figures 25 and 26.

The analytical work indicates that the most promising aircraft type radiator would be similar to those tested except that circular disc fins instead of plane fins should be used with a staggered rather than an in-line tube array. The tube diameter and tube spacing appear to be close to optimum values.

RECOMMENDATIONS

Determine the upper temperature limit for practical radiator operation by endurance testing core elements having fins made of the following materials:

a) Type 316 stainless steel
b) Type 310 stainless steel
c) Nickel-uncoated
d) Nickel with chromium plate
e) Nickel with ceramic coating
f) Nickel with nicrobraze coating

Determine the relative heat transfer performance of the following geometries using 3/16" O.D. tubes spaced on 2/3" centers:

a) In-line tubes, fins interrupted in 2/3" intervals (316 S.S. and Ni fins)

b) In-line tubes, fins with integral ridges (or turbulators) transverse to air flow

c) Staggered tubes, constant thickness disc fins (both 310 S.S. and Ni)

d) Staggered tubes, disc fins tapered from root to tip (Ni)

e) Other promising geometries

PRELIMINARY DESIGN AND ANALYSIS

The NEPA plate and fin type of radiator construction (see NEPA-1520) was predicated on the notion that the radiator air inlet face should be in a plane perpendicular to the axis of the engine. This requirement made it necessary that a high percentage of the face area of the radiator be unobstructed air passage area. Despite the use of a very clever, complex involute type of construction, the NEPA group was unable to avoid a 50°/o increase in engine frontal area arising from the radiator installation. It was felt that an arrangement shown schematically in Figure 1 might be employed to advantage. Simple rectangular radiator cores can be placed around the axis of a turbojet engine in much the same way as the banks of cylinders of an X-type reciprocating air-cooled engine. Helical baffles between the radiator cores can be made to duct the air along the engine axis between the radiator cores, transversely through the cores, and then direct it rearward to the turbine nozzle box. While this arrangement may increase the engine length

[redacted]

Dwg 19418

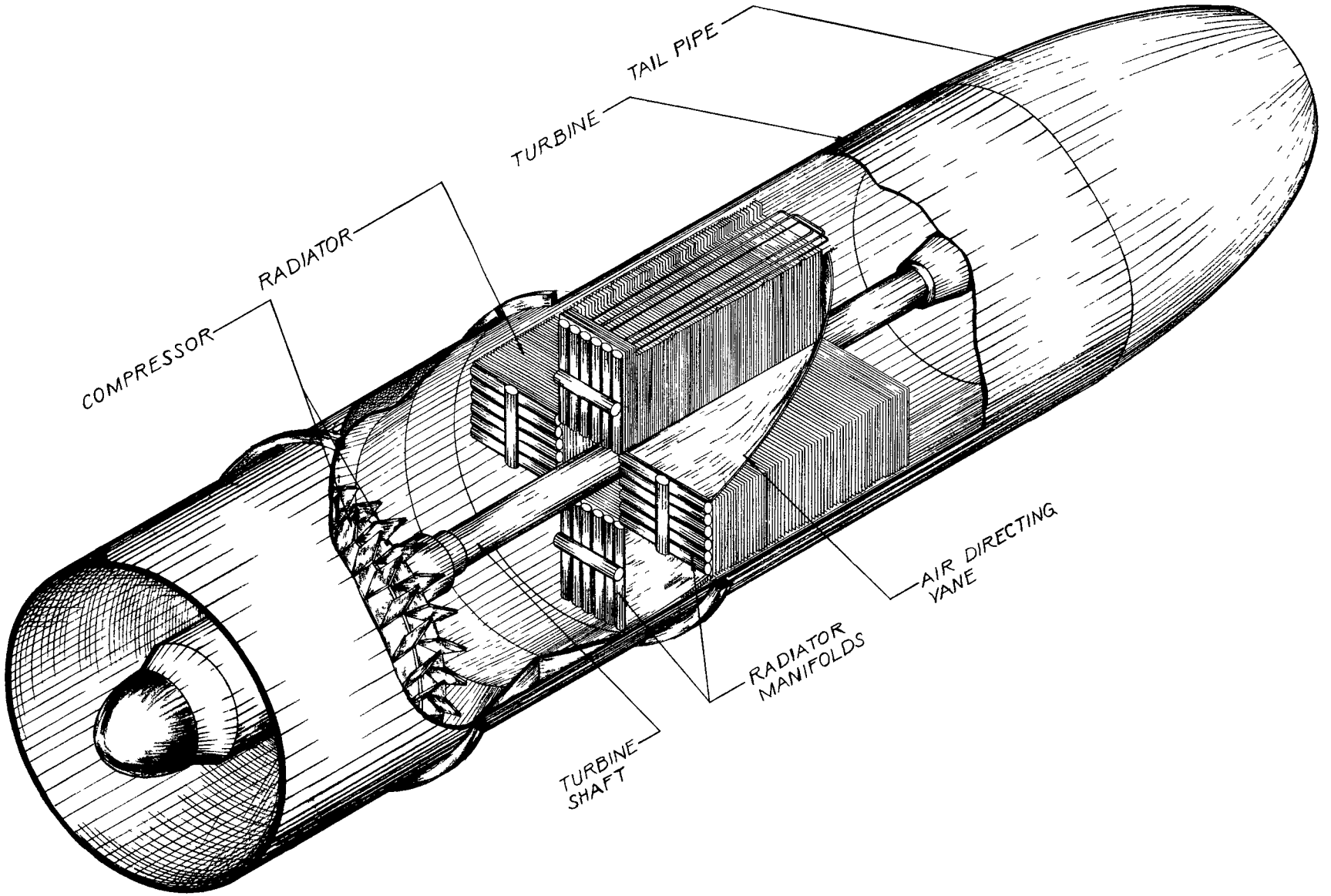

Fig 1 Radiator Installation Arrangement for a Turbojet Engine

over a similar chemically-powered engine, it should not require any increase in engine frontal area. It also has the advantage of allowing turbojet engine control to be effected by means of an air by-pass valve placed in the helical baffle between adjacent radiator cores.

Round tubes cause a greater obstruction to air flow through a radiator than either flat or oval tubes. The increases in engine length and weight caused by the use of round tubes rather than flat or oval ones appeared to be quite small. The advantage of the greater structural strength and stability of round tubes coupled with the markedly easier problem of fabrication made round tubes obviously better for preliminary development work. The use of large, continuous plate fins as opposed to individual disc fins for each tube was carefully considered. It was thought that the former was to be preferred because they clearly give a very stable structure and simply and accurately space the tubes. It has since become apparent that an equally sound structure can be obtained through the use of continuous plates, perhaps .040 in. thick, spaced 2 or 3 in. apart along the tubes with individual disc fins between these plates. This latter arrangement appears from the literature to give a higher performance type of construction from the standpoint of nuclear aircraft power plant requirements.

A paper analysis was made to determine the effects of variations in fin thickness, tube diameter, and tube spacing on radiator core performance for stainless steel fins. The work was then extended to higher conductivity fins of nickel for some of the more interesting tube diameter and spacing combinations. To simplify the design of the die required to fabricate test units, an in-line tube arrangement was adopted. Figures 2A, 2B, and 2C show the effects of fin thickness and tube spacing on the more important performance parameters of a radiator core. These curves were studied carefully and an effort made to assign relative importance to such parameters as the number of feet of brazed seam, the number of feet of tubing, radiator weight, etc., for a full-scale engine installation. The probability of a failure seems to be directly proportional to both the number of feet of tubing required and the number of tube-to-header joints. Both of these vary as the square of the tube spacing which indicates that there is a major incentive to space the tubes as far apart as possible. It is evident from Figures 2A, 2B, and 2C, however, that the average fin efficiency falls off very rapidly, and the radiator weight per effective unit of heat transfer surface is increased as the tube spacing is increased. Other considerations were also judged to be important. The air pressure drop was found to be only a few percent of the compressor air outlet pressure for configurations that seemed of most interest. Since this would probably be less than the diffuser losses between the compressor outlet and the radiator inlets, it appeared that, for this type of construction, the air pressure drop is a secondary consideration. Although smaller tube diameters yield higher radiator performance from both volume and weight standpoints, it was felt that the probability of tubes clogging and leaks developing favored the use of either 3/16 or 1/4 in. tubes over 1/8 in. diameter tubes. Since an adequate supply of 3/16 in. diameter tubing was available for the construction of preliminary tests units, this size was chosen.

Unclassified
Dwg. 19419

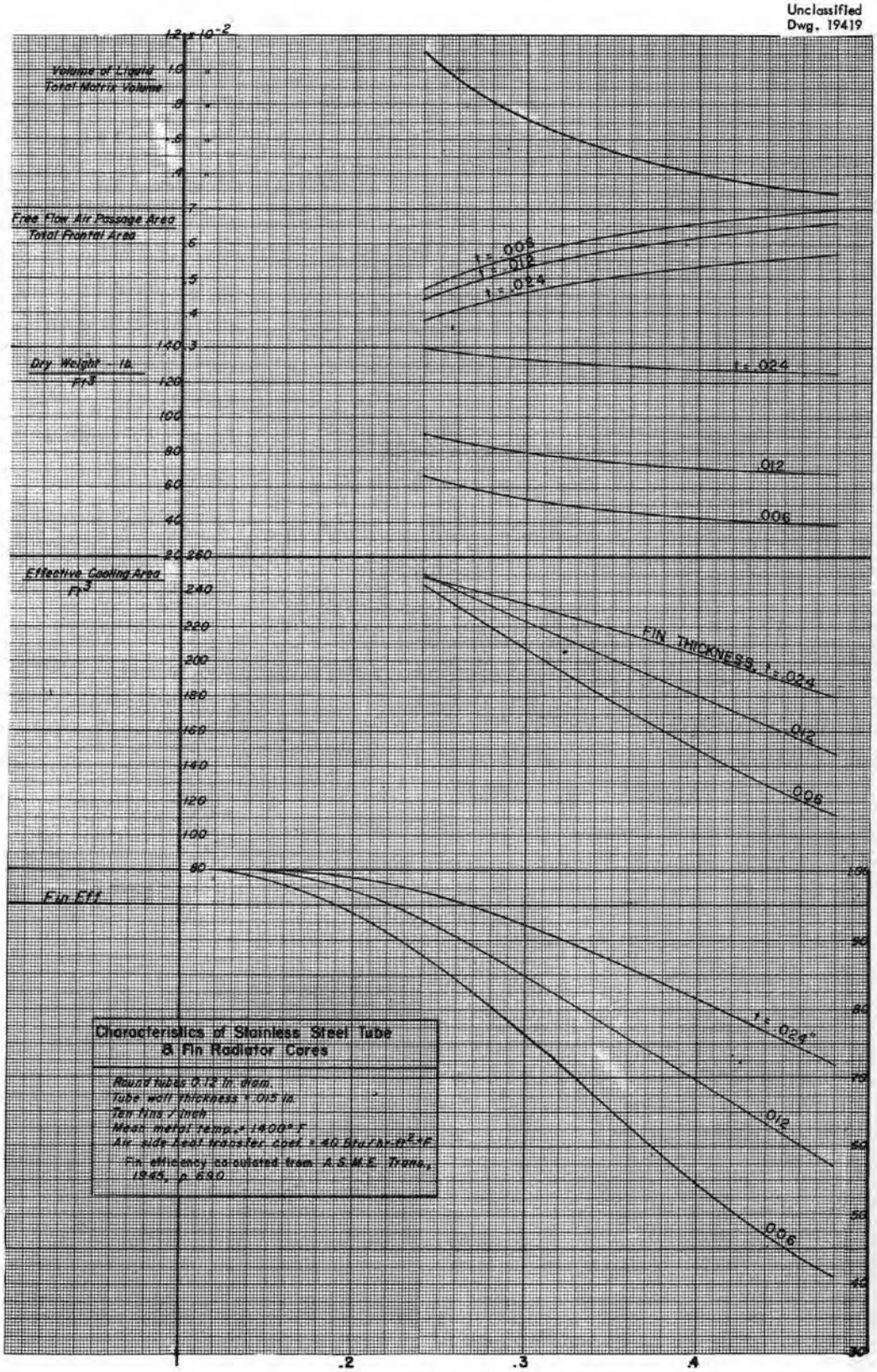

(a) TUBE DIAMETER, D_1 = 0.12 IN

HEAT TRANSFER COEFFICIENT, h = 40 BTU PER FT^2-HR-°F

FIGURE 2 . COMPUTED CHARACTERISTICS OF ROUND TUBE AND PLAIN CONTINUOUS FIN STAINLESS STEEL RADIATOR CORES FOR FINS SPACED 10 PER INCH.

Unclassified
Dwg. 19420

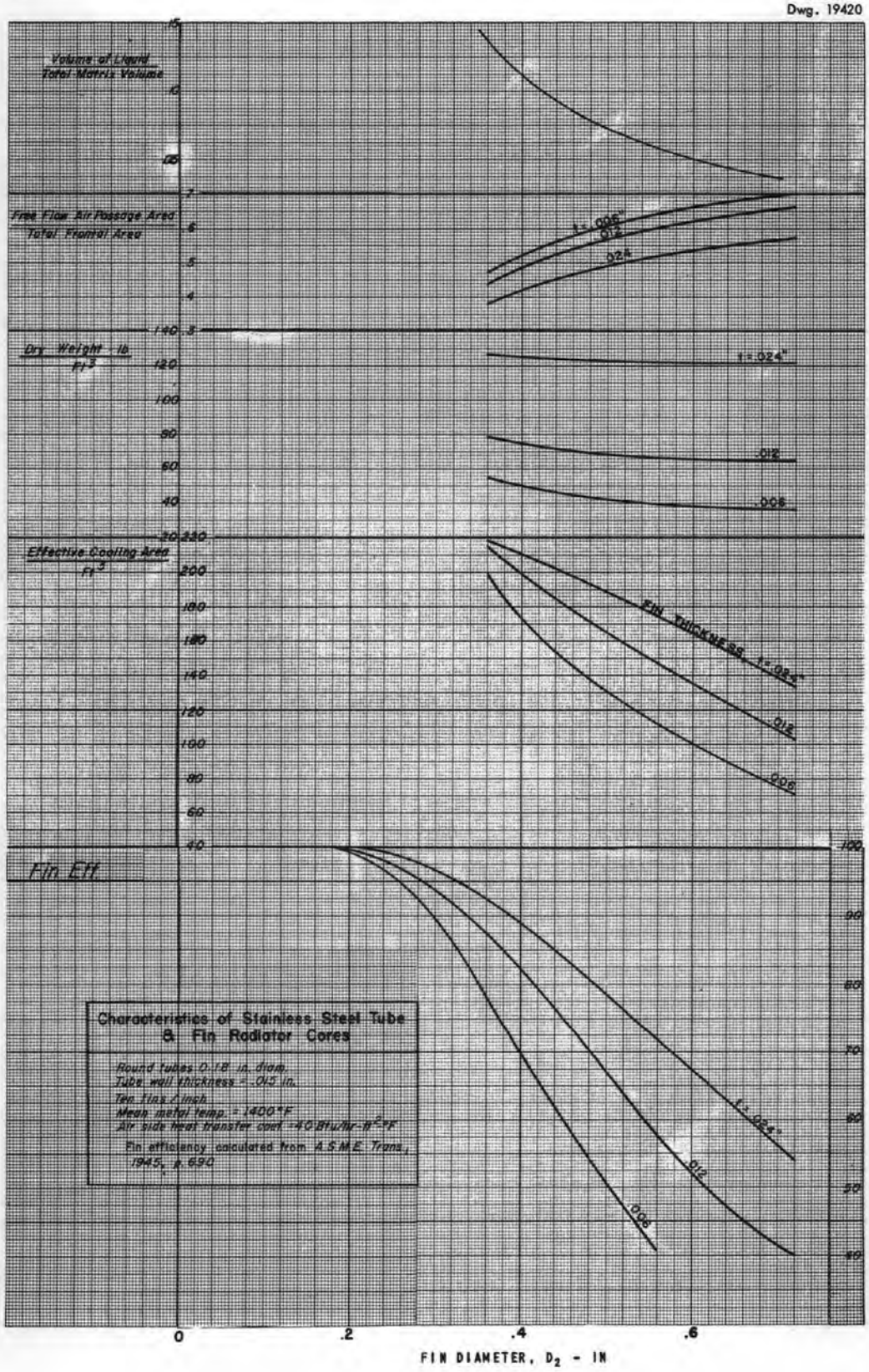

(b) TUBE DIAMETER, D_1 = 0.18 IN

HEAT TRANSFER COEFFICIENT, h = 40 BTU PER FT^2-HR-°F

FIGURE 2 . COMPUTED CHARACTERISTICS OF ROUND TUBE AND PLAIN CONTINUOUS FIN STAINLESS STEEL RADIATOR CORES FOR FINS SPACED 10 PER INCH.

Unclassified
Dwg. 19421

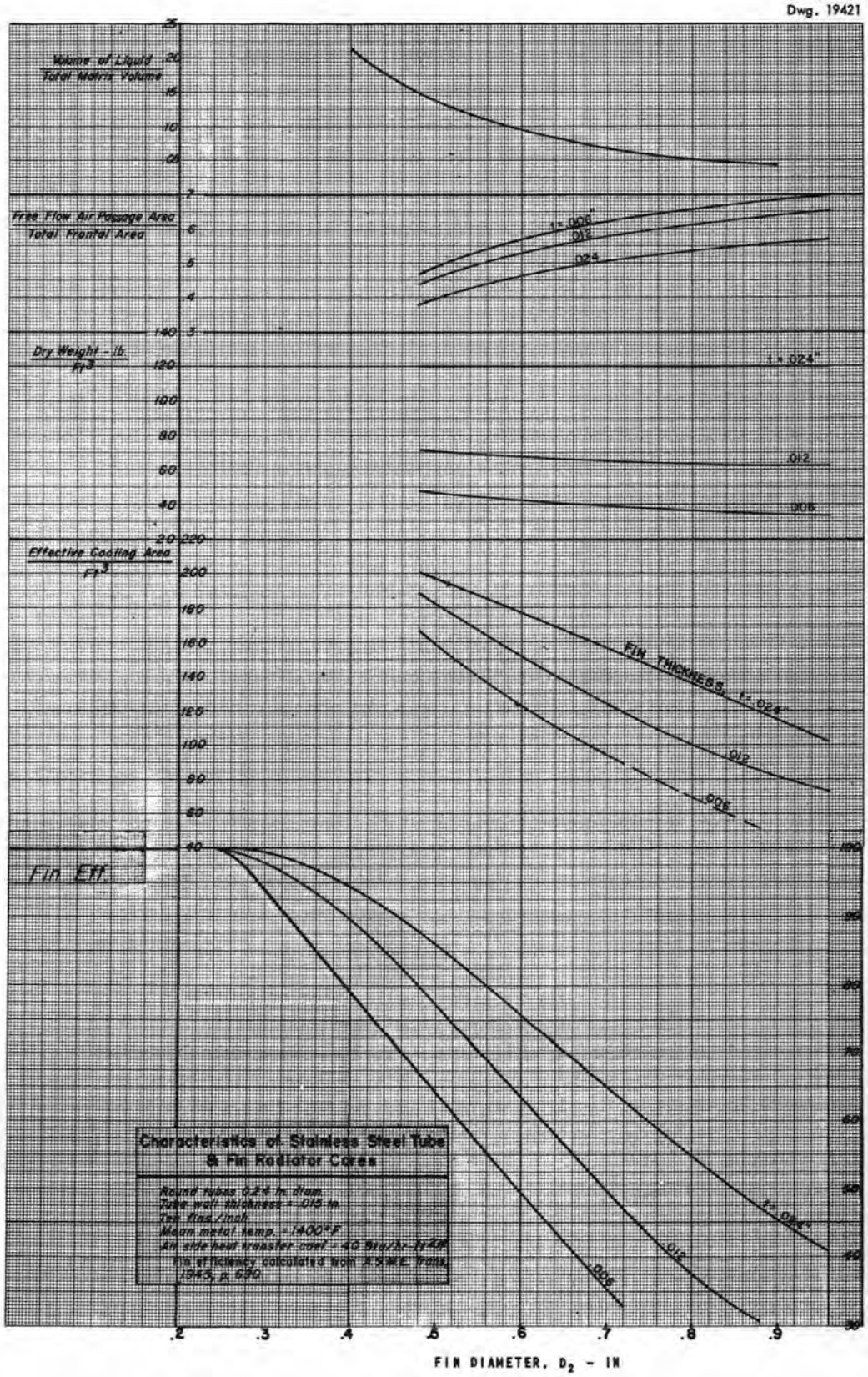

(c) TUBE DIAMETER, D_1 = 0.24 IN

HEAT TRANSFER COEFFICIENT, h = 40 BTU PER FT^2-HR-°F

FIGURE 2 . COMPUTED CHARACTERISTICS OF ROUND TUBE AND PLAIN CONTINUOUS FIN STAINLESS STEEL RADIATOR CORES FOR FINS SPACED 10 PER INCH.

Some studies were made of the effect of sodium pressure drop through the radiator on both stresses and system component weight. It appeared that pressure drops up to 50 psi across the radiator imposed no serious weight or stress penalties in systems that seemed to be of interest.

Other figures of merit in the selection of a radiator core geometry were considered. These included the volume of liquid that would be contained in the radiator and factors associated with that volume, such as liquid cost, potential hazard, and thermal expansion. Thermal lag, engine control, and response characteristics are also important considerations. All of these favor the use of the minimum volume of liquid possible in the radiator core.

Any selection of tube spacing must of necessity represent a compromise. The tube spacing of .667 in. was chosen because it gave a relatively small number of tube-to-header joints, and a small total footage of tubing per cubic foot of radiator. Although the fin efficiency for stainless steel fins used with this tube spacing was low, it was felt that later work could be carried out with nickel fins and the same dies, tools, and fixtures could still be used.

The header and manifold arrangement chosen for the cores built to date can be seen in Figure 6 which shows one of the radiator core elements built for heat transfer and endurance testing. The air enters at the left end through the 2 x 3.33 in. face of the finned region and flows through the 12 in. long passages between the fins from the lower left end to the upper right end. There is a plug in the center of the manifold tube that passes along the side of the radiator in the lower foreground. Hot sodium enters the manifold tube at the lower right corner and passes to the left into the three 2 in. diameter header drums at the air outlet end of the radiator. The hot sodium then flows upward through the tubes in the fin matrix, forward and to the left in the tube cross-over region, then downward and into the three header drums at the air inlet end. Two types of tube cross-over arrangement were used. The first one devised is shown in Figure F-15. It proved to be a bit difficult from the tube bending standpoint. The second arrangement, shown in Figure 6, was relatively easy to build and approaches the ideal pure counter-flow heat exchanger concept almost as closely as the first arrangement. Note that, although this arrangement has but two sets of header joints and appears to give a two-pass cross-flow construction, it actually approaches a four-pass cross-flow heat exchanger in performance.

Designs for three different sets of requirements were prepared. The first design work was on a set of radiators for the J-53 engine so that a comparison with the NEPA radiator design of NEPA-1520 could be made. The second was for a radiator test installation that might be made in a Boeing turbojet engine. The third was for small core element heat transfer and endurance test work. Table I gives the more important data on geometry for both the NEPA plate and fin and the above ORNL tube and fin radiator cores. Figure 3 shows the radiator designed for the Boeing turbojet engine test rig.

TABLE I

Data on Proposed Air Radiator Cores
(All values are estimated and are not based on test data)

	Core Element for Preliminary Testing (Sea-level)	Radiator Core for Boeing Turbojet (Sea-level)	Radiator Core for J-53 (4 required/engine) 45,000 ft.	NEPA Proposal for J-53 Engine in IL-12 Report (45,000 ft.)
Core volume-ft^3	1/16	1.0	4.5/core; 18/eng.	12.35
Type	2-pass, cross-flow	2-pass, cross-flow	2-pass, cross-flow	4-pass, cross-flow
No. of feet of 3/16 in. tubing(including cross-over between passes	45	365	1580'/core;6320'/eng.	
Fin spacing	14/in.	14/in.	14/in.	11/in.
Tube diameter	3/16 in.	3/16 in.	3/16 in.	
Tube spacing	2/3 in.	2/3 in.	2/3 in.	
Fin thickness	.010 in.	.010 in.	.010 in.	.007 in.
Tube thickness	.016 in.	.016 in.	.016 in.	
Tube material	Type 304 SS	Type 304 SS	SS	SS
Fin material	Type 347 SS	Type 302 SS	SS	SS
Core weight(dry without headers)	80 lb/ft^3	80 lb/ft^3	80 lb/ft^3	
Core weight(wet without headers)	82.4 lb/ft^3	82.4 lb/ft^3	82.4 lb/ft^3	
Total core dry weight (with headers)	11 lb	93 lb	1510 lb (per eng)	
Total core weight(wet and with headers)	11.9 lb	99 lb	1580 lb (per eng)	2240 lb
Weight of liquid in core and headers	.9 lb	6 lb	70 lb	240 lb

TABLE I
(Continued)

Data on Proposed Air Radiator Cores
(All values are estimated and are not based on test data)

	Core Element for Preliminary Testing (Sea-level)	Radiator Core for Boeing Turbojet (Sea-level)	Radiator Core for J-53 (4 required/engine) 45,000 ft.	NEPA Proposal for J-53 Engine in IL-12 Report (45,000 ft.)
Length parallel to air flow	12 in.	12 in.	12 in.	12 in.
Length parallel to liquid flow	3 in.	11 in.	36 in. (each core)	
Width	3-1/3 in.	6-2/3 in.	18 in. (each core)	
Inlet face area	1/16 ft^2	1 ft^2	4.5 ft^2/core;18 ft^2/eng.	12.35 ft^2
Free flow ratio (air)	.71	.71	.71	.63
Liquid	Na	Na	Na	Li
Liquid temp. In - ^oF	1600	1600	1600	1600
Liquid temp. Out - ^oF	1200	1200	1200	1140
Air temp. In - ^oF	100	350	289	289
Air flow - lb/sec-ft^2 inlet face area	3.0	3.0	3.3	4.81
Liquid press. drop-psi	7	25	36	50
Air press. drop-psi	1.07	1.00	1.66	1.4
Engine frontal area-ft^2			12.1	18.35
Engine length-in. (Std. Eng. = 180 in.)			192	172

Unclassified
Photo Y-8580

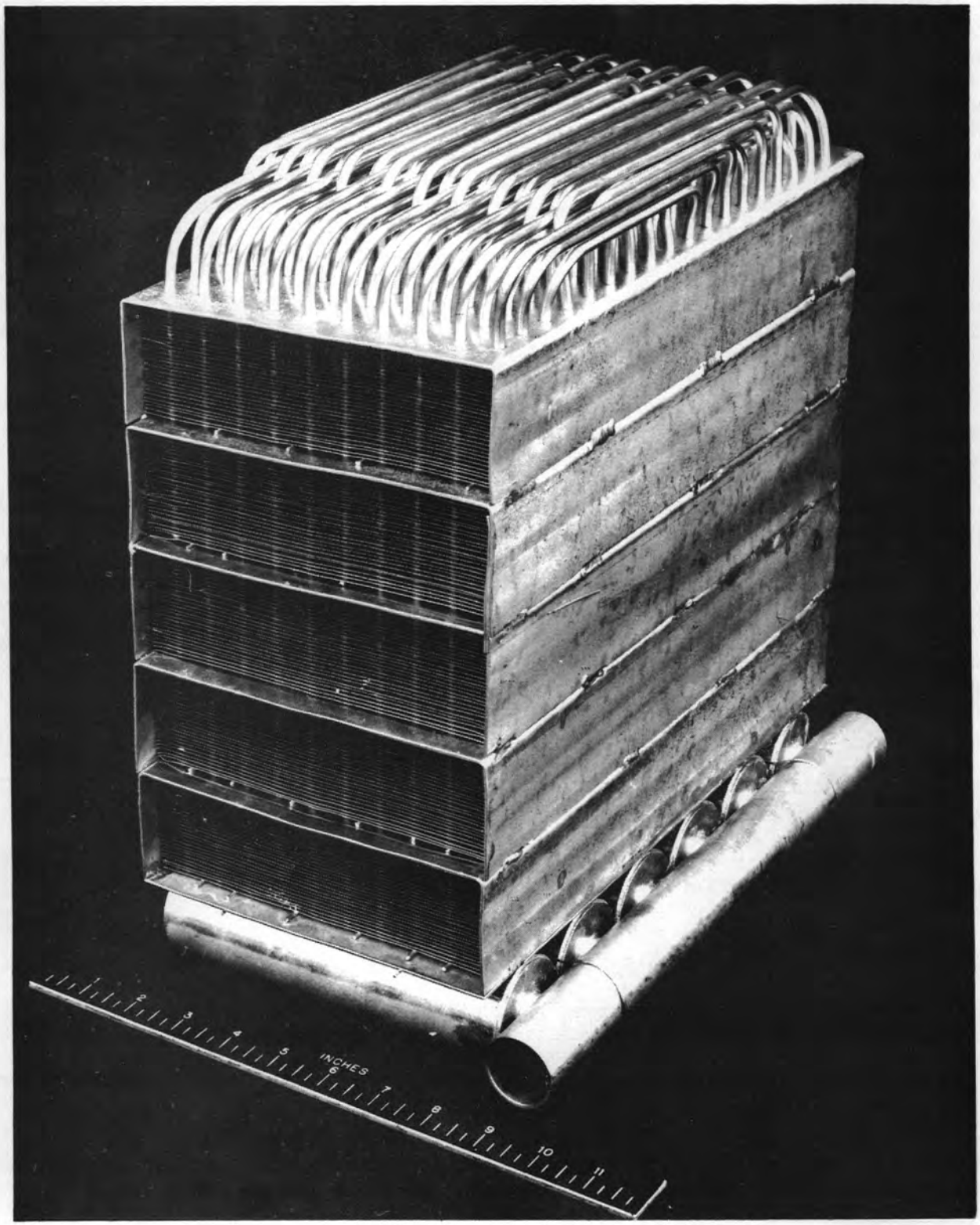

Fig. 3. Type of Radiator to be Used in Boeing Turbojet Engine Test.

HIGH TEMPERATURE BRAZING ALLOYS AND BRAZING TECHNIQUES

The technique of using high temperature brazing alloys to make sound brazed joints has received considerable attention from the Metallurgy Division of the Oak Ridge National Laboratory. To date all of the radiators fabricated have been nicrobrazed. Nicrobraz has good corrosion resistance in sodium and is very oxidation resistant. Its major disadvantage is that the boron and silicon added to the alloy to lower its melting point and increase its fluidity tend to diffuse into the base metal during the brazing operation and embrittle it. This has proved troublesome in the fabrication of the large radiators designed for the Boeing Turbojet Test (see Fig. 3) when several successive brazing operations have been carried out at temperatures of about 2300°F. Some of the embrittled tubes have cracked due to the stresses set up by differential thermal expansion during later brazing operations. The extent of the diffusion of boron and silicon into the tube wall is very sensitive to the brazing temperature and the amount of braze material used, the diffusion being more severe at higher brazing temperatures and with greater amounts of Nicrobraz at the joint. In particularly severe cases the boron and silicon have diffused to the inner surface of the tube wall. Recent experience has indicated that by carefully excluding nitrogen from the system Nicrobraz can be made to flow nicely at furnace temperatures of 2050°F instead of the 2250 to 2300°F that had seemed necessary in earlier work. Brazing at 2050°F greatly reduces boron diffusion into the base metal and the resultant tendency toward tube wall embrittlement.

Other brazing alloys have also been investigated, notably manganese-nickel and gold-nickel alloys. Sixty-forty manganese-nickel alloy has a flow temperature of 1800°F. Tests have indicated that there is little diffusion into the base metal and consequent embrittlement by this alloy and that it is not as temperature or amount sensitive as the Nicrobraz. It appears to have good corrosion resistance in sodium and fair oxidation resistance.

An 82-18 gold-nickel alloy having a flow temperature of 1800°F shows relatively little tendency to diffuse into the base metal but it exhibits poor corrosion resistance in sodium.

The following sections describe in some detail the nicrobrazing procedure and radiator fabrication techniques that have been employed.

Recommended Procedure for Nicrobrazing

Nicrobraz* is a trade-marked product produced by the Wall-Colmonoy Corporation, 19345 John R., Detroit, Michigan. A typical sample contains 70% nickel, 14% chromium, 4.9% boron, 4.6% silicon with the balance iron (from ball milling), and has a melting point of 1950°F. The recommended brazing temperature is 2150°F. It has proved to be a very excellent brazing material for all of the iron-chrome-nickel alloys except that some difficulty has been encountered with type 321 stainless steel. There has also been some difficulty in brazing surfaces that have been ground with zirconia wheels.

*Reference 15, p. 651-662

When first melted the material has a very high fluidity and wets the surfaces exceptionally well. At brazing temperatures, however, it diffuses rapidly into the base material giving a joint having a remelt temperature approaching that of the base metal. If applied in too thick a layer on a surface adjacent to the joint to be brazed, it is inclined to dissolve the surface by alloying and may cause as much as .010" or .020" of material to be melted off and allowed to flow away. Only enough Nicrobraz material to fill the joint should be used.

The Nicrobraz material comes in the form of a 400 mesh powder. It is extremely hard and brittle and has not been produced in sheet or wire form. It can be suspended in a low ash methyl methacrylate cement and painted or dripped with an eyedropper onto a joint. This cement can be extruded to yield ribbons .010" to .020" thick from which washers can be punched and used for brazing. If clearances in the joint of the order of .001" to .003" are employed, painting some of the Nicrobraz methyl methacrylate cement suspension on the outside of the joint is generally satisfactory because upon melting the Nicrobraz material will flow into the joint. However, rapid heating is required because otherwise the Nicrobraz will alloy with the base material before it is well melted and the joint may not fill completely with braze metal.

Apparently because of the affinity of chromium and boron for oxygen and nitrogen, (otherwise, cracked ammonia could be used instead of hydrogen) it is essential that the brazing be carried out in an extremely pure dry hydrogen atmosphere. It has been found that such an atmosphere can be obtained by passing water-pumped hydrogen first through a Deoxo Catalytic Unit (to convert any oxygen present to water) and then through a Lectrodryer to remove virtually all of the moisture and reduce the dew point to at least -65°F. Because the development of the technique of controlling these units, particularly regeneration of the Lectrodryer is rather difficult, it is very important that the dew point of the hydrogen be checked with a dew point indicator. Commercial sources and approximate price data of these three items of equipment are as follows:

Deoxo Catalytic Unit
50 ft^3/hr size -- $45.00
Baker Company, Inc.
Newark, New Jersey

Lectrodryer
100 ft^3/hr -- $300.00
Pittsburgh Lectrodryer Company
Pittsburgh, Pennsylvania

Dew Point Indicator -- $340.00
Illinois Testing Laboratory
420 N. LaSalle Street
Chicago 10, Illinois

Satisfactory nicrobrazing work is done commercially at Wall-Colmonoy by placing units to be brazed inside of what are in effect metal bell jars with a sand seal around the outside of the lower rim. Many operators prefer to weld the work to be brazed into an airtight can. This insures that no back diffusion of air or furnace gases will take place through joints or a sand barrier if the hydrogen flow rate happens to drop off momentarily. When using canning techniques, it is also recommended that the hydrogen be passed through a preheater before it enters the can containing the work to be brazed. This can be done rather easily by bending a 20 ft length of 1/4 inch stainless steel pipe into a flat spiral much like a watch spring. This preheater can be mounted within a few inches of the can so that it can be pushed into the furnace along with the work. A rough rule of thumb for a satisfactory hydrogen flow rate is that there should be about 30 cu ft/hr of hydrogen per cubic foot of can. This can be established easily with a small rotometer.

When the work is first pushed into the furnace, decomposition of the methyl methacrylate cement will cause the dew point of the hydrogen leaving the muffle to rise rapidly to perhaps $0^{\circ}F$. The dew point should then drop back down to $-65^{\circ}F$ or lower or a satisfactory job of brazing will probably not be obtained. It has been found that an initial furnace temperature of $2100^{\circ}F$ gives good results for small units; i.e., cans of 1 cu ft or less. Furnace temperatures somewhat higher may prove better for larger units. When the work is pushed into the furnace, the temperature normally drops several hundred degrees Fahrenheit and will rise again to the value set on the controls. It appears that the controls should be set to give soaking temperatures of $2100^{\circ}F$ because the flow of hydrogen over the work cools it to a level somewhat below the furnace temperature.

Commercial sources of hydrogen cylinders are such that there is often a considerable amount of water in the cylinders along with the hydrogen. If the hydrogen is used until the pressure drops below about 500 psi, so much water vapor may be present in the hydrogen that the Lectrodryer will be overtaxed. That is, below cylinder pressures of 500 psi the partial pressure of the water vapor will become a significant percentage of the total pressure of the gas leaving the cylinder.

Careful and thorough regeneration of the Lectrodryer in accordance with the manufacturer's specifications is essential to insure a sufficiently dry hydrogen atmosphere throughout the entire 1 to 2 hr. of brazing, as well as during the preliminary purge period. When putting the unit into operation, the entire system including the can should be first purged with helium or another inert gas to eliminate the oxygen, and then purged with hydrogen which should be ignited and allowed to burn at the outlet from the muffle. The system should be purged with hydrogen for at least an hour at a flow rate of about 10 $ft^3/hr\text{-}ft^3$ of system volume.

One should not attempt to weld in the vicinity of a brazed joint after nicrobrazing because of the embrittling effect of traces of the brazing alloy. Cracking may be prevalent in the weld and in regions surrounding the weld. If welding should prove essential, the surface should be machined or filed to make certain that no Nicrobraz material gets into the weld zone.

The film of Nicrobraz material in the vicinity of a joint appears to be even more oxidation-resistant than stainless steel. This suggests that radiators might be assembled and the Nicrobraz material applied by dusting it on. This would serve to cover the fins with an oxidation-resistant coating and at the same time would take care of the tube-to-fin joints.

A few additional remarks on technique may prove helpful to the novice in nicrobrazing. These are as follows:

1. The amount of braze material to be applied at each joint can be learned only through experience.

2. If the work is placed in a can that is welded shut, the hydrogen flow may be cut to approximately 1/3 after the brazing temperature has been reached to prevent cooling by the hydrogen.

3. The time in the furnace depends on the type of furnace (high or low speed) and the total heat capacity of the assembly to be brazed.

4. Commercial sources of hydrogen vary in quality from one section of the country to another. It may be necessary to try several sources before a satisfactory supply can be found.

5. The hydrogen may be burned in the furnace or it may be returned to the atmosphere and burned there.

6. The surfaces of the work brazed should come out very bright and clean as if electrolytically polished. Even badly oxidized regions in the vicinity of welds that may have been made to hold the parts together during brazing will be reduced and appear bright and clean. If the hydrogen supplied is not dry enough, the surfaces of stainless steel parts will be coated with a gray-green film, and inspection will show that the brazing material has not melted and flowed properly but remains in dirty, partly sintered granules on the surface. Nickel parts will come out bright whether the hydrogen is dry or not, but satisfactory brazing cannot be obtained except with very dry hydrogen.

7. Recent experience has indicated that purging the system with nitrogen prior to the brazing operation may result in faulty brazed joints. It is believed that some nitrogen may remain in the system even after the hydrogen purging operation and form nitrides, thus raising the melting point of the Nicrobraz. This will cause the braze material to sinter partially rather than melt and flow into the joint. Tests show that it is much better to use helium in place of nitrogen to purge the system.

8. Use of a heavy liquid cement to suspend the Nicrobraz is not recommended since tests at ORNL have shown that even after heating at 1200°F for an hour some heavy liquid cement that had been used had not evaporated but still was present as a rubbery mass. This may well prevent the Nicrobraz from flowing properly. Use a thin cement consisting mostly of solvent.

Suggested Procedure and Specifications for Radiator Fabrication

1. In the first brazing operation braze all connections except those to the header plugs on the anti-manifold side. The assembly can be prepared for brazing so that it is almost entirely self-jigging. The flanges at the ends for the connecting air duct should be welded on and the two long seams welded in the 2-1/4" x 3-1/2" duct enclosing the finned region. The long tubular manifold will be supported by the air duct flanges, and the manifold ends of the header drums will be supported by the manifold tube. Six tabs bent out from a sheet metal angle will support the other end of each header drum. Use a sheet of plain carbon steel shim-stock (about .020 in.) between the assembly to be brazed and the can to prevent the formation of a brazed connection to the can caused by excess braze material running to the bottom of the assembly.

2. After brazing inspect the unit visually for good fillets in tube-to-header joints and for dissolving away of the tube walls caused by use of an excess of brazing material.

3. Using rubber gaskets, clamp plates over the openings in the header drums and the manifold tube. Applying helium at 15 psi, submerge the unit in hot water (about 160°F). Wipe off all air bubbles. Watch carefully for 30 minutes looking for bubbles to form at the joints.

4. Apply brazing material lightly to patch any leaks found in (3) or any poor joints found in (2). Install header drum plugs with brazing material and carry out second brazing operation.

5. Repeat inspections carried out in (2) and (3) above except using helium at 60 psi. If leaks develop, patch with brazing material and braze a third time. (Note: bubbles the size of the head of a pin requiring 10 minutes to form indicate leaks that may be tolerated. No more than two such leaks may be permitted in one radiator core.)

6. Do not try to patch any leaks in nicrobrazed joints by welding.

SUGGESTED JIGGING FOR BRAZING

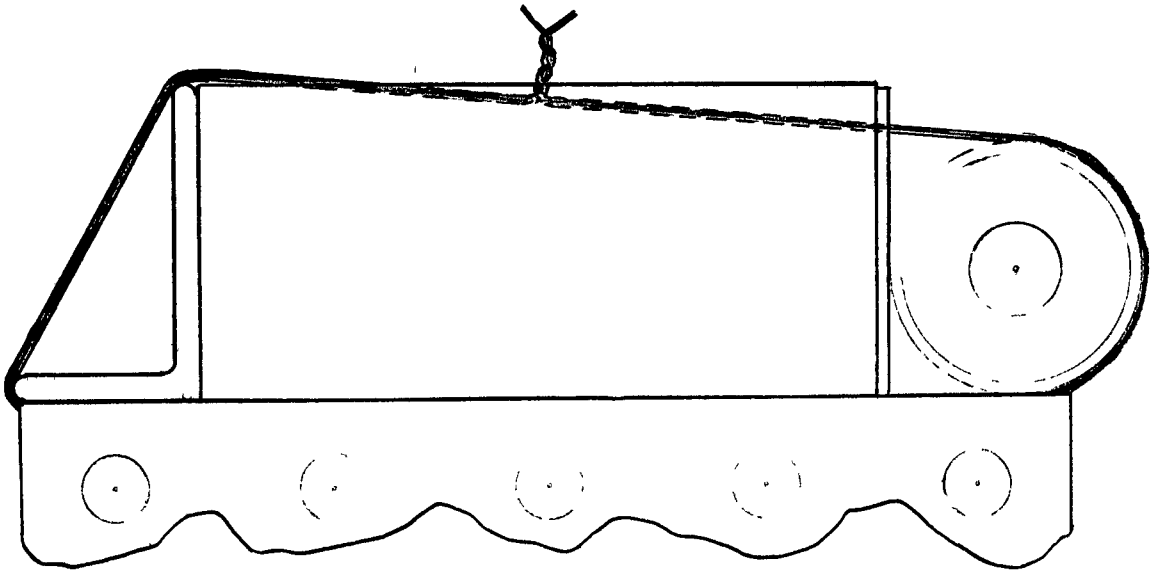

Manifold and Angle Held Snuggly Together at Each End With Baling Wire

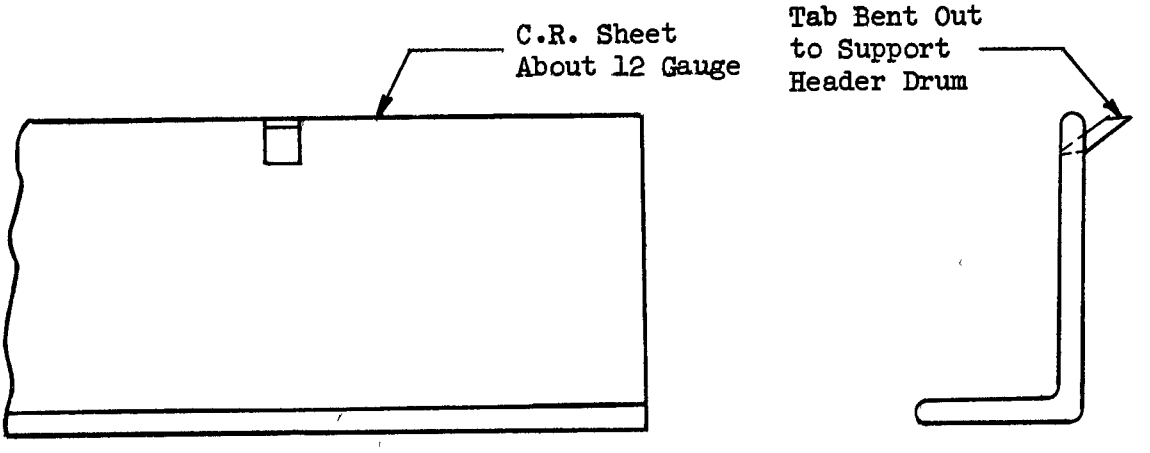

HEAT TRANSFER ANALYSIS

In approaching the basic design problem from the heat transfer standpoint it was immediately evident that the temperature drop from the liquid metal to the tube wall would be trivial and that the heat transfer resistance on the air side of the radiator would be controlling. Thus large extended surfaces composed of either plate fins, circular disc fins, discontinuous strip fins, or pin fins must be employed. The problem is complicated by the large temperature differences through the heat exchanger so that far from isothermal conditions prevail.

Discontinuous strip fins and pin fins were investigated experimentally by Norris and Spofford, reference 13. They were able to correlate their results by the following empirical correlation.

$$\frac{h}{cG}\left(\frac{c\,\mu}{k}\right)^{2/3} = 1.0\left(\frac{Z_p G}{\mu}\right)^{-1/2}$$

where h - heat transfer coefficient
c - specific heat
k - thermal conductivity
G - mass flow
μ - viscosity
Z_p - the heated perimeter

This same relation was also satisfactory for correlating the experimental results of Johnson, reference 9, using circular disc fins. Although this is a laminar flow solution it has been found to hold for the above types of surface for Reynolds numbers (based on length) up to 10,000.

The heat transfer coefficient for laminar flow and constant wall temperature for flow between infinite parallel plates can be predicted by the analysis of Norris and Streid, reference 14. Their solution approximates the heat transfer coefficient for plate fins in which a large fin pitch is employed. Their correlation has also been shown to fit the experimental data of Kays, reference 10, for plate fin radiators. Using the logarithmic mean temperature difference, the following expressions were derived by Norris and Streid for the heat transfer coefficient.

$$\frac{hD}{k} = 1.85\left(\frac{cGD^2}{kL}\right)^{1/3} \quad \text{for} \quad \left(\frac{cGD^2}{kL}\right) > 70$$

$$\frac{hD}{k} = 7.60 \quad \text{for} \quad \left(\frac{cGD^2}{kL}\right) < 70$$

where L - heated length
D - equivalent diameter (twice the gap for infinite parallel plates)

The heat transfer coefficient for turbulent flow for plate fin radiators can be predicted approximately by the formula proposed by Colburn, reference 2.

$$\frac{h}{cG}\left(\frac{c\mu}{k}\right)^{2/3} = 0.023\left(\frac{DG}{\mu}\right)^{-0.2}$$

When the wall or fin temperature of the radiator is much larger than the mean air temperature, the heat transfer coefficient on the air side is generally lower than the value predicted by the isothermal heat transfer correlations just presented. The isothermal heat transfer correlations can sometimes be corrected to apply to non-isothermal conditions by evaluating the properties of the air stream at a particular temperature. Deissler, reference 4, made an analysis for non-isothermal laminar heat transfer for a Prandtl Number of 1 for flow through circular tubes. He found that evaluation of the thermal conductivity at the following particular temperature in the isothermal heat transfer correlations brought the predicted value into agreement with his non-isothermal analytical result.

$$t_{-0.27} = -0.27(t_o - t_b) + t_b$$

where t_o - absolute wall temperature (^oR)
t_b - absolute bulk mean temperature (^oR)

Deissler, reference 5, has also made a similar analysis for the turbulent flow region. When the gas is being heated he recommended evaluating the physical properties at the following temperature

$$t_{0.4} = 0.4(t_o - t_b) + t_b$$

When the gas is being cooled the following temperature was employed for evaluating the physical properties in the isothermal heat transfer correlations.

$$t_{0.6} = 0.6(t_o - t_b) + t_b$$

These latter two particular temperatures were shown to correlate the non-isothermal turbulent flow heat transfer experiments with air at NACA in Cleveland, reference 8.

The experimental results obtained at ORNL on the 15 fins/in. continuous plate-fin radiator were compared to the heat transfer coefficient predicted by Norris and Streid's analysis using the non-isothermal correction proposed by Deissler above. The experimental heat transfer coefficients fell in general below the theoretical predictions as shown in Figure 4.

An analytical study was made on plate-fin type radiators in order to determine the design which would transfer the maximum amount of heat to the air stream for a given radiator weight. Plate-fin type radiators were chosen for the analysis not only because they could be fabricated easily but also because they were expected to give the maximum pressure drop efficiency for extended surfaces. The efficacy of this selection has been shown in a recent study by Kays, reference 10, in which a rectangular channel was found to give a higher heat transfer-friction power characteristic in the laminar region than a circular tube, and gave approximately the same characteristic in the turbulent flow region. A set of calculations was made covering a range of fin thicknesses, fin pitch, and tube spacing for a fixed mass flow per unit of frontal area and for fixed thermal boundary conditions. The isothermal correlations for the heat transfer coefficient presented by Norris and Streid, and by Colburn, were used in the calculations. If the pressure drop is held to 5°/o of the inlet absolute pressure and a stainless steel radiator is employed, the optimum feasible design appeared to be one consisting of 1/8 in. tubes, 0.010 in. thick fins, 30 fins/in. and 3/8 in. tube spacing. The complete analysis is presented in reference 6. A comparison of relative weight per unit of heat transferred for a fixed mass flow per unit of frontal area and fixed thermal boundary conditions is plotted versus fin pitch in Figure 5 for stainless steel fins having a thickness of 0.010 in. with a tube spacing of three times the tube diameter for 1/8, 1/4, and 1/2 in. O.D. tubes.

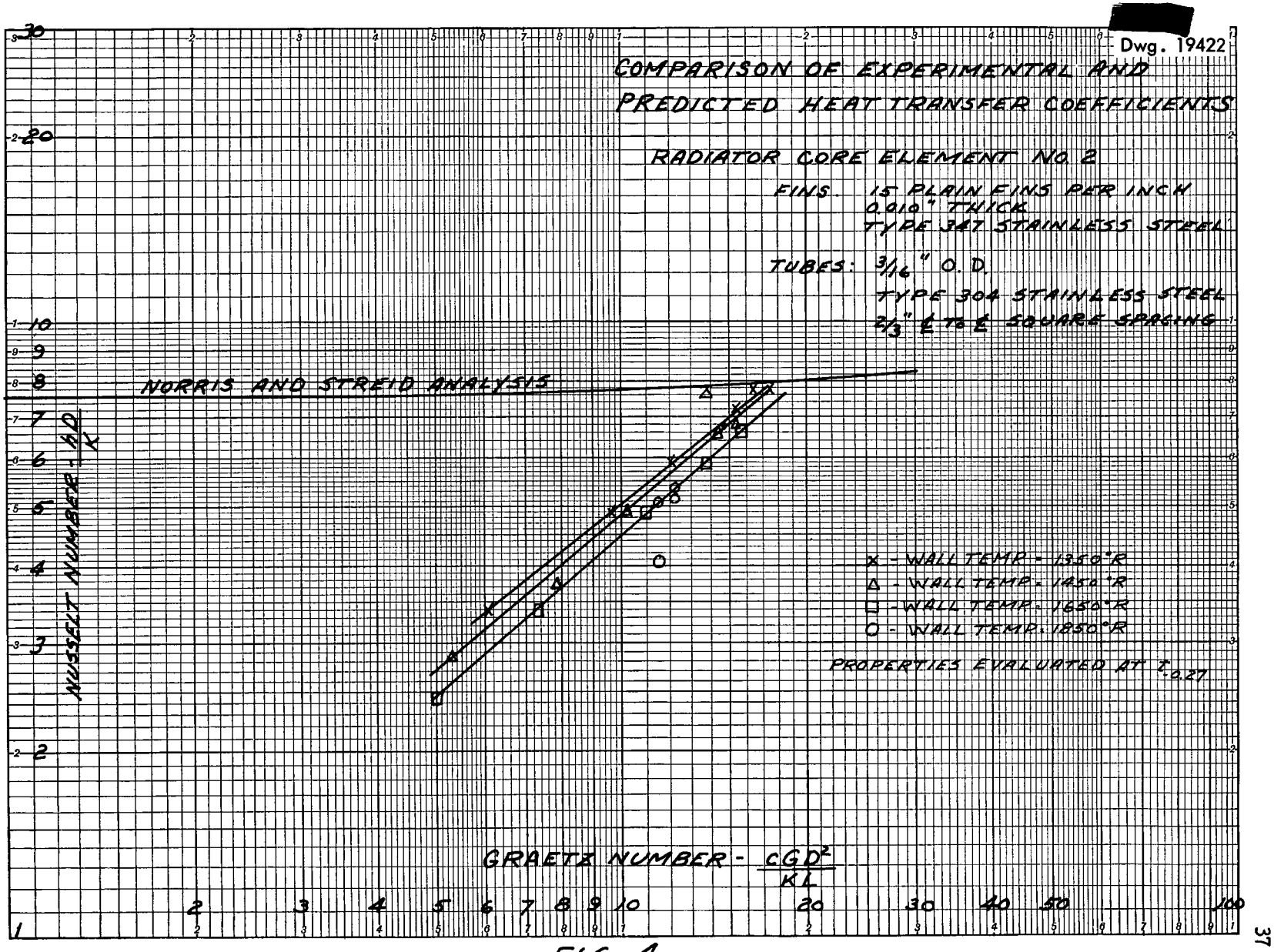
Dwg. 19422
COMPARISON OF EXPERIMENTAL AND
PREDICTED HEAT TRANSFER COEFFICIENTS
RADIATOR CORE ELEMENT NO. 2
FINS: 15 PLAIN FINS PER INCH
0.010" THICK
TYPE 347 STAINLESS STEEL
TUBES: 3/16" O.D.
TYPE 304 STAINLESS STEEL
2/3" ℄ TO ℄ SQUARE SPACING
NORRIS AND STREID ANALYSIS
X - WALL TEMP - 1350°R
Δ - WALL TEMP - 1450°R
□ - WALL TEMP - 1650°R
O - WALL TEMP. 1850°R
PROPERTIES EVALUATED AT $T_{0.27}$
NUSSELT NUMBER - $\frac{hD}{K}$
GRAETZ NUMBER - $\frac{CGD^2}{KL}$

FIG-4

[redacted]
Dwg. 19423

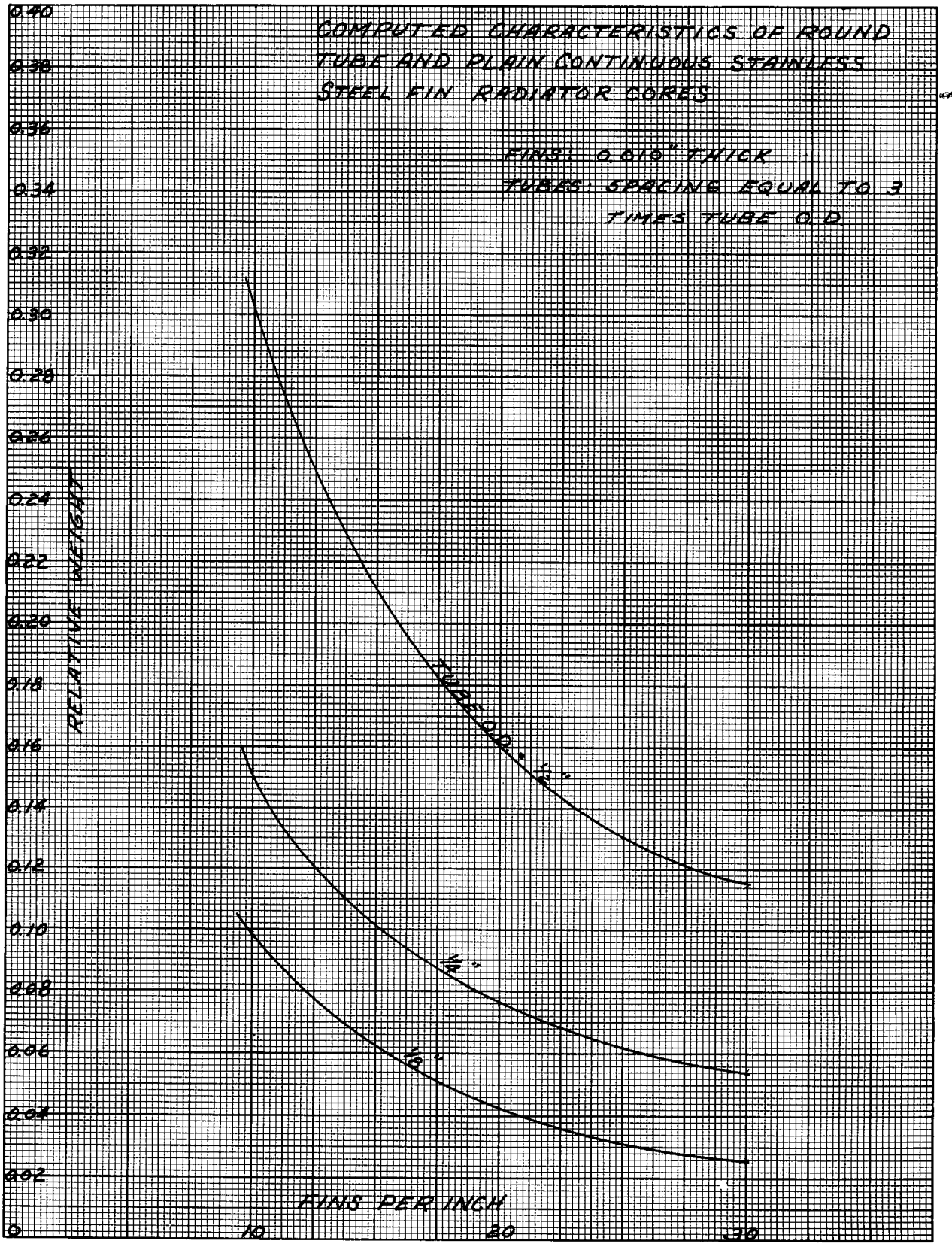

FIG-5

DESCRIPTION OF RADIATOR CORE ELEMENTS TESTED

Radiator Core Element No. 1

The first radiator core element tested was a continuous fin and tube heat exchanger similar to that shown in Figure 6, except that it had 10.5 fins/in. The tubes were arranged to give three parallel two-pass groups, 15 tubes per group, placed in series in such a way that the over-all performance was roughly equivalent to a conventional four-pass heat exchanger. Table III lists the important dimensions of the radiators and the materials of construction.

The header and manifold arrangement chosen for the cores built to date can also be seen in Figure 6. There is a plug in the center of the manifold tube that passes along the bottom of the radiator in the lower foreground. Hot sodium enters the manifold tube at the lower right corner of the radiator and passes to the left into the three 2 in. diameter header drums at the air outlet end of the radiator. The hot sodium then flows upward through the tubes in the fin matrix, forward and to the left in the tube cross-over region, downward and into the three header drums at the air inlet end, and out through the manifold to the heating circuit. The air enters the left end of the radiator through the face of the finned region and flows through the passages between the fins from the lower left end to the upper right end.

Radiator Core Element No. 2

The second radiator core element tested was a round tube and continuous plate fin heat exchanger. Figure F-15 shows this core element after termination of the endurance test. Note the damage done to the fins at the lower left hand corner of the radiator where the sodium leak occurred. This radiator differed from the first one tested in that it had 15 fins/in. and used a different tube cross-over arrangement.

Radiator Core Element No. 3

The third radiator core element tested had 15 fins/in. with the fins interrupted at two-inch intervals in the direction of air flow, each fin section containing 15 tubes. The tube cross-over arrangement was the same as that used for the first radiator tested.

Radiator Core Element No. 4

Calculations indicated that a core element 2-2/3 in. long in the direction of air flow using 30 fins/in. might give approximately the same performance as the previous radiators tested. The radiator was made 4 in. long to permit the

use of headers similar to those employed on the previous radiators (see Fig. 7). Because of the close spacing of the fins, 20 mil nichrome wire was placed between adjacent fins parallel to the direction of air flow to prevent the fins from warping during the nicrobrazing operation.

Although heat transfer coefficients as high as 70 - 80 Btu/hr-ft^2-$^\circ$F had been computed for the very close fin spacing the experimental data gave values of 3 to 7 Btu/hr-ft^2-$^\circ$F. The poor performance apparently was caused by poor bonding in the nicrobrazed tube-to-fin joints because, when the sodium inlet temperature was raised to 1550°F, the entire fin matrix did not glow red as it had in the other radiators when tested at this temperature.

The poor brazing was most likely caused by the insertion of the wire spacers between the fins after the radiator had been prepared for nicro-brazing since it was observed that some of the brazing compound was scraped off by the wires. It is evidently advisable to put the wire spacers between the fins while assemblying any other radiators of this type in the future.

The test of this radiator was halted after 200 hr. of operation because its poor performance hardly justified further testing. Fabrication and testing of another of these radiators is planned when priorities permit.

Table II shows a list of the radiator core elements that have been tested and those proposed for testing. Figures 8 and 9 are typical assembly drawings that show two types of disc fin radiators proposed for testing.

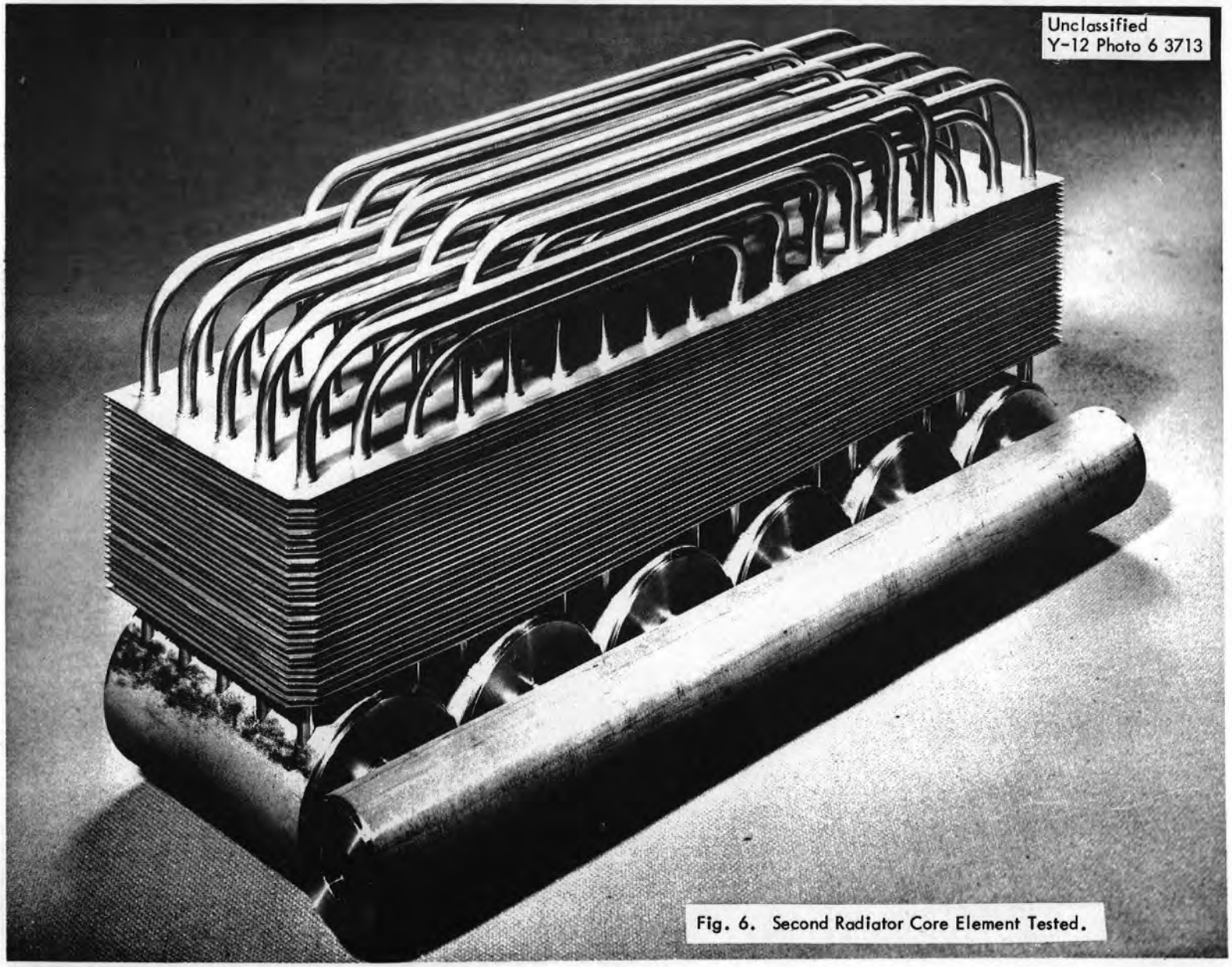

Fig. 6. Second Radiator Core Element Tested.

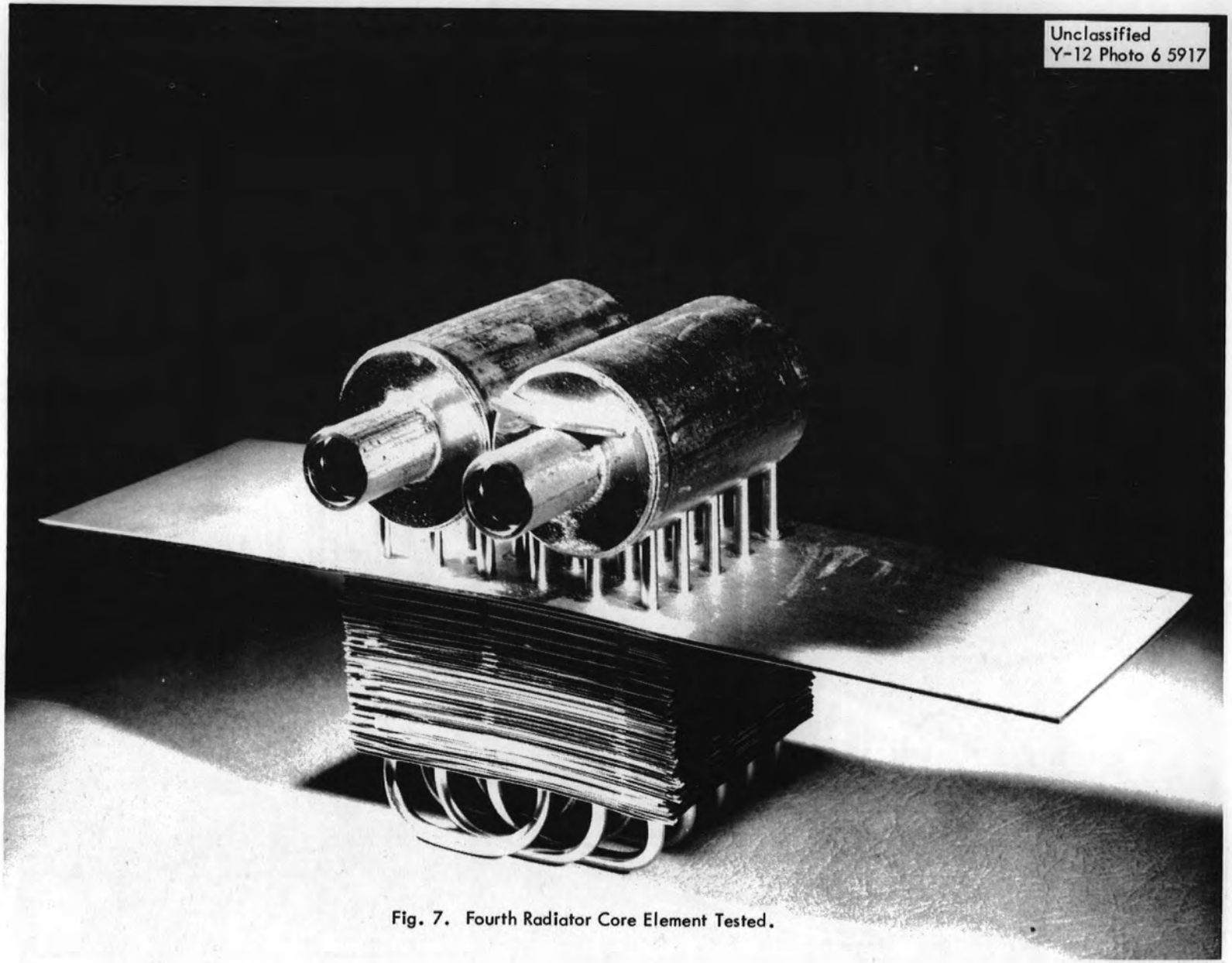

Fig. 7. Fourth Radiator Core Element Tested.

TABLE II

TYPES OF TUBE AND FIN RADIATOR CORE ELEMENTS
PROPOSED FOR DEVELOPMENT TESTING

Tube Diameter = 3/16" O.D.
Tube Material - Type 316 Stainless Steel (if available)
Tube Spacing Transverse to Air Flow - 2/3"
Tube Spacing in Direction of Air Flow - 2/3"
Air Passage Length - 12"
Air Inlet Face - 2" x 3-1/3"

Type	Fin Description	No. Fins per Inch	Fin Material	Tube Arrangement	Status as of October 14, 1952
A	Plain plate	10.5	S.S.	In-line	Test completed May, 1952
B	Plain plate	15	S.S.	In-line	Test completed June, 1952
C	Plate interrupted every 2"	15	S.S.	In-line	Test completed November, 1952
D	Plate interrupted every 2/3"	15	S.S.	In-line	Ready for test (March, 1953)
E	Plate interrupted every 2", with electroformed turbulators	15	Ni	In-line	Fins being fabricated for ORNL
F	Disc fins, stamped, ceramic coated	15	Ni	In-line	Fabrication technique being developed at ORNL
G	Disc fins, stamped	15	S.S.	In-line	Suggested Wright Field project
H	Disc fins, stamped	15	Ni	In-line	Suggested Wright Field project
I	Disc fins, stamped	15	Ni	Staggered	Suggested Wright Field project
J	Disc fins, coined	15	Ni	Staggered	Suggested Wright Field project
K	Disc fins, stamped, chrome plated (Possibly .0003")	15	Ni	In-line	
*L	Plain plate *Air passage length	30 4"	Ni	In-line	First test terminated December, 1952

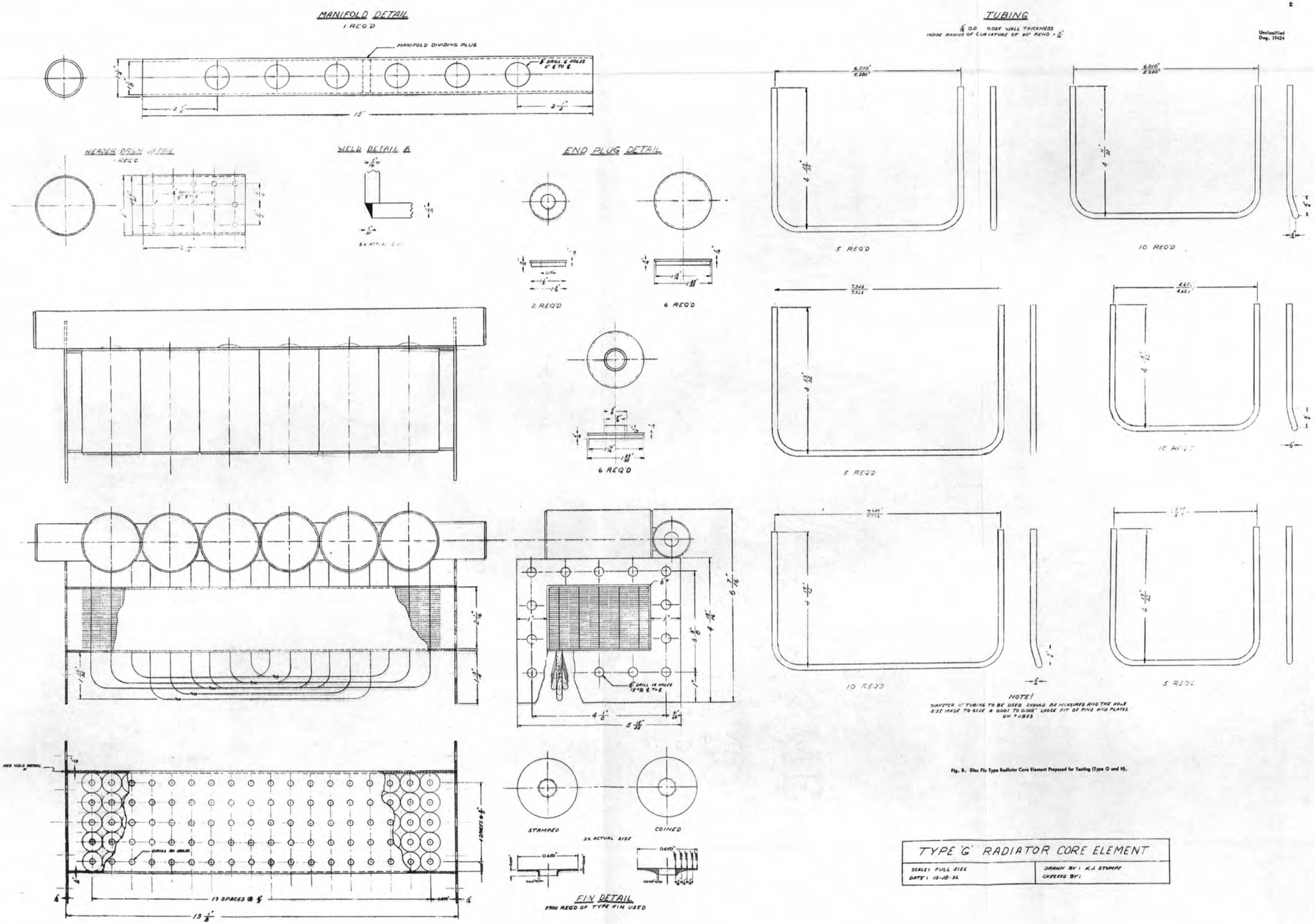

Fig. 8. Disc Fin Type Radiator Core Element Proposed for Testing (Type G and H).

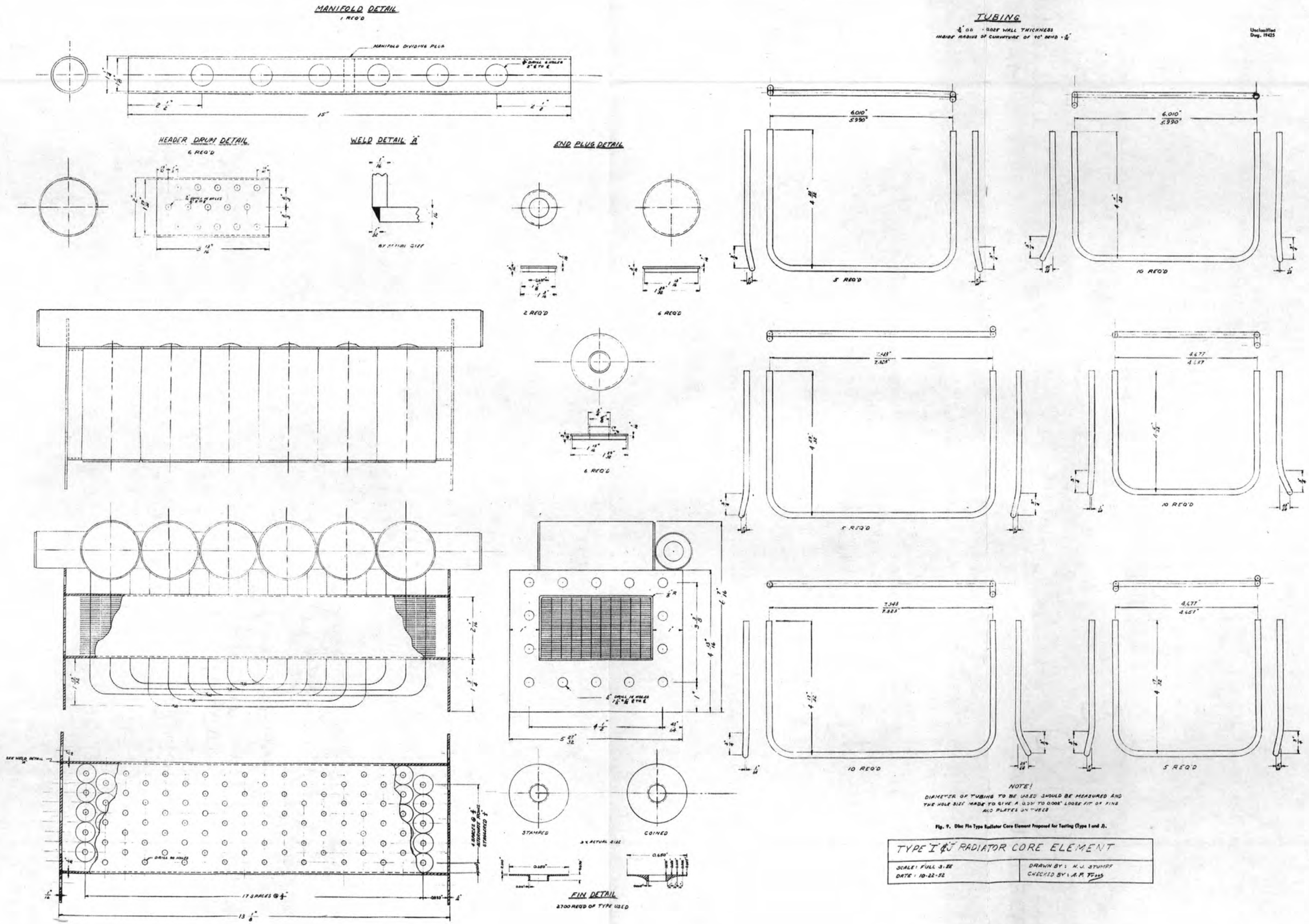

Fig. 9. Disc Fin Type Radiator Core Element Proposed for Testing (Type I and J).

DESCRIPTION OF TEST LOOP*

A picture of the test loop is shown in Figure 10. The heat source was a direct electrical resistance system capable of delivering 60 Kw at a sodium outlet temperature of 1600°F. The source was made up of two 50 ft. parallel paths of 1/4 in. Type 316 stainless steel pipe coupled to a high current Thomson welding transformer. A picture of the heating coils is shown in Figure 11. The sodium was pumped through the loop with a modified General Electric G-3 electromagnetic pump. The pump was operated at temperatures as high as 1300°F delivering 3.5 gallons per minute at a head of 10 lb./in^2. Air was supplied to the radiator by a model 7E Buffalo Blower capable of producing a static head of 12.5 in. of water over the range of air flows used in the test. Recently a Roots-Connersville gas pump driven by a varidrive unit was installed which is capable of delivering the required volume at a static head of 50 in. H_2O with the added advantage of greater air flow range and better regulation.

Primary electromagnetic flow meter elements were located on the main stream and the by-pass circuits. Trapped gas pressure measuring volumes were connected to ordinary bourdon tube pressure gages with approximately 4 ft. of 1/8 in. copper tubing. These units have operated effectively with NaK, but with sodium they will generally cause trouble after a few hundred hours because of sodium vapor condensation plugs, unless the temperature of the free liquid surface in the well can be kept below 275°F.

A by-pass filter circuit has been designed into the system to utilize the header tank as a cold trap to trap out the oxides. The flow through this circuit was originally restricted by a 1/8 in. orifice in one of the flanged joints to prevent the cold trap from running above 300°F. Clogging of this orifice and/or the filter caused the flow rate through the by-pass system to drop to practically zero after approximately 100 hr. of operation. After this happened, oxide plugging of the colder radiator tubes would begin to cause losses in the heat transfer performance. This plugging could be relieved by shutting off the air flow and running the radiator isothermally at 1200°F for about an hour. After normal operation was resumed, the plugging would start again and after a few hours a drop in heat transfer performance would again be observed. A valve was finally installed in place of the orifice so that the by-pass flow rate and hence the temperature of the by-pass circuit could be controlled. At the present time this by-pass circuit is operated at temperatures between 600 and 800°F below the main stream with approximately 1/8 of the total system flow continuously paralleled through the header tank and filter. A heater is used to keep the filter temperature about 50°F above the header tank (cold trap) temperature. Operation in this manner has proved very successful.

Experience up to the present time indicates that even though the oxide concentration in the system caused plugging of some of the heat exchanger tubes before the by-pass filter system was set up properly, it did not cause any noticeable corrosion.

---

*Reference 18, p.5.

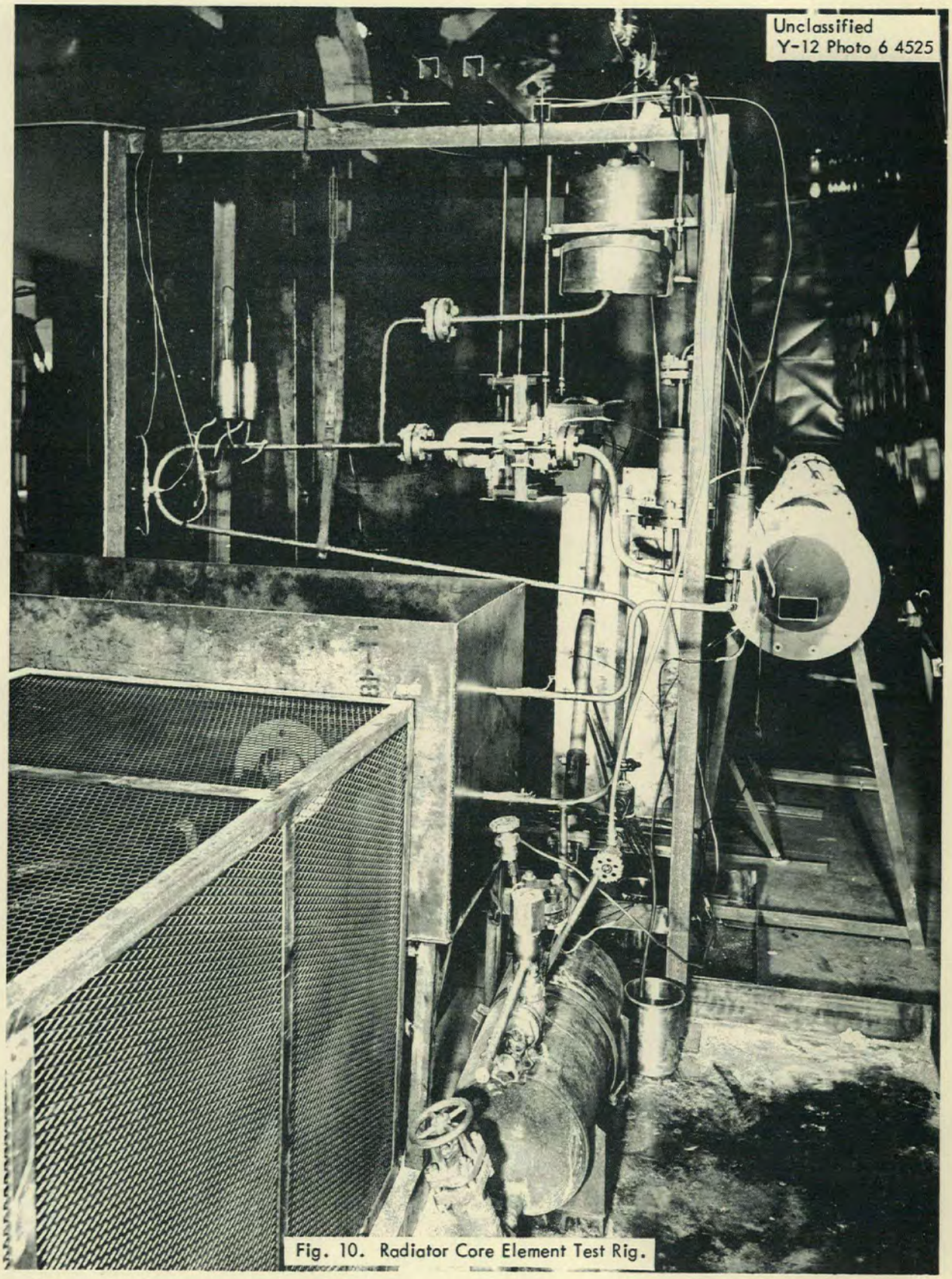

Fig. 10. Radiator Core Element Test Rig.

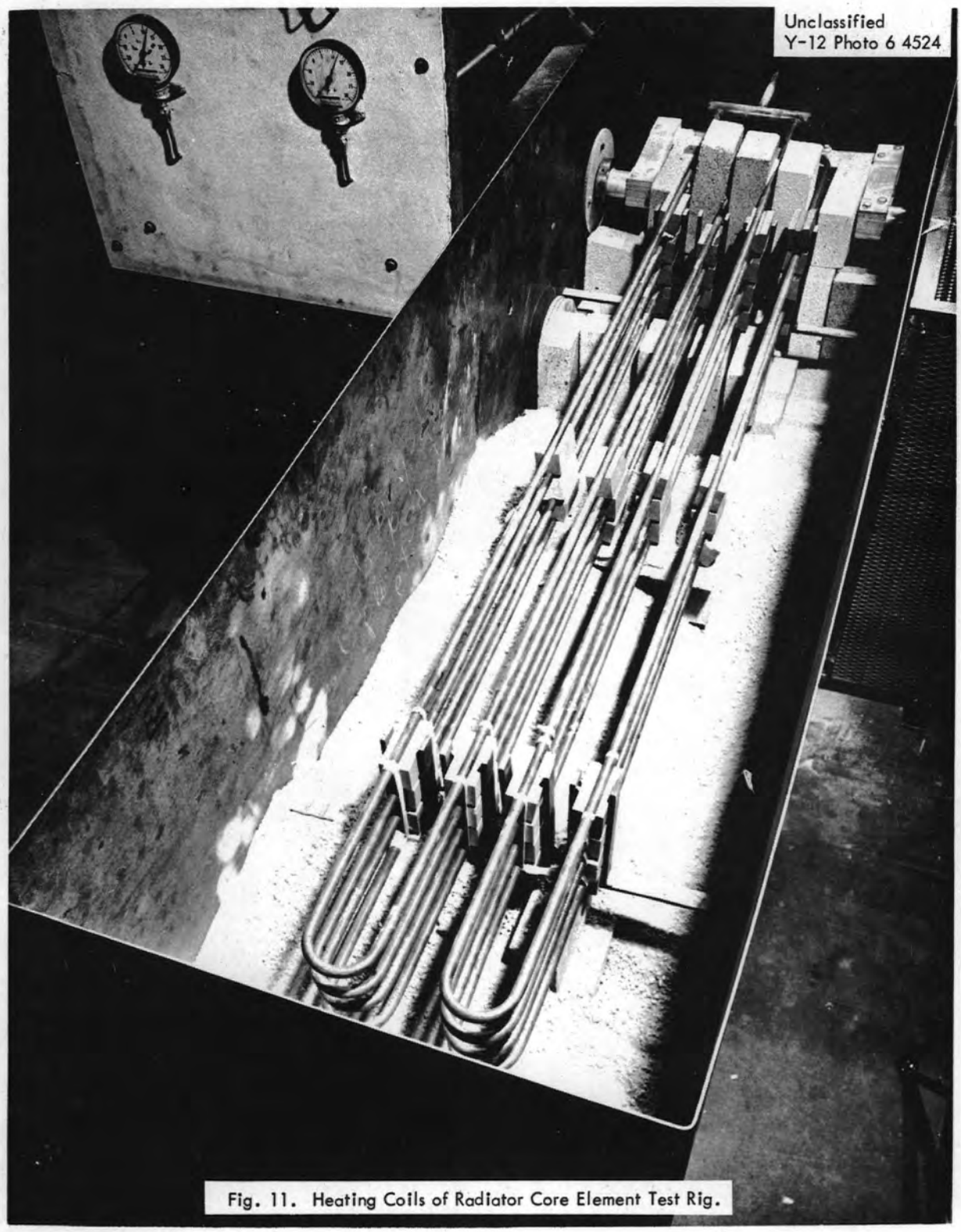

Fig. 11. Heating Coils of Radiator Core Element Test Rig.

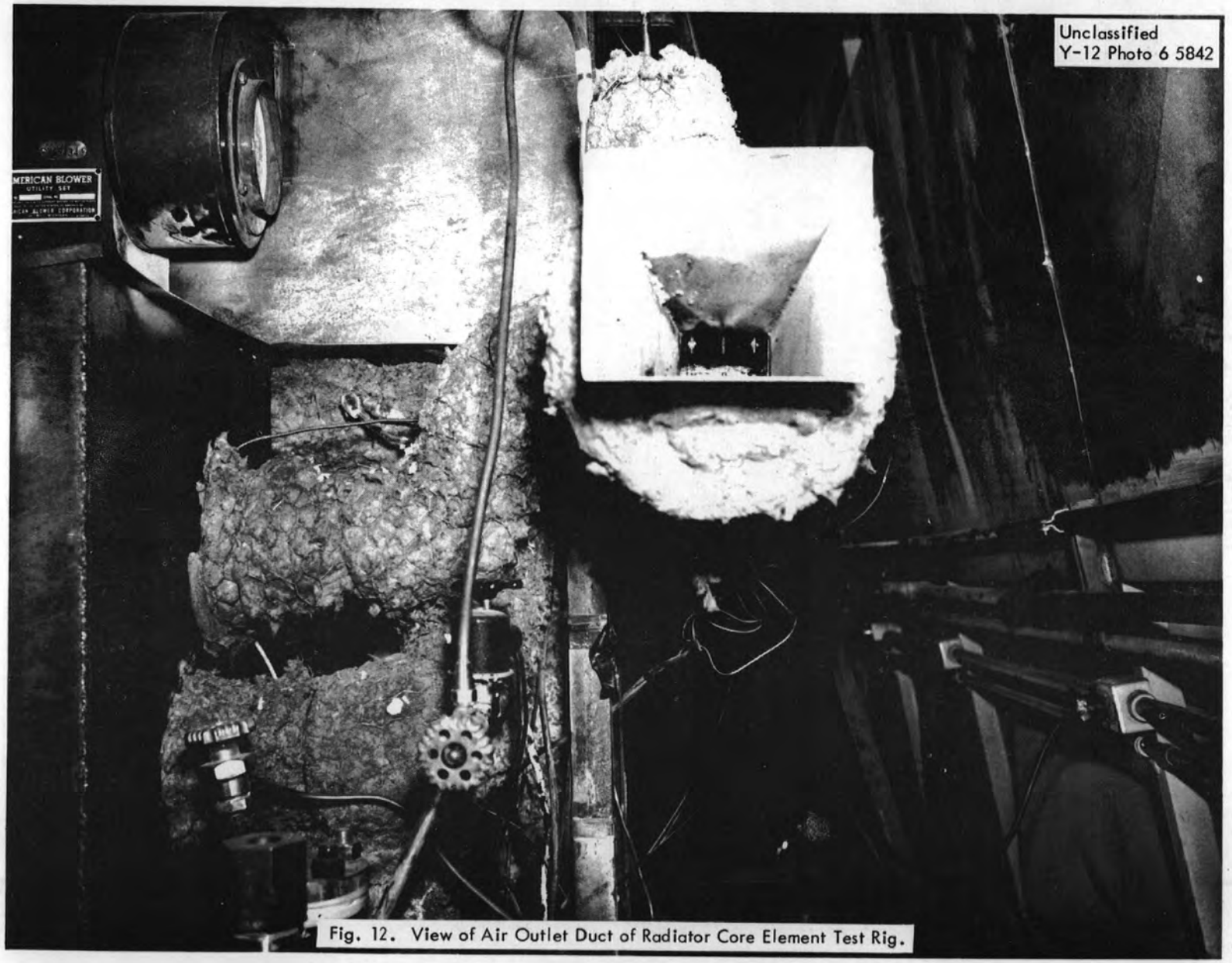

Fig. 12. View of Air Outlet Duct of Radiator Core Element Test Rig.

RADIATOR TEST DATA

The following series of graphs summarizes the radiator core element test data obtained during the past year. During this period four core elements were fabricated and tested. Detailed data on their construction is given in Table III.

The test data for the last core element tested (30 fins/in) is not included among these charts. The heat transfer performance of this radiator was far below the predicted value and did not compare favorably with the data obtained from the first three core elements tested, and hence would be of little interest. As explained in an earlier section, it was felt that poorly brazed tube-to-fin joints accounted for the poor performance of this radiator.

It is interesting to note from Figures 13A, 13B, and 13C that for the uninterrupted fin radiator core element the heat transfer coefficient decreased with increasing sodium inlet temperature while for the interrupted fin type the heat transfer coefficient increased with increasing sodium inlet temperature. As previously mentioned, it is felt that this effect is dependent on which of the two factors predominates at elevated temperatures - increased thermal conductivity of the air or increased viscosity causing a thickening of the boundary layer.

It is also of interest to note that the air pressure drop through the interrupted fin core was less than that through the plain fin core. No satisfactory explanation has been given for this but it is felt that experimental inaccuracies may have been responsible.

The method of computing the radiator performance parameters from the experimental data is shown in Appendix A together with tables of these data for radiators No. 1, No. 2, and No. 3.

[redacted]

Dwg. 19426

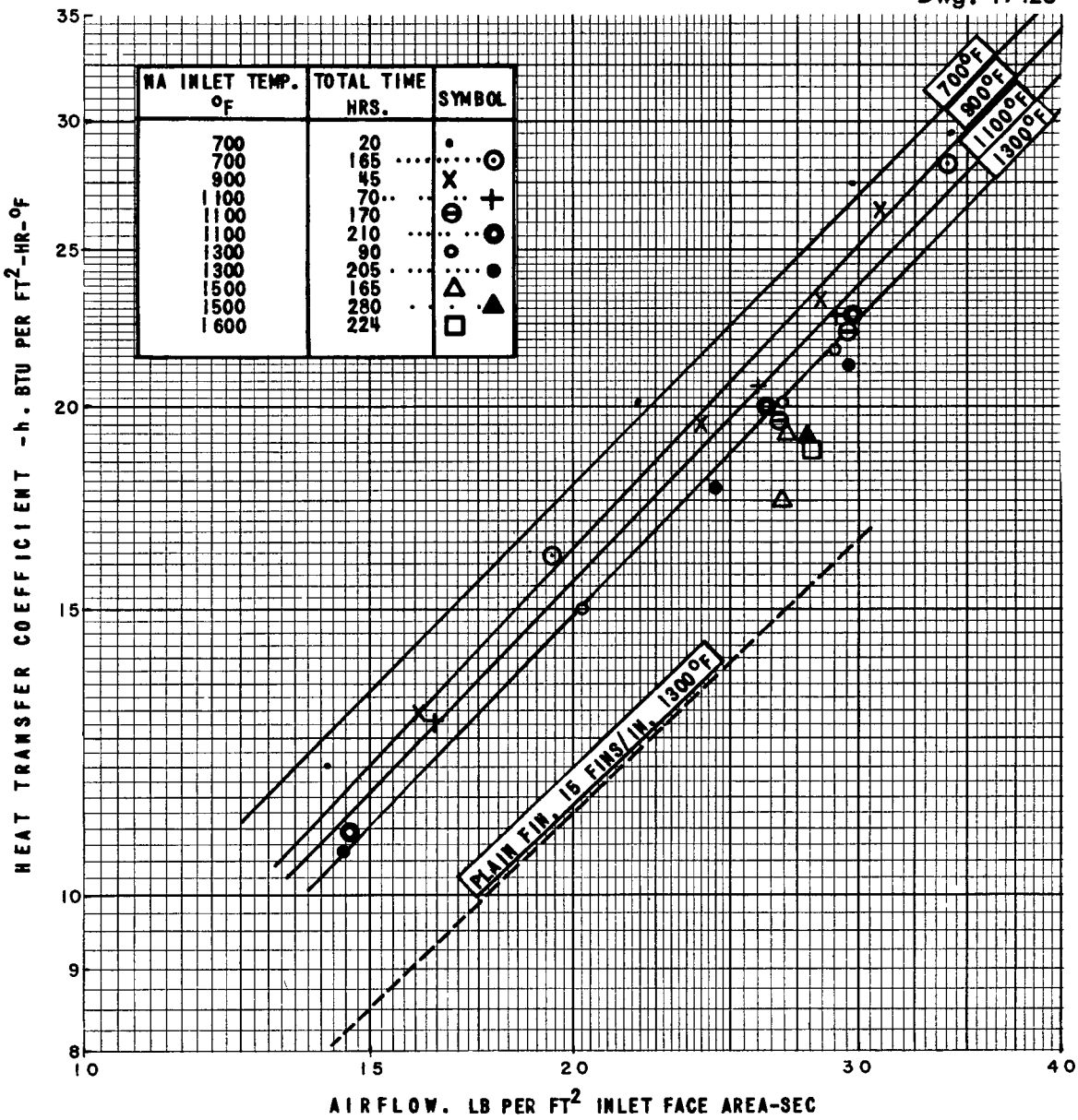

(a) RADIATOR CORE ELEMENT NO. 1 (PLAIN FIN, 10.5 FINS/IN)
FINS: TYPE 347 STAINLESS STEEL, 0.010" THICK
TUBES: 3/16" O.D., 2/3" ℄ - ℄, SQUARE SPACING

FIGURE 13. SODIUM TO AIR RADIATOR CORE ELEMENT HEAT TRANSFER PERFORMANCE (h vs. AIR FLOW).

[redacted]

Dwg. 19427

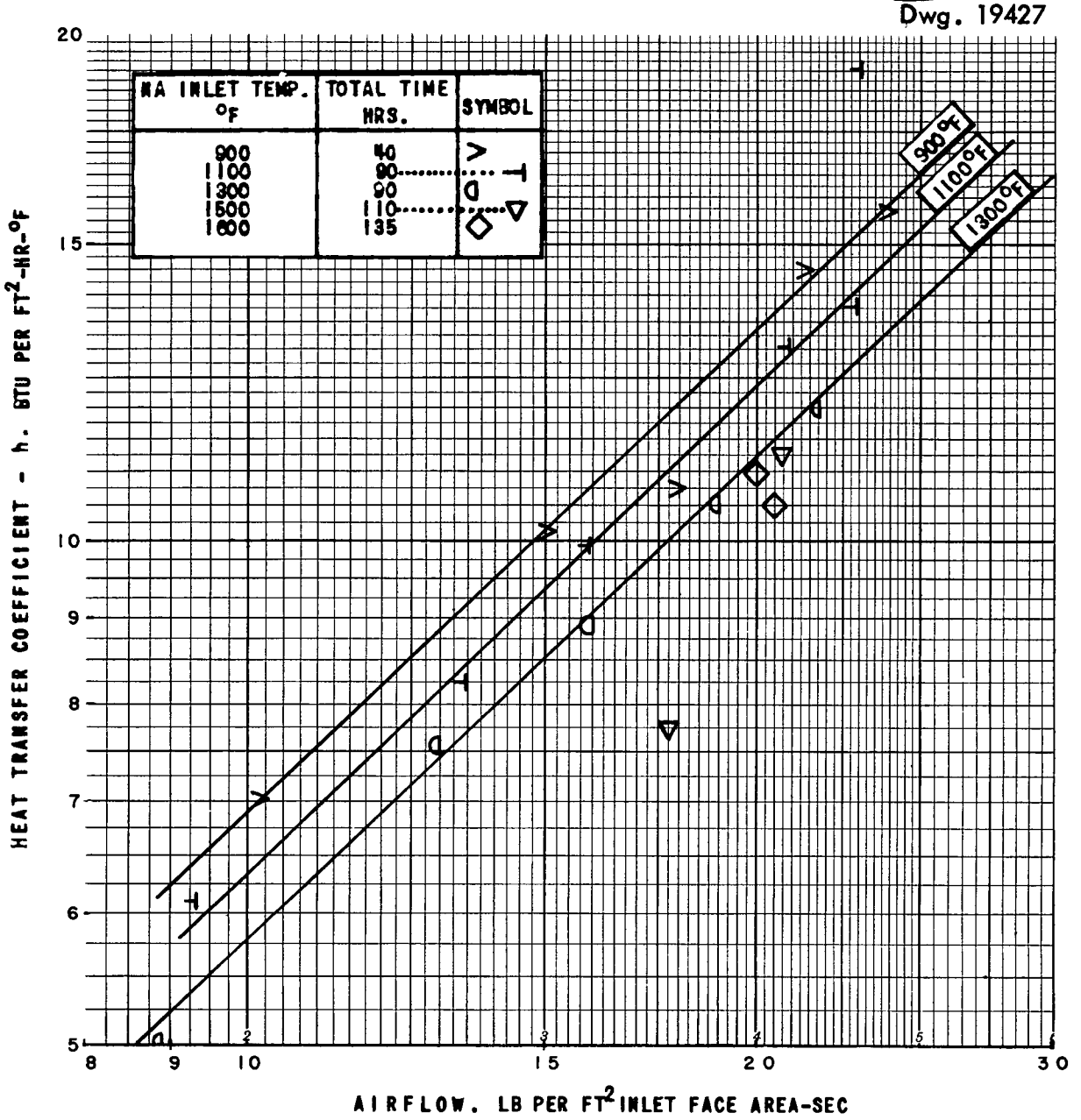

(b) RADIATOR CORE ELEMENT NO. 2 (PLAIN FIN. 15 FINS/IN)

FINS: TYPE 347 STAINLESS STEEL. 0.010" THICK
TUBES: 3/16" O.D., 2/3" ℄ - ℄. SQUARE SPACING

FIGURE 13. CONTINUED. SODIUM TO AIR RADIATOR CORE ELEMENT HEAT TRANSFER PERFORMANCE. (h vs. AIR FLOW).

[redacted]

Dwg. 19428

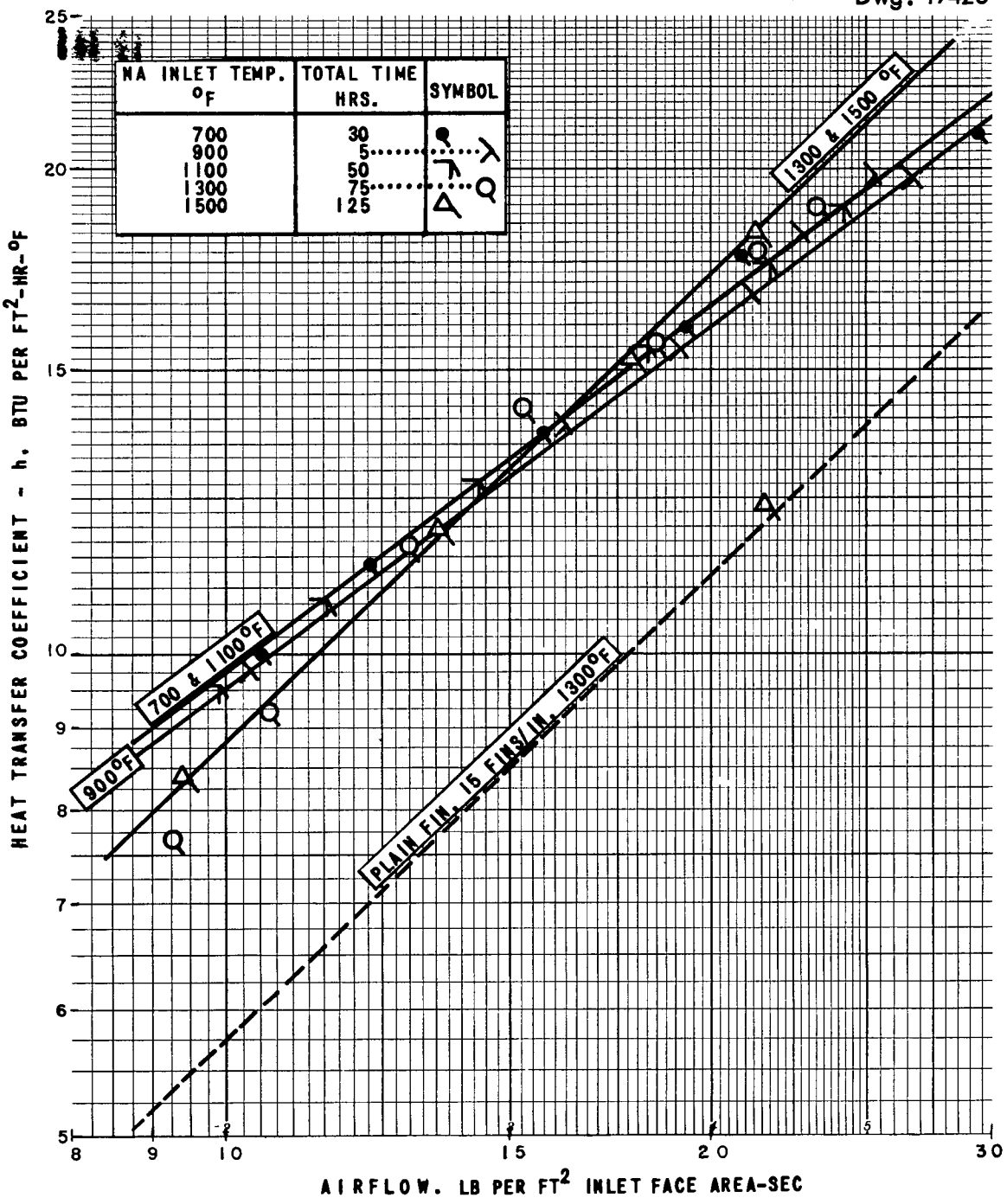

(c) RADIATOR CORE ELEMENT NO. 3 (INTERRUPTED FIN, 15 FINS/IN)
FINS: TYPE 304 STAINLESS STEEL, 0.010" THICK
TUBES: 3/16" O.D., 2/3" ℄ - ℄, SQUARE SPACING

FIGURE 13. CONCLUDED. SODIUM TO AIR RADIATOR CORE ELEMENT HEAT TRANSFER PERFORMANCE. (h vs. AIR FLOW).

[redacted]

Dwg. 19429

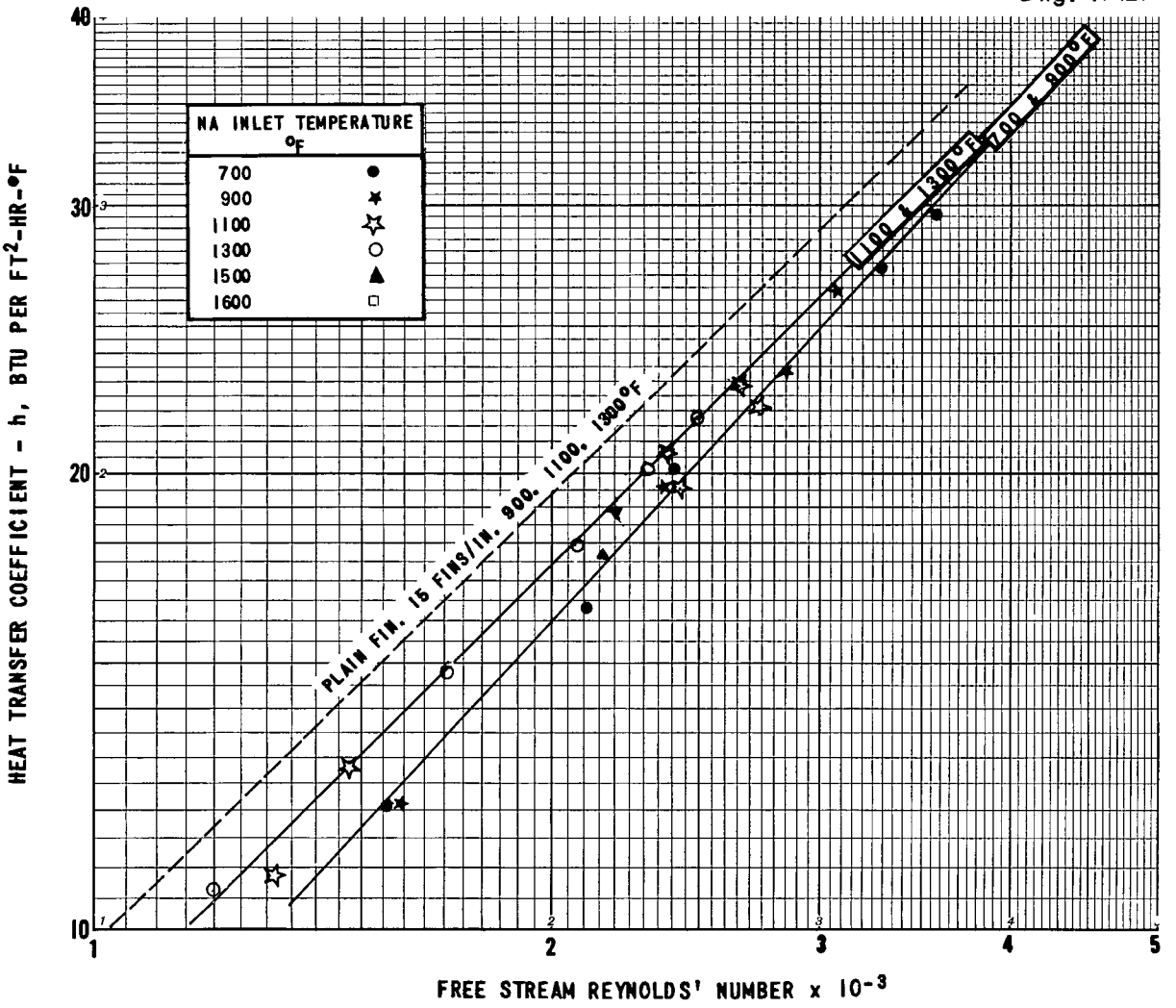

(a) RADIATOR CORE ELEMENT NO. 1 (PLAIN FIN. 10.5 FINS/IN)
FINS: TYPE 347 STAINLESS STEEL, 0.010" THICK
TUBES: 3/16" O.D., 2/3" ℄ - ℄, SQUARE SPACING

FIGURE 14. SODIUM TO AIR RADIATOR CORE ELEMENT HEAT TRANSFER PERFORMANCE, (h vs. R_e).

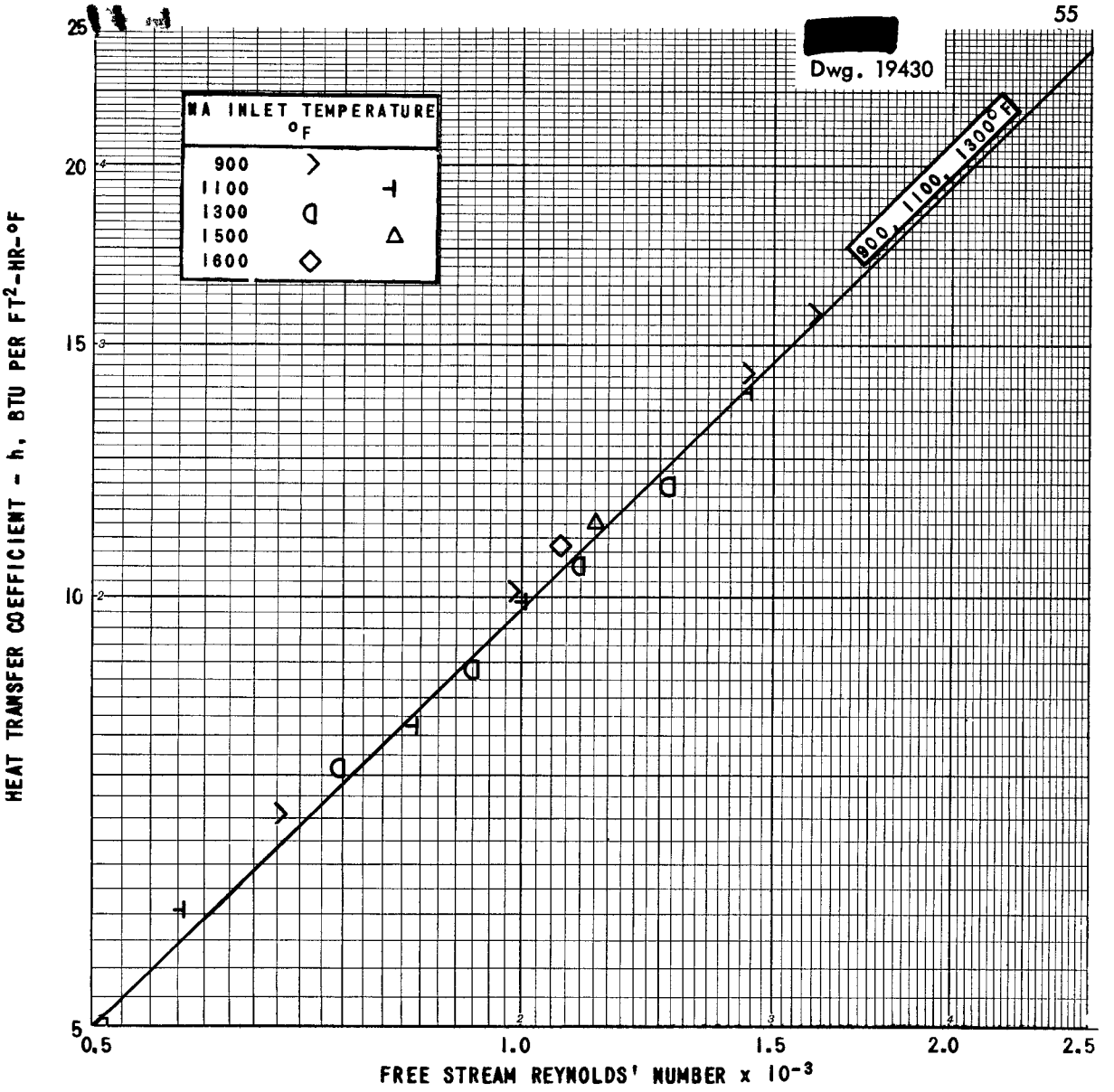

(b) RADIATOR CORE ELEMENT NO. 2(PLAIN FIN, 15 FINS/IN)
FINS: TYPE 347 STAINLESS STEEL, 0.010" THICK
TUBES: 3/16" O.D., 2/3" ℄ - ℄, SQUARE SPACING

FIGURE 14 . CONTINUED. SODIUM TO AIR RADIATOR CORE ELEMENT HEAT TRANSFER PERFORMANCE. (h vs. R_e).

[redacted]

Dwg. 19431

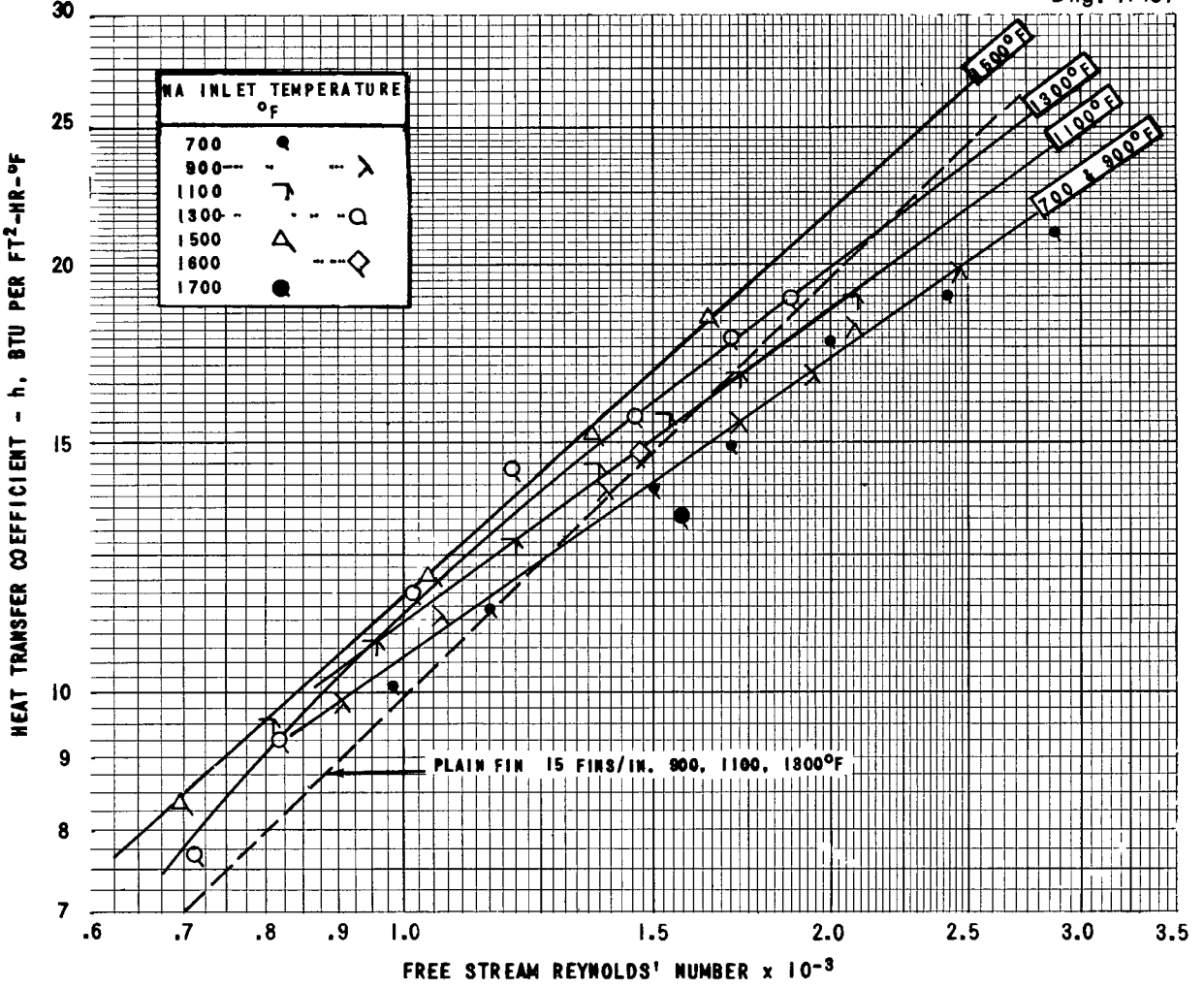

(c) RADIATOR CORE ELEMENT NO. 3 (INTERRUPTED FIN. 15 FINS/IN)
FINS· TYPE 304 STAINLESS STEEL 0.010" THICK
TUBES· 3/16" O D.. 2/3" ℄ - ℄. SQUARE SPACING

FIGURE 14 . CONCLUDED SODIUM TO AIR RADIATOR CORE ELEMENT HEAT TRANSFER PERFORMANCE. (h vs R_e)

[redacted]

Dwg. 19432

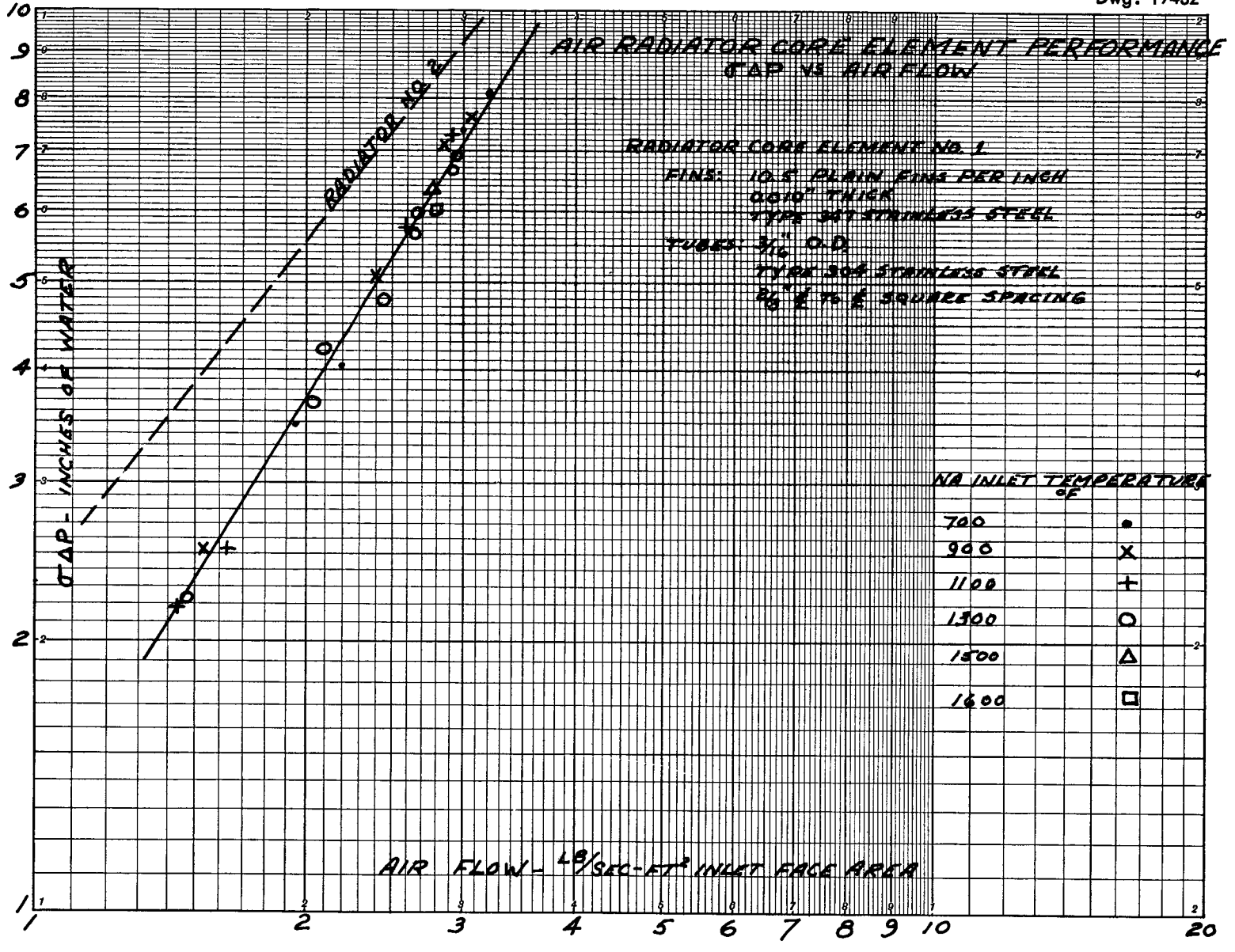

FIG. 15-A

[redacted]

Dwg. 19433

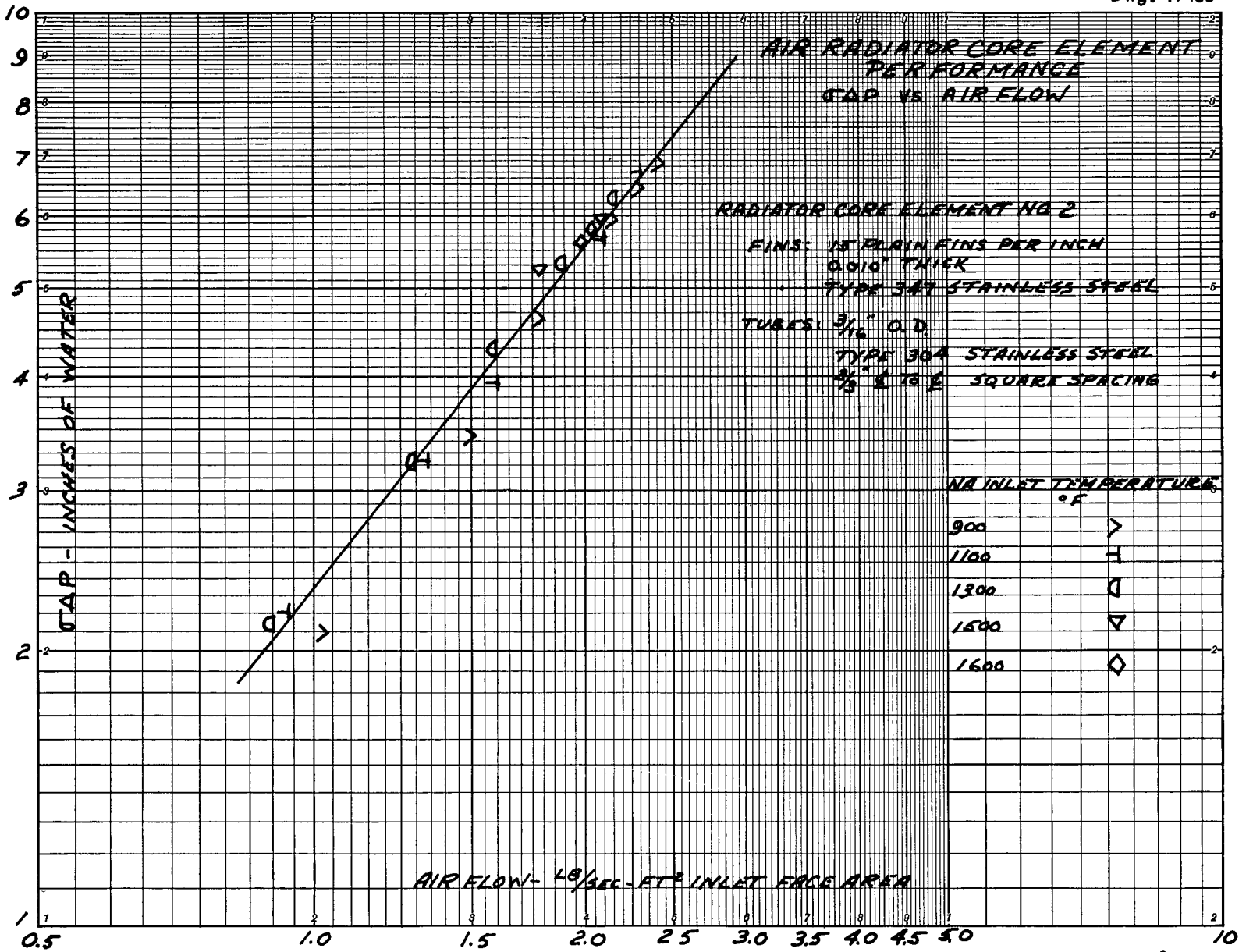

FIG-15-8

[redacted]

Dwg. 19434

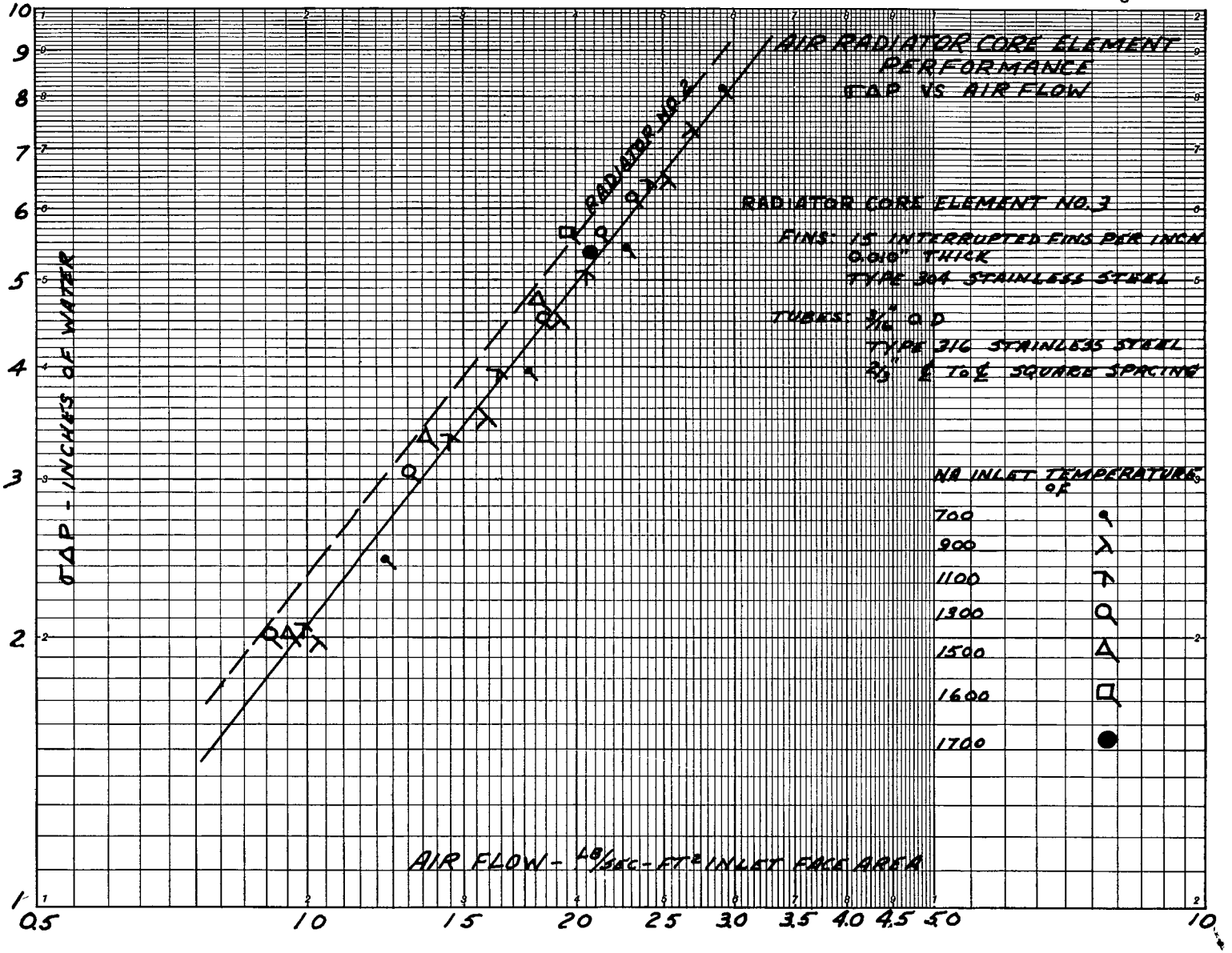

FIG. 15-C

[redacted]

Dwg 19435

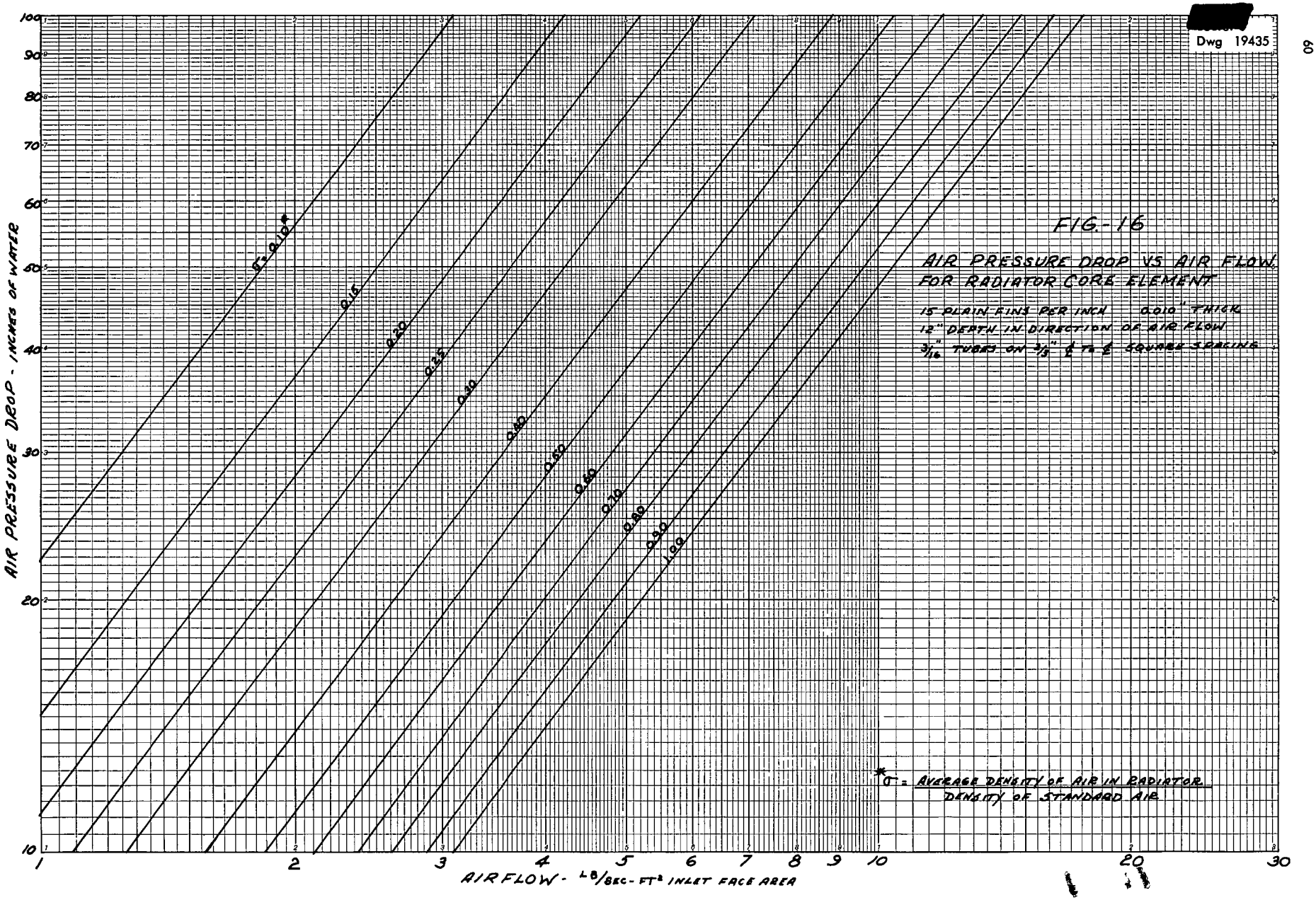

FIG.-16

AIR PRESSURE DROP VS AIR FLOW FOR RADIATOR CORE ELEMENT

15 PLAIN FINS PER INCH 0.010" THICK
12" DEPTH IN DIRECTION OF AIR FLOW
3/16" TUBES ON 3/8" ℄ TO ℄ SQUARE SPACING

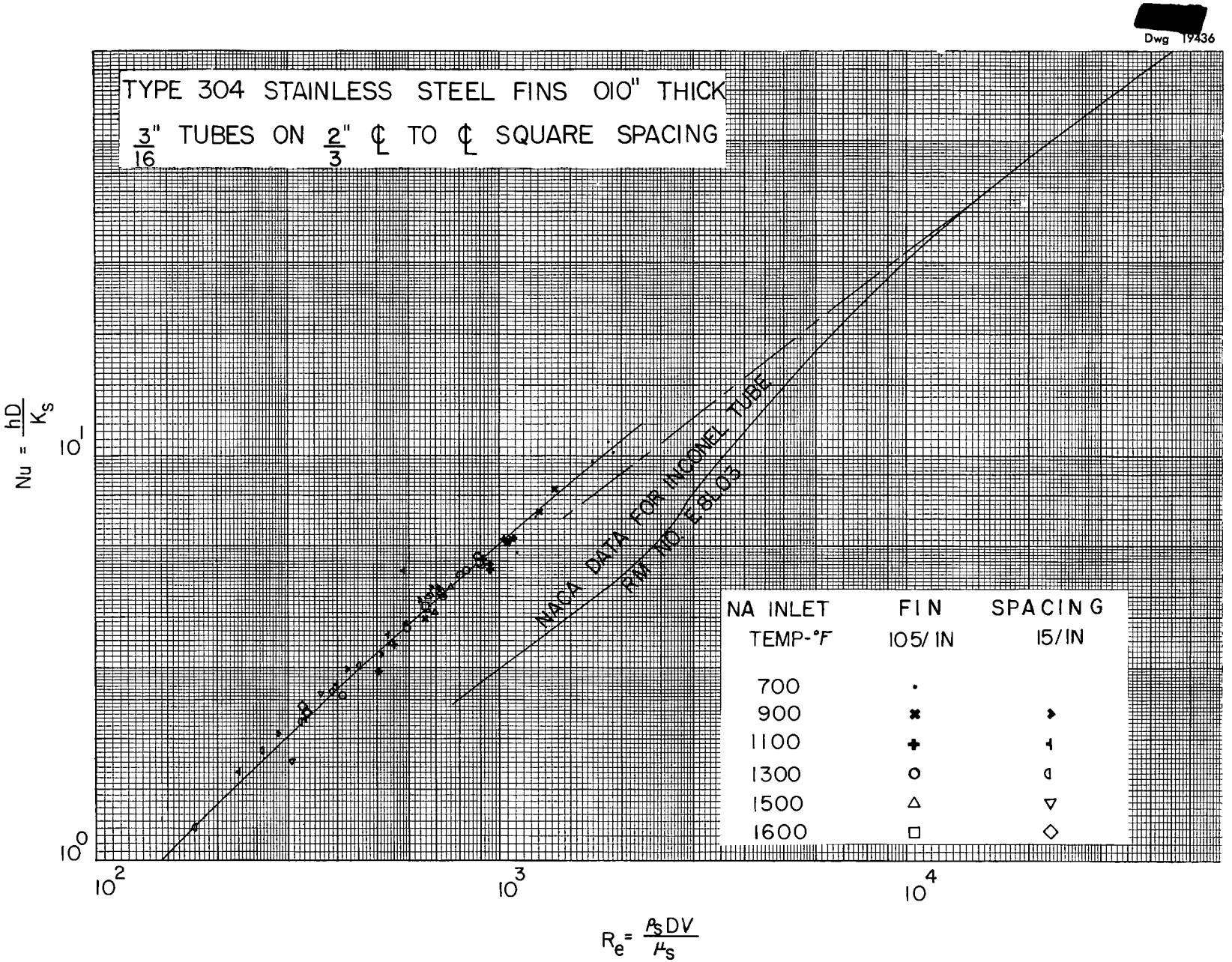

FIGURE 17 SODIUM TO AIR RADIATOR CORE ELEMENT HEAT TRANSFER PERFORMANCE, (Nu vs Re)

TABLE III

DESIGN DETAILS OF AIR RADIATORS

	Radiator No. 1	Radiator No. 2	Radiator No. 3	Radiator No. 4
Fins per inch	10.5	15	15	30
Fin thickness (in.)	0.010	0.010	0.010	0.010
Distance between fins (in.)	0.085	0.057	0.057	0.023
Fin length (direction of air flow)(in.)	12	12	12	4
Fin width (in.)	3.375	3.375	3.375	3.375
Fin material	347 stainless steel	347 stainless steel	304 stainless steel	Nickel
Number of active fins	21	28	29	60
Tube O.D. (in.)	0.1875	0.1875	0.1875	0.1875
Tube wall thickness (in.)	0.015	0.015	0.025	0.025
Tube spacing (in.)	0.667 ℄ - ℄ square array	0.667 ℄ - ℄ square array	0.667 ℄ - ℄ square array	0.667 ℄ - ℄ square array
Number of tubes	90	90	90	30
Tube material	304 stainless steel	304 stainless steel	316 stainless steel	316 stainless steel
Height of radiator fin region (in.)	2	2	1.9	2
Face area ($in.^2$)	6.75	6.75	5.76	6.46
Air passage free flow area ($in.^2$)	4.23	4.08	3.43	2.84
Sodium passage free flow area ($in.^2$)	1.753	1.753	1.336	0.445

Radiator No. 1, No. 2, and No. 4 have uninterrupted fins.

Radiator No. 3 has interrupted fins. A cut was made at five places along the fins perpendicular to the direction of air flow. There are 15 tubes in each section.

Radiator No. 3 has a section of the fins at the top center plugged with brazing material. It was estimated that this decreased the face area and free flow area by 10%.

CHARTS FOR THE ANALYSIS OF TEST DATA

Figure 18 is a chart in which logarithmic mean temperature difference is plotted as a function of the temperature differences at the inlet and at the outlet faces of the heat exchanger. In the radiator tests of this report the greatest temperature difference was that between the sodium and the air at the air inlet face, while the least temperature difference was that between the sodium and the air at the air outlet face.

While it is most convenient to reduce test data to figures of merit for heat exchanger performance on the basis of the conventional relationships between heat transfer coefficient and fluid flow rate, the design of radiators for turbojet or ram-jet engines is most easily carried out through the use of charts giving the parameter heating (or cooling) "effectiveness" as a function of both air flow rate and radiator air passage length. If an attempt is made to design a radiator to meet specified engine performance conditions simply through the use of heat transfer coefficient data, a considerable amount of tedious trial and error calculation is required because there is no explicit relation between the conditions given and the logarithmic mean temperature difference. This tedious trial and error work can be avoided through the use of Figure 19 which relates the logarithmic mean temperature difference and the heating effectiveness. Heating effectiveness is ordinarily defined as the temperature rise (or drop) in one fluid stream divided by the difference in temperatures between the two fluid streams at their respective inlets to the heat exchanger. Heating effectiveness is commonly expressed as either a ratio or as a percentage (for it can never be greater than $100^{\circ}/o$). Appendix B gives an illustration of the use of the graph of Figure 19.

The over-all heat transfer coefficient differs from the local heat transfer coefficient because of the temperature gradient along the fins. Figure 21 shows a set of curves for fin efficiency as a function of the local heat transfer coefficient "h" and the thermal conductivity "K" of the fins. These were computed from Reference 16. Figure 20 was prepared from Figure 21 to show the local heat transfer coefficient as a function of over-all heat transfer coefficient for stainless steel fins to facilitate reduction of test data. Note that it was necessary to prepare curves for each of a series of mean metal temperatures because variations in the thermal conductivity of stainless steel are important.

Figure 22 is a chart giving heating effectiveness as a function of radiator depth in the direction of air flow for various radiator air flow rates for the best geometry tested to date. Graphs of this type are particularly useful in the calculation of turbojet and ram-jet performance where the heat is supplied by NaK-to-air radiators.

Unclassified
Dwg 19437

FIG. - 18

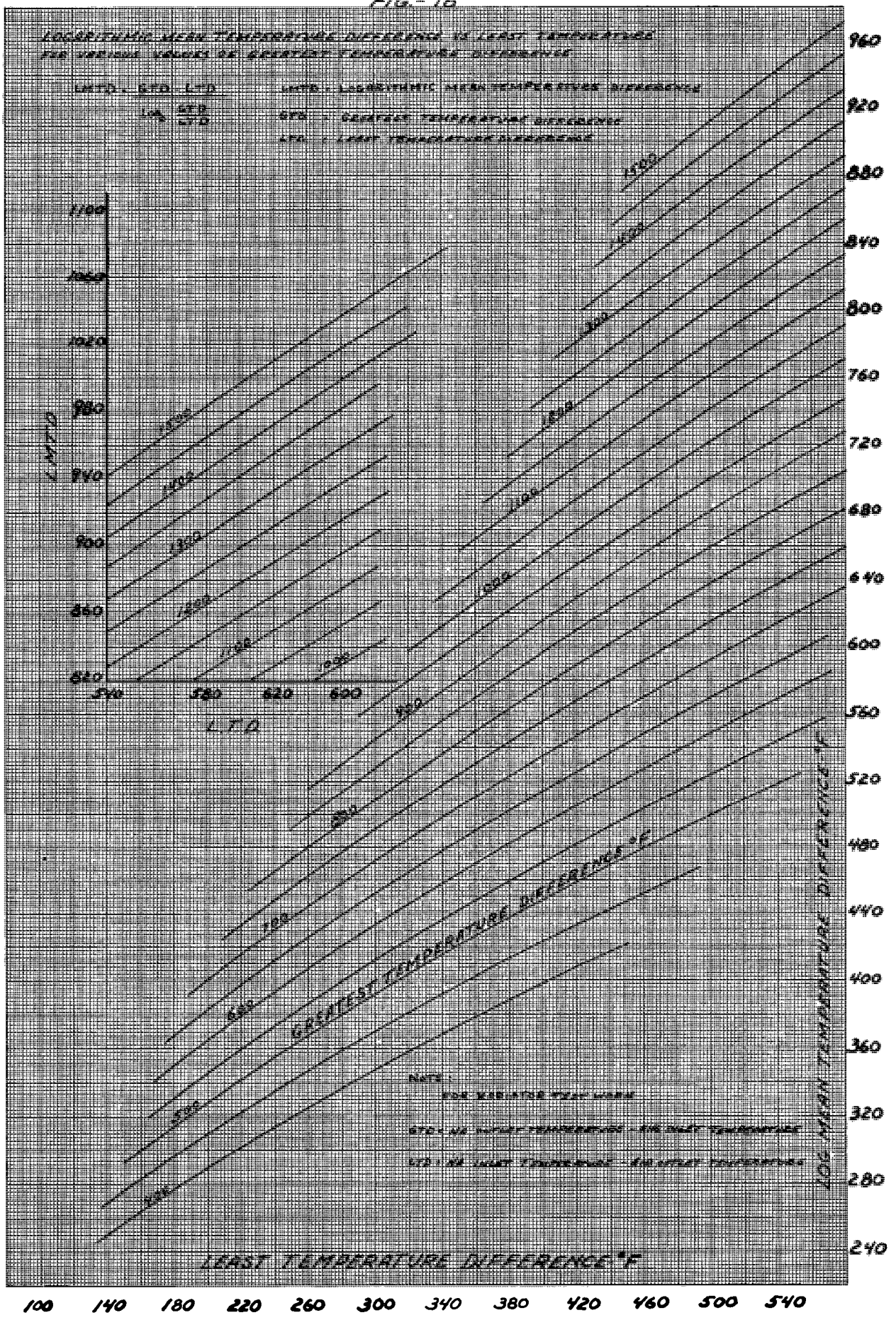

Unclassified
Dwg 19438

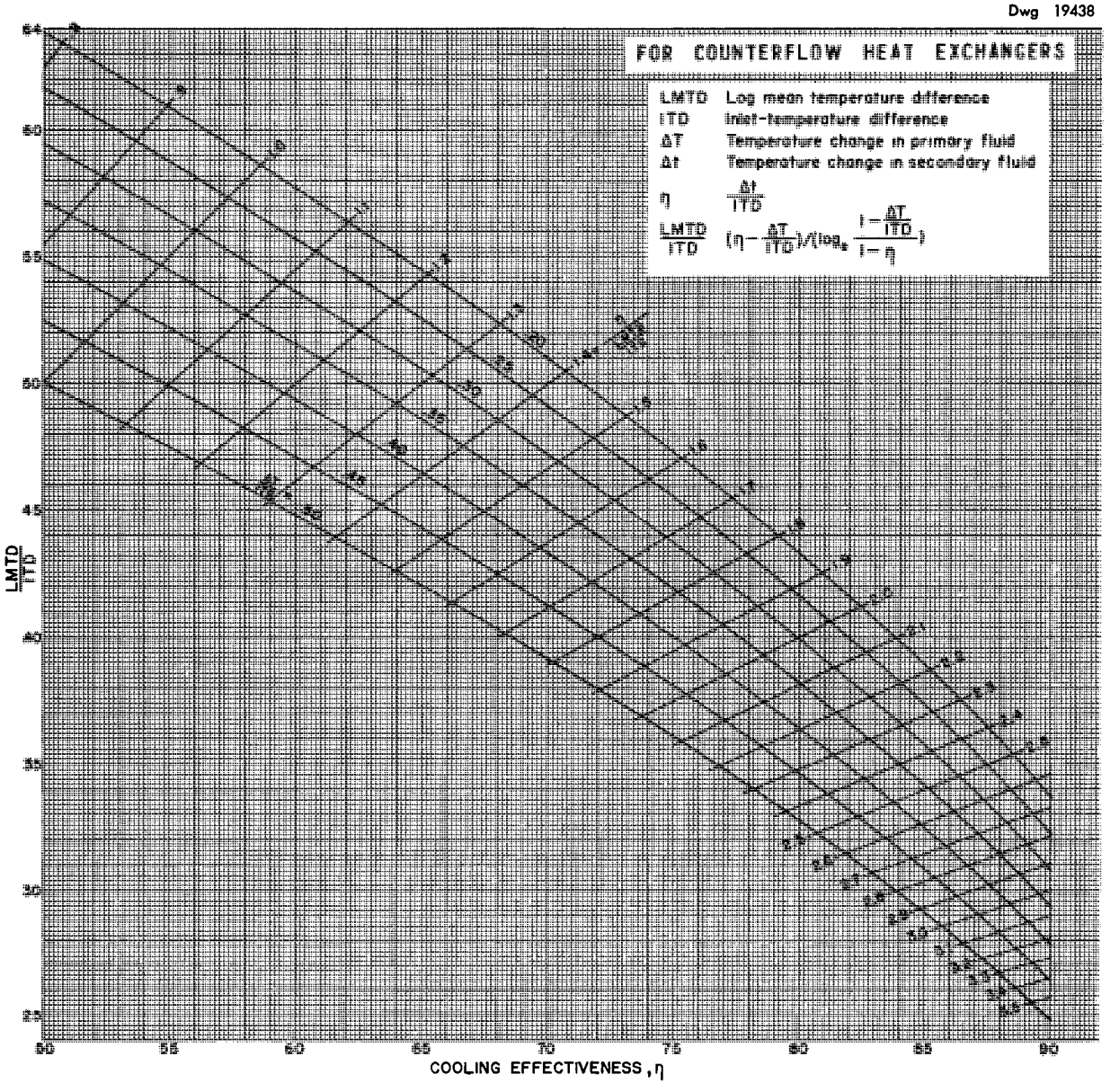

FIGURE 19 LOGARITHMIC MEAN TEMPERATURE DIFFERENCE AGAINST COOLING EFFECTIVENESS FOR VARIOUS RATIOS OF PRIMARY FLUID TEMPERATURE CHANGE TO INLET-TEMPERATURE DIFFERENCE

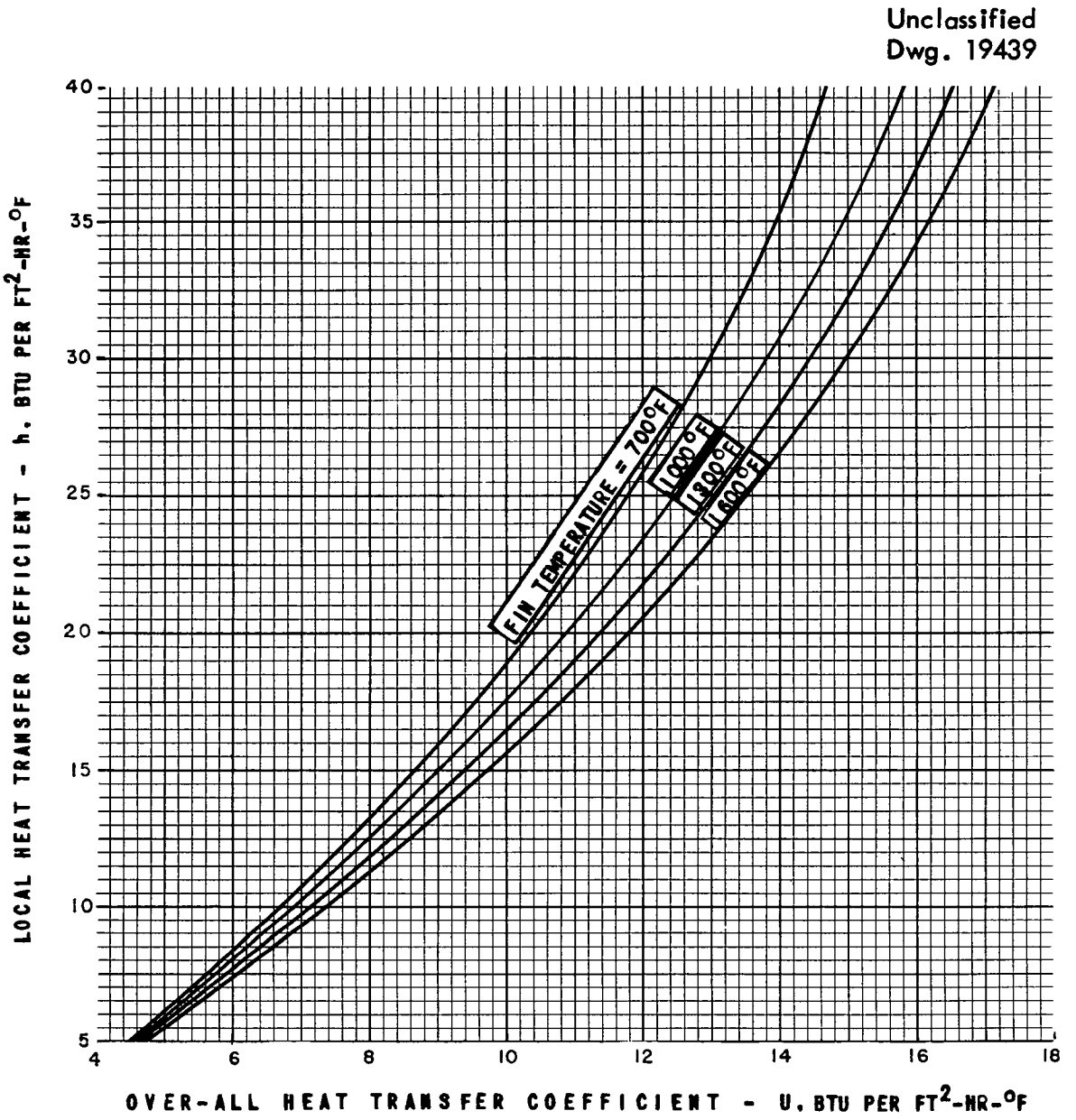

FIGURE 20. LOCAL VS. OVER-ALL HEAT TRANSFER COEFFICIENTS FOR .667" O.D. DISC FINS OF 18-8 STAINLESS STEEL, .010" THICK, ON .1875" O.D. TUBES.

Unclassified
Dwg. 19440

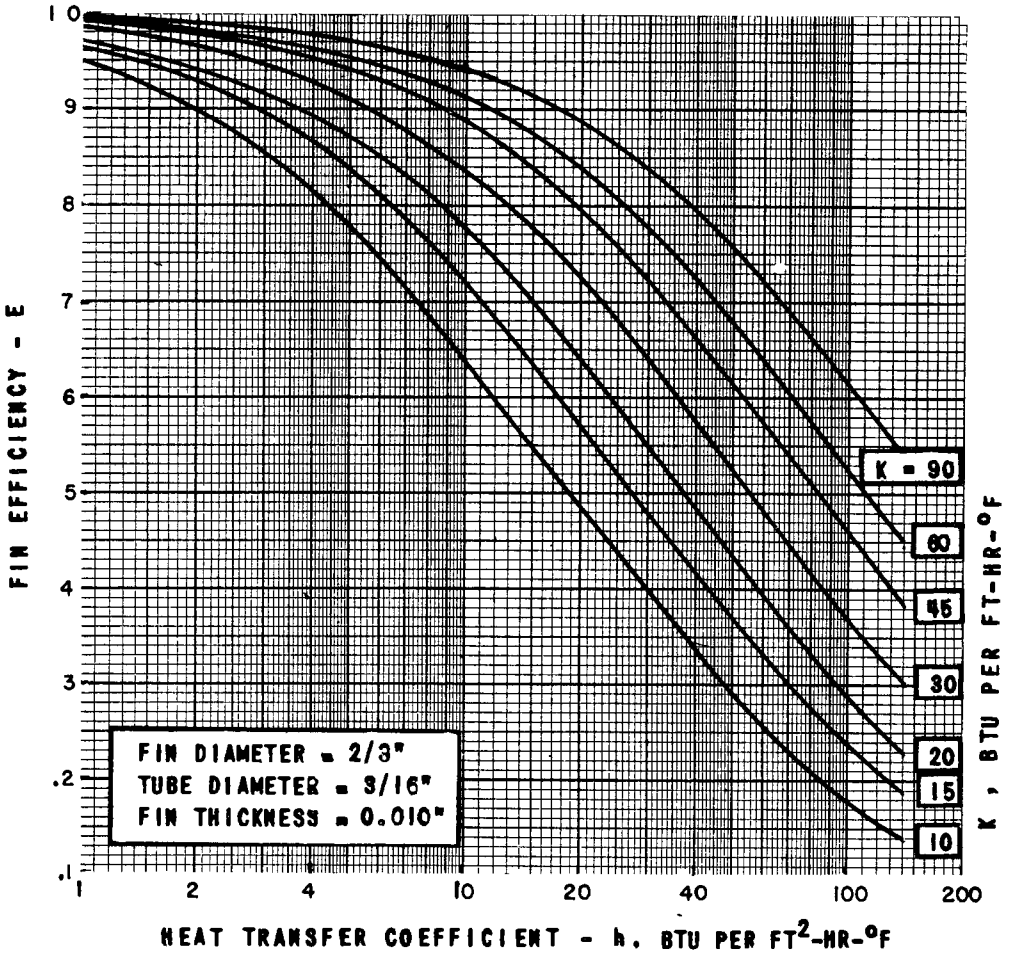

FIGURE 21. FIN EFFICIENCY VS. HEAT TRANSFER COEFFICIENT FOR VARIOUS THERMAL CONDUCTIVITIES.

[redacted]

Dwg. 19441

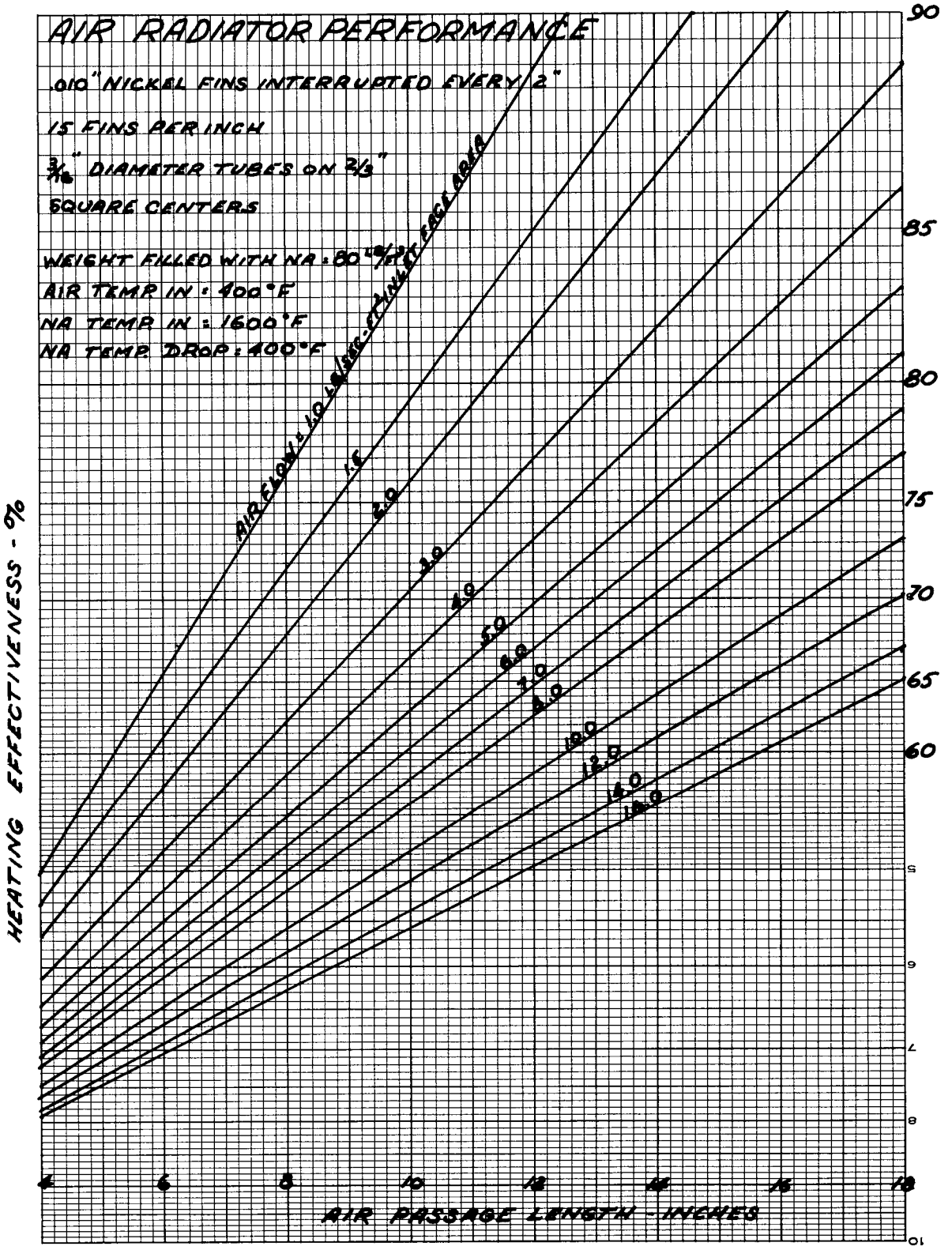

FIG-22

ENGINE PERFORMANCE STUDIES

Turbojet Engine Performance

It is not possible to balance the relative importance of such radiator parameters as air pressure drop, heat transfer coefficient, radiator weight in pounds per cubic foot, etc., except through a study of the over-all performance of a turbojet or ram-jet engine installation. This over-all performance may be expressed in two common figures of merit; namely, pounds of thrust per pound of air passing through the engine per second and pounds of engine per pound of thrust. Mr. B. F. Ruffner of Boeing suggested that engine performance be evaluated at sea level, 15,000 ft , 35,000 ft , 45,000 ft , and 55,000 ft and at flight Mach numbers of .3, .6, and .9 at the lower altitudes, and .9, 1.2 and 1.5 at the higher altitudes. On the basis of the results of such a study the performance of radiators of different materials or different geometries can be compared to give some concept of the relative importance of the various design parameters.

Some initial calculations were made for the GE J-53 engine so that comparisons might be made with the proposal in NEPA Report No. 1520. Since this engine appeared to be inherently heavy, some further calculations were based on the Sapphire engine. These assumed that removal of the combustion chambers would compensate for the weight increase resulting from the additional structure that might be required for a liquid metal radiator installation. Thus the total engine weight was taken as the weight of the radiators plus the dry weight of the standard Sapphire turbojet. Since examination of ORNL Report No. ANP-57 indicated that a compression ratio somewhat lower than the standard Sapphire compression ratio of 6.85 should give better performance, calculations were carried out for engine compression ratios of both 4 to 1 and 6.85 to 1. Several curves of engine weight, radiator weight, and total weight, all in pounds per pound of thrust were plotted as a function of radiator depth to investigate the effects of compression ratio. It was found that only at sea level did the 6.85 compression ratio give the better performance. The radiator core matrix chosen for all of the engine performance estimates in this report was the best for which test data were available at the time of writing; namely, plain fins interrupted in the direction of air flow with 15 fins/in. and 3/16 in. diameter tubes on square centers. While no test data were available for nickel fins with a ceramic coating, it was felt that the performance with these fins could be estimated with little error from data for stainless steel fins.

Since the engine installation weight should probably include not only the radiators and turbojet engine but also the weight of pumps and lines for the liquid metal circuit, a brief study of optimum line size was carried out. It is obvious that as the line size is reduced the pumping power is increased so that the weight of the pump and pump drive system must increase. Whether the weight of the pipes will increase or decrease as pipe diameter is reduced is not obvious, because increases in system pressure drop resulting from

reduced line sizes might require pipe walls so much thicker that an increase in pipe weight with a reduction in pipe diameter might conceivably result. Figure 24 shows the results of a rough study on the effect of pipe sizes on pump and line weight for a typical turbojet engine installation. It was assumed that 20 ft. of pipe would be required from the reactor to the turbojet engine. It was also assumed that the total weight of the pump and pump drive mechanism charged to the installation should be 2 lb. per horsepower input to the pump shaft. This was based on some rough estimates of the weight penalties associated with compressor air bleed-off from the turbojet compressor and an air turbine drive. The wall thickness of the liquid metal pipes was taken as .10 in. or a stress limited value, whichever was the greater. The stress limited value was calculated from line pressures using an allowable stress of 1500 psi at 1600°F, and an allowable stress of 11,000 psi at 1100°F. It was deduced from these curves that a rough estimate of pump and line weight was given by multiplying the power supplied to the radiators in kilowatts by .04 to get pump and line weight in pounds. These studies also showed that if the engine installation is designed to give peak performance at sea level instead of high altitude the use of 3/16 in. O.D. tubing in the radiators results in excessive pressure losses. This condition can be alleviated through the use of larger tubing in the fin matrix (perhaps 1/4 in. O.D.) and by changing the radiator proportions to provide more tubes operating in parallel.

The first set of calculations made on turbojet engine performance covered a range of radiator inlet face areas and radiator depths (air passage lengths) Thus with a given radiator core geometry a wide variety of potential installation possibilities was considered.

Results of the calculations for performance of the Sapphire for several flight conditions are shown in Figures 23A, 23B, and 23C. Note that the curves give relatively broad, flat peaks so that it is evident that the performance is not too sensitive to radiator inlet face area or radiator depth. The air pressure drops are relatively small — of the same order as the diffuser losses to be expected between the compressor outlet and the radiator inlet.

Examination of the first set of curves prepared indicated that the radiator face areas chosen were not small enough to bracket the optimum values. In order to get some idea of the best performance without making a new set of curves it was estimated that a 12 ft^2 face area and a 12 in. depth would yield optimum performance. The curves of Figure 25 were then prepared to show the performance of the engine for a wide range of flight conditions with this particular radiator core installation. Subsequent work along these lines has indicated that a 10 ft^2 face area and a 14 in. depth would yield a small improvement in performance. To accommodate this 2 in. increase in depth it would be necessary to use three radiators arranged in the form of a three-pointed star rather than four radiators in the cross-shaped array of Figure 1. The three-pointed star arrangement gives a somewhat greater free flow area and a decreased length along the engine axis as compared to the cruciform arrangement.

[redacted] Dwg 19442

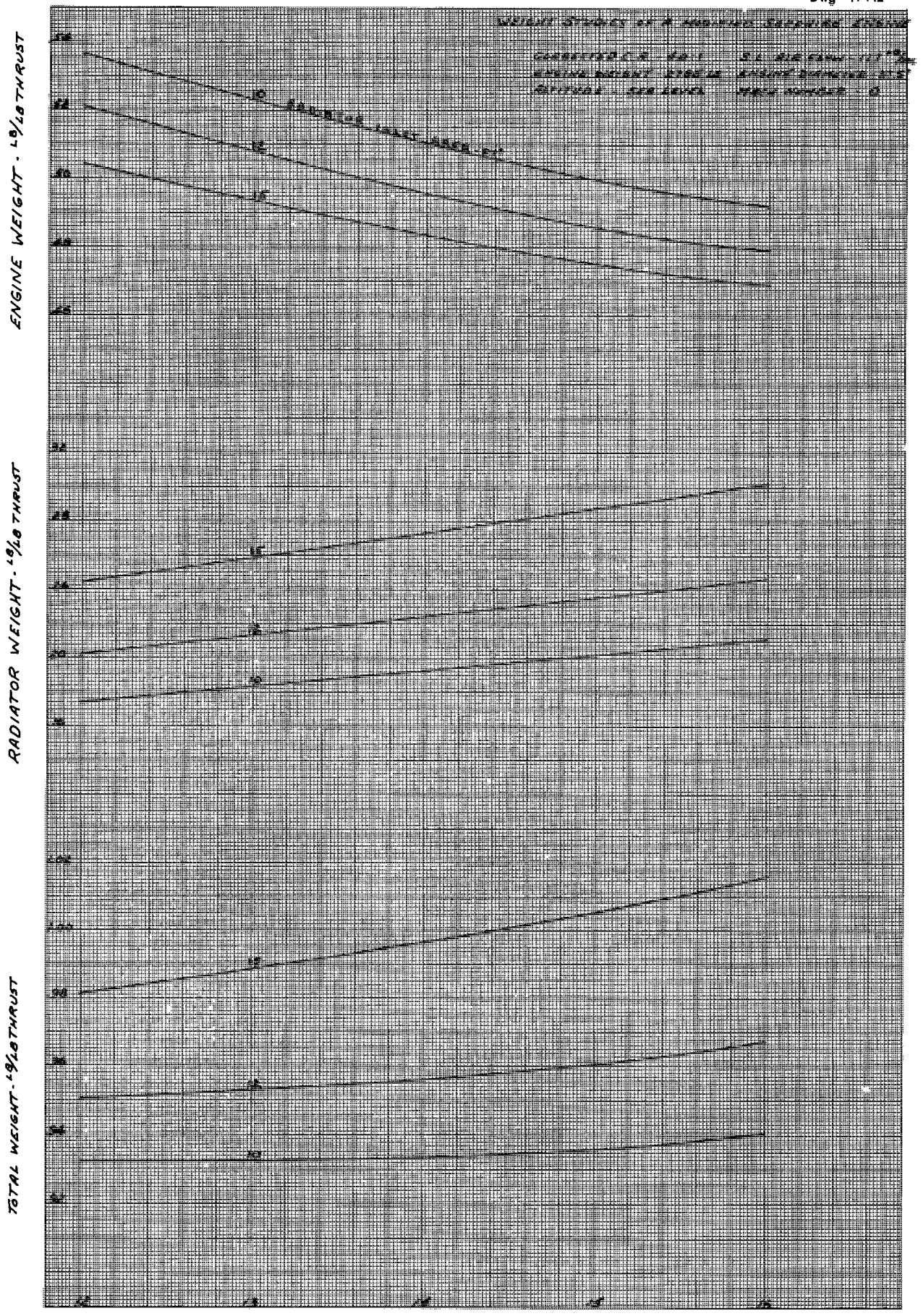

FIG-23-A

[redacted]
Dwg 19443

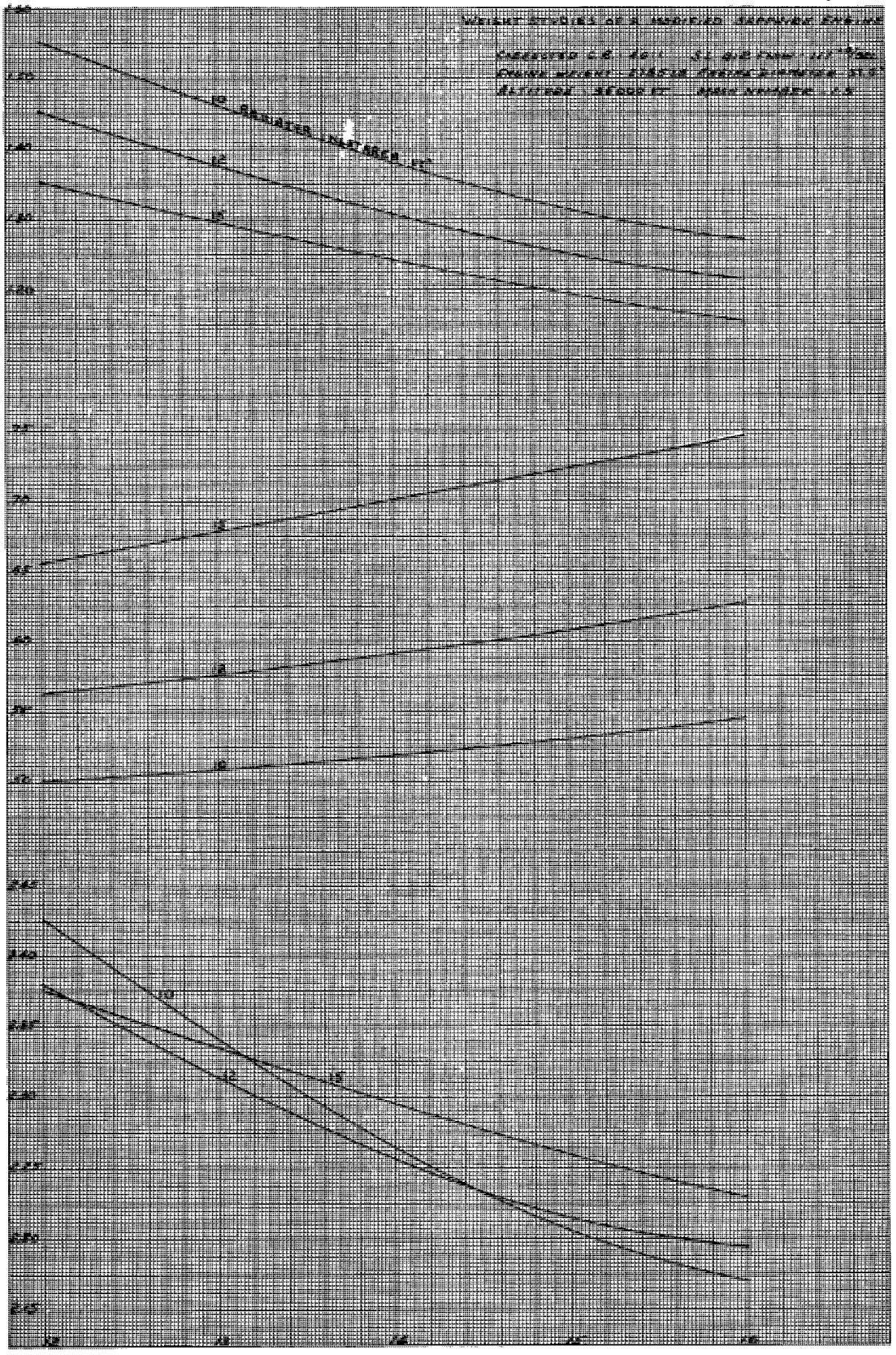

FIG-23-B

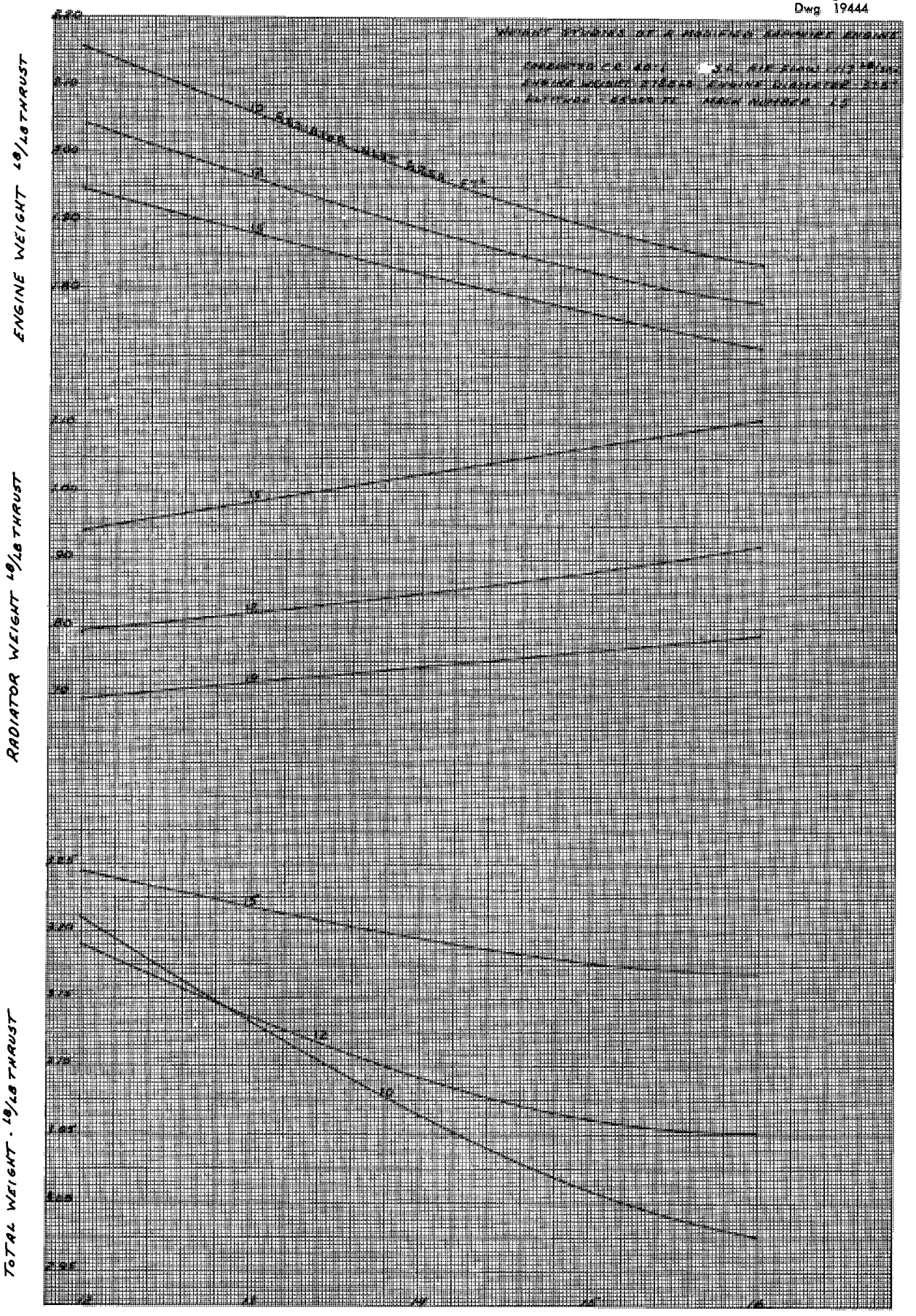
ENGINE WEIGHT LB/LB THRUST
RADIATOR WEIGHT LB/LB THRUST
TOTAL WEIGHT - LB/LB THRUST
RADIATOR DEPTH - INCHES

FIG-23-C

[redacted] Dwg 19445

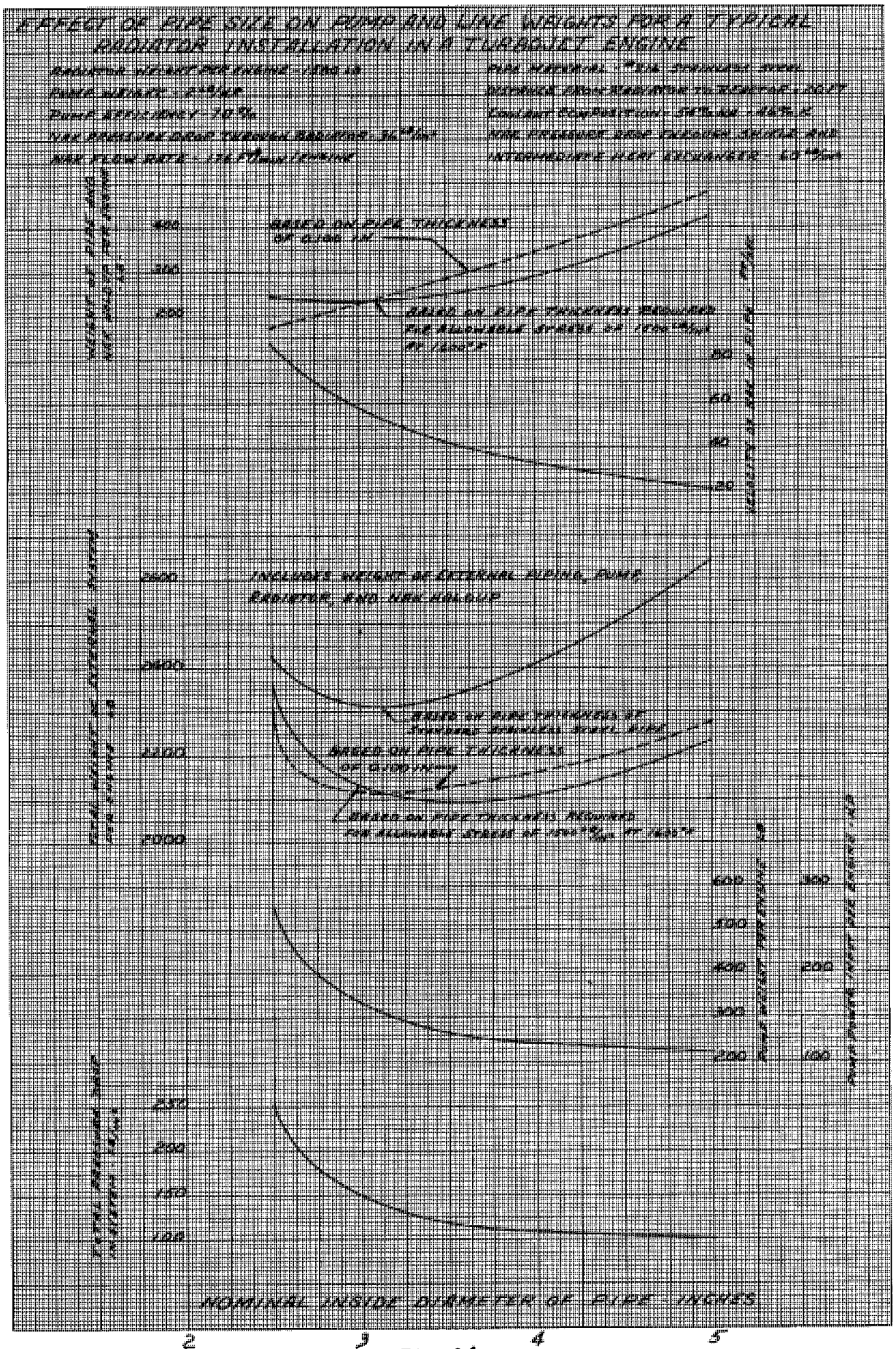

FIG-24

ESTIMATED PERFORMANCE OF A MODIFIED SAPPHIRE TURBOJET ENGINE

CORRECTED C R - 40 1 RADIATOR WEIGHT - 1080 LB ENGINE DIA - 37.5 IN
ENGINE WEIGHT - 2785 LB RADIATOR DEPTH - 12 IN S L AIR FLOW - 117 LB/sec
RADIATOR INLET FACE AREA - 12 FT² NA ΔT THROUGH RADIATOR - 400°F

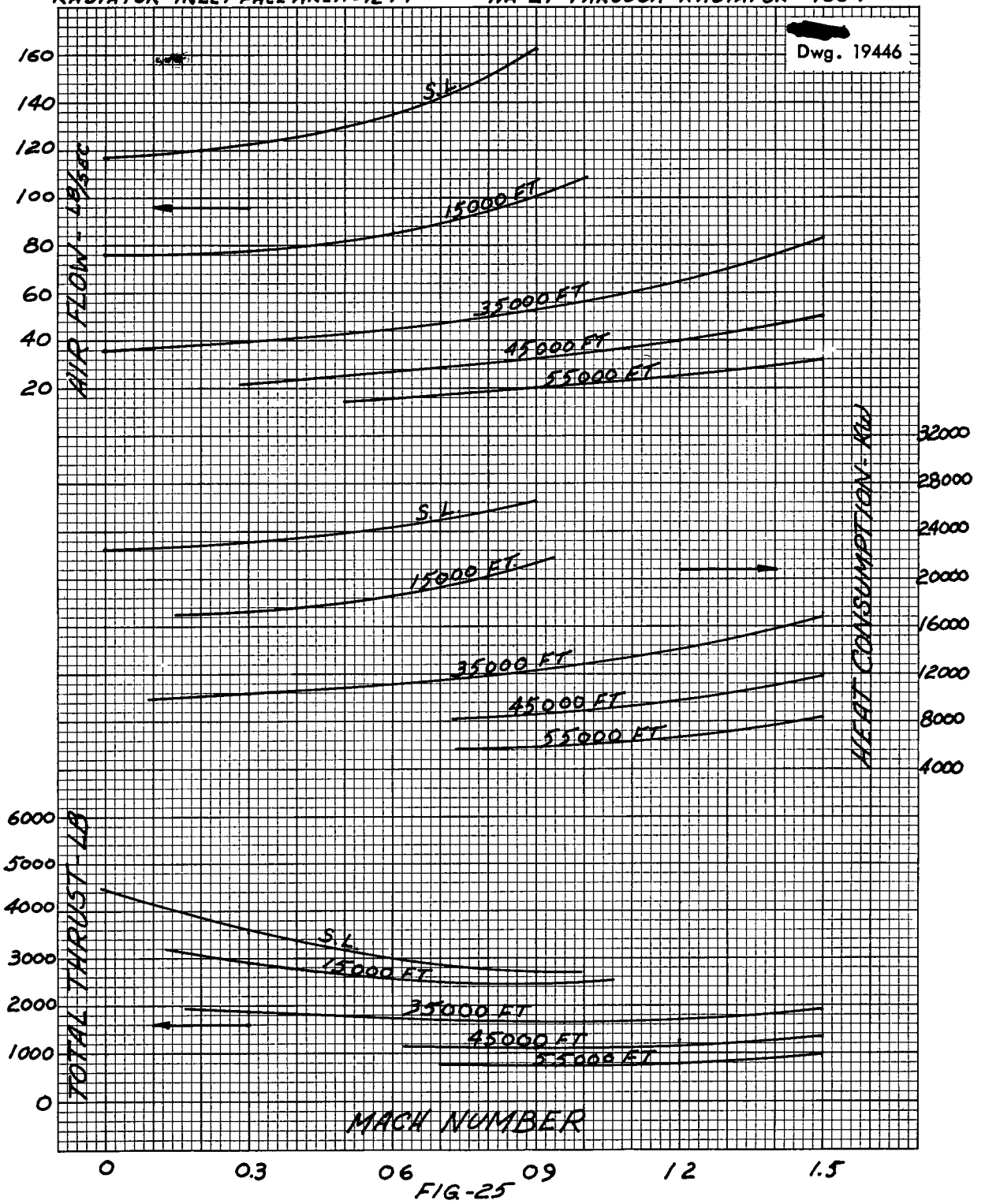

FIG-25

ESTIMATED PERFORMANCE OF A MODIFIED WRIGHT TURBOJET ENGINE

76 CORRECTED C R - 4 0 1 RADIATOR WEIGHT - 1080 LB ENGINE DIAMETER - 44.5 IN
ENGINE WEIGHT - 3100 LB RADIATOR DEPTH - 12 IN S.L. AIR FLOW - 220 LB/SEC
ENGINE LENGTH - 140 IN. NA ΔT THROUGH RADIATOR - 400°F RADIATOR INLET FACE AREA - 12 FT²

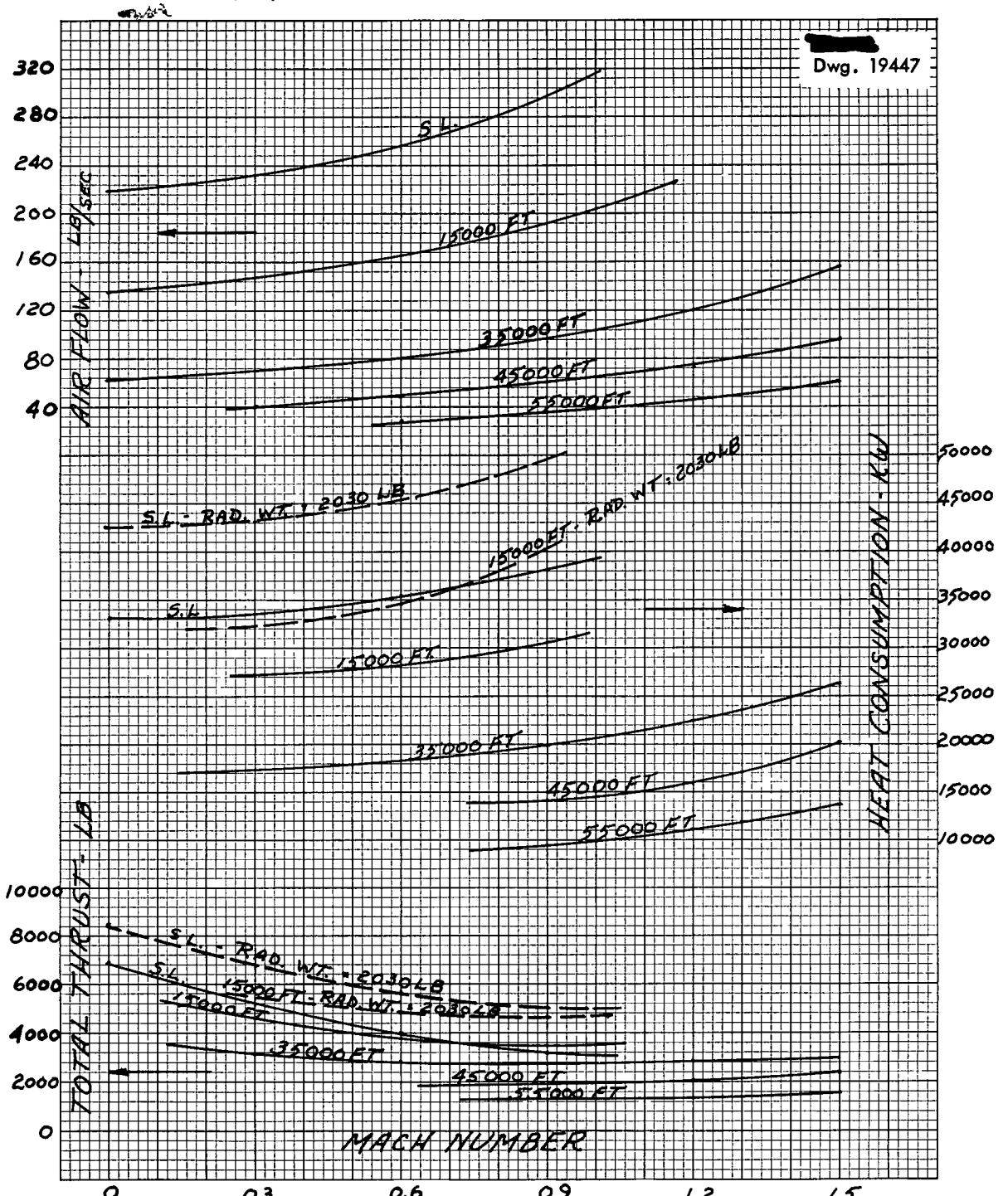

FIG - 26

The results of this preliminary work indicated that a larger engine having a lower weight per pound of air handled would be highly desirable. Engineers of the Wright Aeronautical Company suggested that an engine they have under development might be modified to meet these requirements. By removing the burners and the center spool of this two-spool engine while adding two stages to the remaining compressor they estimated that a considerable weight saving could be effected. Thus this engine having a rated air flow of 220 lb/sec, modified to accommodate four radiators, would weigh approximately 3100 lb. No curves similar to those of Figure 23 have been made as yet for this modified Wright turbojet engine, but its performance with two particular sets of radiators was estimated and is given in Figure 26. The solid lines indicate the performance of this engine using the same size radiators as were used in the Sapphire engine. The dotted lines indicate the expected performance with much larger radiators.

Ram-jet Engine Performance

A series of ram-jet performance calculations was prepared which may prove useful in connection with rough design estimates of possible missile power plants. The assumptions made for these calculations are included in Figures 27A and 27B.

The initial set of computations determined the specific thrust and specific heat consumption of a ram-jet using sodium-to-air radiators as the heat source for various radiator air outlet temperatures and flight Mach numbers of 1.5, 2.5, and 3.5. This data was applicable for altitudes above 35,000 ft.

The next set of calculations estimated the performance of a ram-jet using particular radiator configurations and air flows. As shown in Figures 27A and 27B the radiator depth in the direction of air flow was varied from 3 to 12 in. for air flows of 4 to 16 lb/sec-ft^2 of radiator inlet face area. At a Mach number of 1.5 the air pressure drop through the radiators became excessive and no further performance calculations were made at this speed. There is little incentive to use air flows in excess of 16 lb/sec-ft^2 of radiator inlet area since the total power plant weight is decreased only slightly and in some cases may increase.

It can be seen from these curves that the total power plant weight given in pounds per pound of thrust is approximately that to be expected from a reciprocating engine, excluding fuel load. In these ram-jet performance studies a weight penalty of 0.5 lb/lb of thrust has been included for the unshielded reactor. Previous weight studies made on a modified Sapphire turbojet engine have shown that the total power plant weight of this type of a power plant, excluding any reactor weight penalty, is greater than that of the ram-jet.

Some estimates of the required radiator sizes for various air flows, radiator depths, and number of engines used has indicated that for air flows of 12 to 16 lb/sec-ft^2 it may be feasible to pass the air straight through the ram-jet in an axial direction. This would eliminate the need for any elaborate ducting with its consequent pressure loss and undesirable flow patterns as was necessary in the turbojet installation. In some instances, the required radiator frontal area is only 81 $^o/o$ of the duct inlet area which makes this arrangement quite attractive. Even for air flows as low as 8 lb/sec-ft^2 the radiators may still be installed in this manner if they are mounted at an angle to the plane perpendicular to the axis of the ram-jet. Another incentive to use higher air flows is that the required duct size is decreased.

It was also felt that these ram-jet performance calculations may prove of interest in connection with the possible use of ram-jet engines as auxiliary power plants that might be operated at high altitudes and high air speeds, since the output of the reactor is not affected by altitude and there is a much larger amount of power available at high altitudes than could be utilized by the turbojet engines.

The radiator data used in making these calculations was the best available at the time of writing, namely test data from a core element using flat plate, nickel fins, 15 to the inch, and interrupted every 2 in. in the direction of air flow. Since further radiator development work is expected to improve the heat transfer performance and decrease the weight of these heat exchangers, particularly the ceramic coated, nickel disc fin, staggered tube type, these ram-jet performance estimates may be conservative.

[redacted]

Dwg 18964

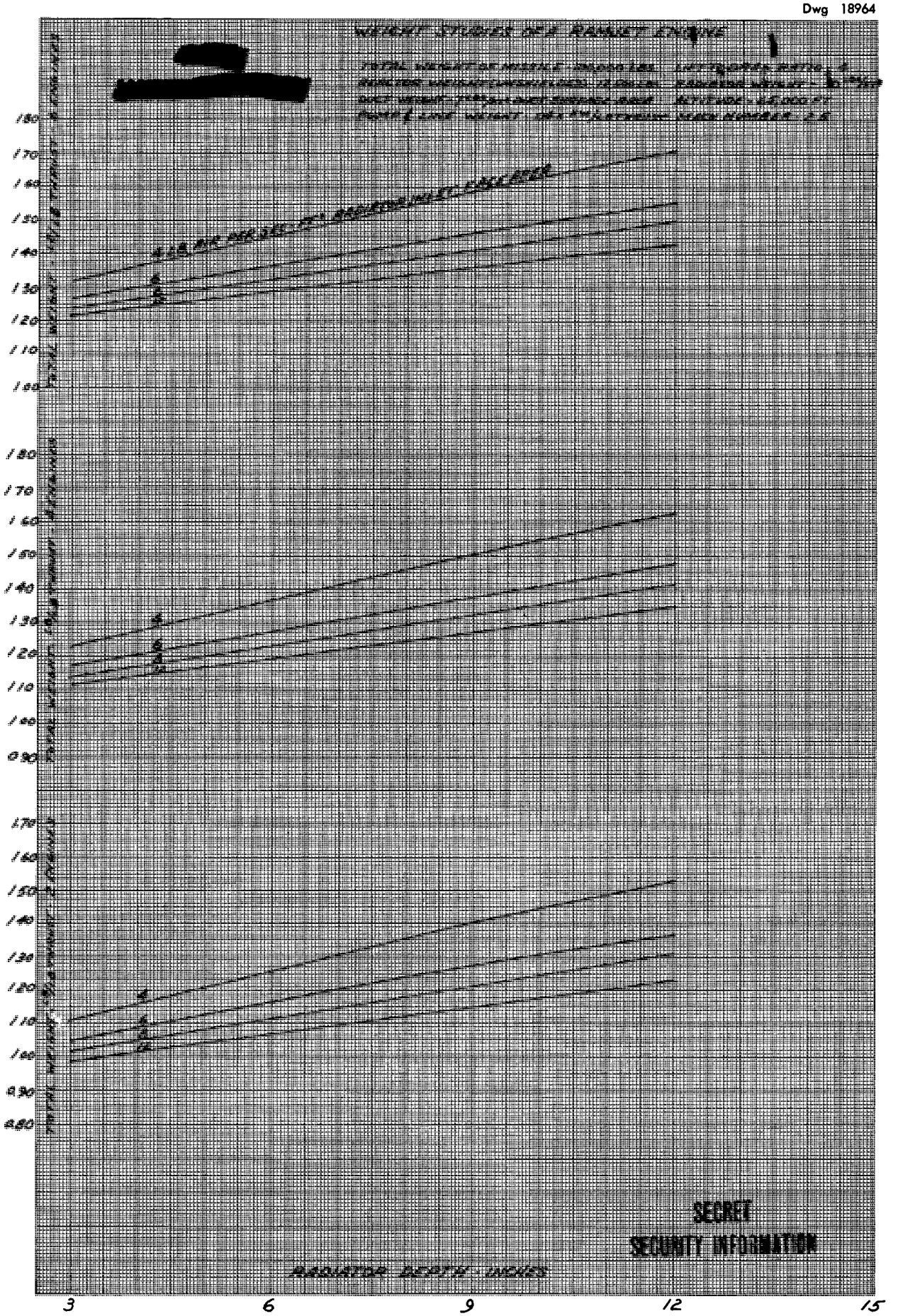

FIG-27-A

[redacted]

Dwg 18965

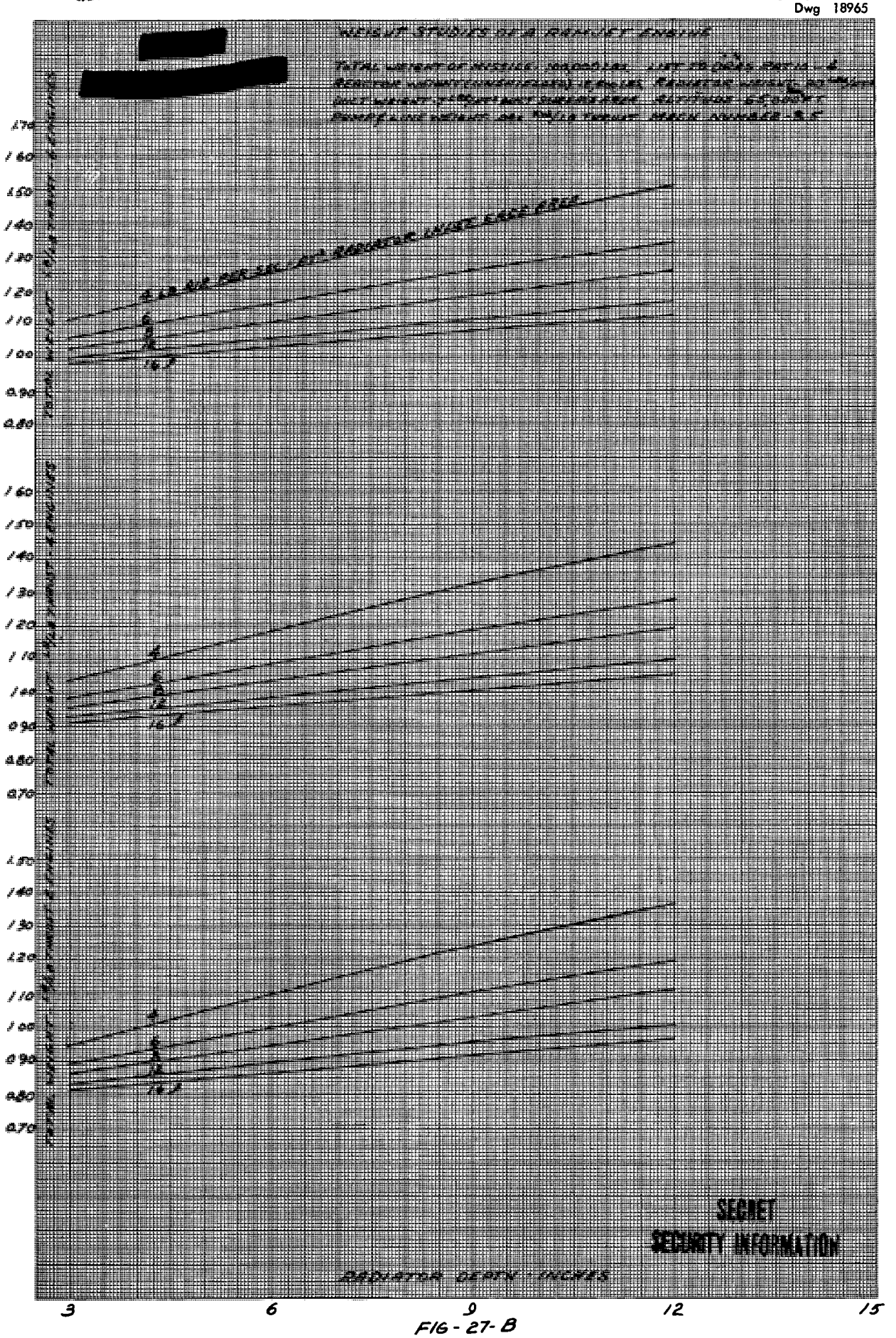

FIG - 27- B

APPENDIX A

RADIATOR CORE ELEMENT TEST INSTRUMENTATION AND COMPUTATION

The details of the instrumentation employed and the methods used to compute radiator core element performance have an important bearing on the significance of many of the curves presented in this report. The instrumentation for each of the items of data affecting radiator performance is described below. Complete data sheets are then presented followed by a table specifying the calculation procedure for each column of the data sheets.

Instrumentation

1. Air inlet temperature - Taken as room temperature at blower inlet

2. Air outlet temperature - Six modified Probert Probes were arranged in a shielded duct 9 in. downstream from the radiator. The air outlet temperature was taken as the average of these six readings. The probes were arranged as shown below.

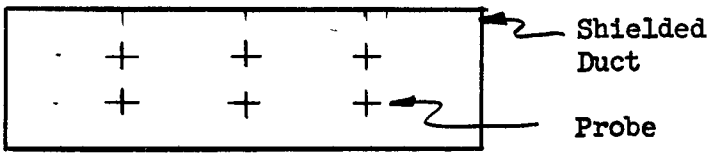

3. Sodium inlet temperature - Two thermocouples were welded to the sodium inlet line to the radiator. They were covered with Sauereisen and 6 in. of slag wool insulation The sodium inlet temperature was taken as the average of these two readings. The Brown recorder was checked with a Leeds and Northrup potentiameter over the Na temperature range and the error was less than 1°F at 1600°F.

4. Sodium outlet temperature - Similar to the above arrangements for sodium inlet temperature.

5. Sodium flow rate - A venturi tube was connected to a bourdon tube type of differential pressure gage. It was calibrated with water and the readings corrected for the difference in density between water and sodium. An electromagnetic flowmeter was checked against the venturi tube and a calibration chart was constructed to convert millivolts to gallons per minute. The electromagnetic flowmeter was found to be more accurate than the venturi tube at low flow rates. The venturi tube was not used for later test data because the pressure gage line plugged.

6. Pressure drop across radiator- This was taken to be the static pressure drop between a point 18 in. before the radiator and 8 in. after the radiator. It was measured by a manometer in inches of water. Readings were corrected for the difference in flow passage area between the two stations. The arrangement used is shown below.

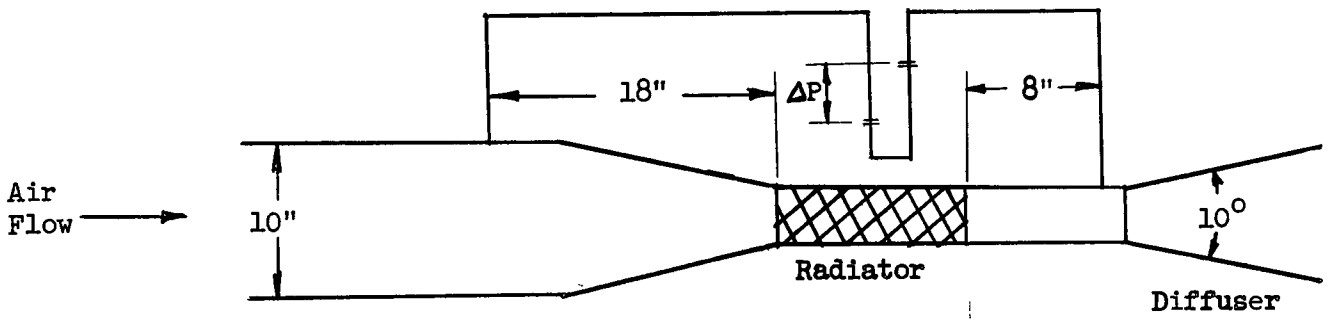

7. Air flow rate - The static pressure drop across a 2.8 in. diameter sharp-edged orifice was measured with an inclined manometer. The orifice was preceded by 18 ft. of 10 in. diameter straight pipe. A calibration chart was constructed using A.S.M.E. standard orifice data to give the air flow rate in lb/sec. in terms of the pressure drop across the orifice in inches of water.

8. Inlet air pressure - The static pressure well upstream from the radiator was measured by means of a manometer and this was added to the barometric pressure in the room.

A heat balance was made by comparing the heat lost from the sodium to the heat gained by the air. These values usually differed by 10 - 15 $^{o}/o$. This discrepancy was probably due to the inaccuracy of the sodium flow measurements as these fell in the lower portion of the range of the sodium flow metering instruments.

PERFORMANCE DATA FOR RADIATOR NO 1

Plain Fin - 10 5 Fins Per Inch
Face Area - 0.0469 Ft^2
Free Flow Area - 0.0294 Ft^2
Distance Between Fins - 0.0071 Ft

Date	Hours Total Time	1. Ma Flow, GPM	2. Ma Inlet Temp., °F	3 Ma Outlet Temp., °F	4 Ma Temp Drop, °F	5. Orifice Air Press, Inches H_2O	6 Orifice Air Press, Inches Hg Abs	7 Air Inlet Temp., °F	8 Air Outlet Temp, °F	9 Air Temp Rise, °F	10 Air Density, lb/ft^3	11 Orifice Diff. Press., Inches H_2O	12 Air Flow, lb/sec	13 Max Temp Diff, °F	14 Cooling Effectiveness, %	15 Heat From Ma, Btu/sec	16 Mean Air Temp, °R	17. Heat to Air, Btu/sec	18 Outlet Temp Diff. OTD, °F	19 Inlet Temp Diff ITD, °F	20 Log Mean Temp Diff. LMTD, °F	21. Air Flow, lb/sec/ft^2 Free Flow Area	22. Air Flow, lb/sec/ft^2 Face Area	23 Mean Air Density, lb/ft^3	24. Press Drop Across Radiator, Inches H_2O	25. ΔP for Radiator, Inches H_2O	26. Over-all Heat Transfer Coefficient, U	27. Local Heat Transfer Coefficient, h, Btu/hr-ft^2-°F	28 Viscosity of Air, lb/ft sec x 10^7	29. Free Stream Reynolds Number, R_D
															BAR = 29 25" Hg.																
4-15-52	20	3.0	700	630	70	3.2	29 48	80	550	470	0726	.29	067	620	75.8	7.7	775.0	7.65	150	550	308	2.28	1.43	.0506	3.85	2.55	7.60	12.1	208.2	1554
		3 0	700	610	90	6.4	29.72	80	520	440	0732	.66	.103	620	71 0	9 9	760.0	11.00	180	530	324	3.51	2.20	.0520	6.00	4.08	10.40	20 1	207.0	2403
		3 0	700	584	116	11.2	30.07	80	485	405	0741	1 20	.140	620	65.4	12.8	742 5	13 77	215	504	340	4.76	2.98	.0539	10.40	7.33	12.40	27.4	205.3	3294
		3.0	700	575	125	12.4	30.16	80	475	395	.0743	1.40	152	620	63 7	13.8	737.5	14.57	225	495	343	5 16	3.24	.0544	11.40	8.11	12.90	29.5	204.7	3582
															BAR = 29.45" Hg.																
4-16-52	45	3.0	900	788	112	4.4	29.77	79	674	595	.0722	.36	076	821	72 5	11 7	836.5	11.04	226	709	421	2.46	1.54	.0465	4.15	2.52	8.03	12.9	230.5	1590
		3.0	900	755	145	8.6	30.08	79	630	551	.0730	.78	.112	821	67 1	15.1	814.5	15.15	270	676	442	3 83	2.40	.0483	8.10	5.11	10.50	19.5	228.5	2378
		3.0	900	734	166	11.8	30.32	77	605	528	0736	1.10	.133	823	64.2	17 4	801.0	17.15	295	657	451	4.52	2.83	.0493	11.05	7.12	11.65	23.2	227.2	2823
		3.0	900	728	172	12.5	30.36	77	600	523	0736	1.30	.145	823	63.6	17.8	798.5	18.56	300	649	453	4.94	3.09	.0495	11.72	7.58	12.55	26.3	226.9	3089
															BAR = 29.58" Hg.																
4-17-52	70	3.3	1105	974	131	4.7	29.93	79	824	745	.0732	.35	.077	1026	72.6	14 5	911.5	14.20	281	896	530	2.61	1.63	.0433	4.50	2.55	8.19	12.7	252.9	1471
		3.3	1100	920	180	9.8	30.30	79	760	681	.0743	.90	.122	1021	66 7	20.0	879.5	20 40	320	841	557	4.15	2.60	.0455	9 35	2.59	11.20	20.5	249 7	2360
		3.3	1095	895	200	12.5	30.50	80	730	650	0749	1.20	.137	1015	64 0	22.1	865.0	21.90	365	815	562	4.66	2.92	.0468	11.80	7.22	11.91	22.7	248.0	2668
															BAR = 29.40" Hg.																
4-18-52	90	3 0	1250	1004	246	12.5	30.46	81	839	758	.0746	96	.126	1169	64.8	24.4	920.0	23.60	411	923	635	4.29	2.68	.0439	10.40	5.97	11.38	20.1	262.6	2318
		3.0	1295	1072	223	7.2	29.93	82	915	833	.0718	.57	.095	1213	68.6	21.9	958.5	19 60	380	990	639	3.23	2.02	.0406	7.00	3.72	9.40	15.0	268.4	1710
		3.0	1288	1035	253	10.8	30.18	84	865	781	.0735	.96	.125	1204	65.0	24.8	934.5	24 20	423	951	650	4.25	2.67	0428	10.30	5.76	11.39	20.1	266.2	2268
		3.0	1285	1009	276	12.3	30.13	83	844	761	.0741	1 12	.136	1202	63.3	27 1	923.5	25.65	441	926	655	4.62	2.90	0436	11.70	6.67	12.00	21.7	264.7	2482
															BAR = 29.47" Hg.																
4-21-52	165	3.0	1432	1190	242	8.5	30.09	87	996	909	0729	.62	098	1345	67.6	23.0	1001 5	22 20	436	1103	718	3.33	2.09	.0398	8.20	4.27	9.45	14.6	281 1	1684
		3.0	1471	1161	310	11.5	30.32	84	977	893	.0738	97	.126	1387	64.4	29.5	990.5	28.00	578	1077	800	4.29	2.69	.0405	10.95	5.80	10.71	17.5	281.6	2161
		3.0	1491	1170	321	11.4	30.31	84	988	904	.0737	97	.126	1407	64 2	30 1	996.0	28.40	503	1086	758	4.29	2.69	.0403	11.00	5.79	11.45	19.4	283.0	2150

PERFORMANCE DATA FOR RADIATOR NO 1

Plain Fin - 10 5 Fins Per Inch
Face Area - 0 0469 Ft^2
Free Flow Area - 0.0294 Ft^2
Distance Between Fins - 0.0071 Ft

Date	Hours Total Time	1. Na Flow, GPM	2. Na Inlet Temp., °F	3 Na Outlet Temp., °F	4 Na Temp Drop, °F	5 Orifice Air Press, Inches H_2O	6 Orifice Air Press, Inches Hg Abs	7 Air Inlet Temp., °F	8 Air Outlet Temp, °F	9 Air Temp Rise, °F	10 Air Density, lb/ft³	11 Orifice Diff. Press, Inches H_2O	12 Air Flow, lb/sec.	13 Max Temp Diff, °F	14 Cooling Effectiveness, %	15 Heat From Na, Btu/sec	16. Mean Air Temp., °R	17 Heat to Air, Btu/sec.	18 Outlet Temp Diff. OTD, °F	19 Inlet Temp. Diff. ITD, °F	20 Log Mean Temp Diff LMTD, °F	21. Air Flow, lb/sec/ft² Free Flow Area	22 Air Flow, lb/sec/ft² Face Area	23 Mean Air Density, lb/ft³	24. Press Drop Across Radiator, Inches H_2O	25 Δ P for Radiator, Inches H_2O	26 Over-all Heat Transfer Coefficient, U	27 Local Heat Transfer Coefficient, h, Btu/hr-ft²-°F	28 Viscosity of Air lb/ft sec x 10^7	29 Free Stream Reynolds Number, R_e
															BAR = 29.44" Hg															
		2.8	1499	1174	325	11.6	30 30	84	991	907	0737	.96	125	1415	64.1	28.2	997 5	28.20	500	1090	757	4 25	2.66	0402	11.10	5.83	11.41	19.3	283.6	2129
															BAR = 29.39" Hg.															
	165	3 7	700	550	150	12.3	30 35	88	466	378	0737	1 40	.150	612	61 8	17 3	737 0	13 80	234	462	335	5 12	3.21	.0548	11 35	8.13	12.60	28.2	203.0	3576
		3.7	700	590	110	5 5	29 79	88	518	480	0724	.53	091	612	70.3	12.7	763.0	9.50	182	502	316	3 09	1.94	0520	5 15	3 50	9.20	16.2	205 7	2137
															BAR = 29.46" Hg															
	170	2.6	1114	905	209	10 4	30.22	84	737	653	0739	.96	.126	1030	63 4	18 4	870 5	20 20	377	821	570	4 29	2.68	0462	9 90	5 98	10 84	19 5	249.6	2438
		2 6	1119	896	223	12.2	30.36	84	728	644	.0742	1.20	.140	1035	62.2	25.5	866.0	22 20	391	812	577	4 76	2 97	.0466	11.60	7.07	11.78	22 3	249 4	2711
															BAR = 29 42" Hg															
4-22-52	185	3.0	1465	1175	290	12.4	30 33	86	964	878	.0739	1.06	.131	1379	63.7	27 6	985.0	28.60	501	1089	757	4 42	2.77	0410	11 80	6.32	11.57	19.8	282 0	2244
		3.5	1460	1200	260	12.4	30.33	86	970	886	0739	1.05	.130	1374	64.5	26.2	988.0	28.70	490	1114	760	4 46	2.80	.0408	11 85	6.32	11.55	19.8	283.0	2219
		4.0	1445	1215	230	12.4	30.33	86	966	880	.0739	1.05	.130	1359	64.8	29.2	986 0	28.50	479	1129	760	4 46	2.80	0409	11.85	6.34	11.49	19 8	283.0	2219
			1463	1120	343	12.4	30 33	87	939	852	0739	1.08	.134	1376	61.9	29.3	973 0	28.40	524	1033	747	4 56	2.86	.0415	11.90	6.46	11.61	20.1	279.2	2318
															BAR = 29.36" Hg.															
4-23-52	205	3.5	1285	1005	280	12.4	30.27	83	829	746	0742	1.15	.138	1202	62.1	30.5	916.0	25.50	456	922	664	4.69	2.94	0440	11.90	6.84	11 75	21.2	264.5	2520
		3.5	1282	1004	278	12.4	30 27	83	827	744	0742	1.15	.138	1199	62.1	31 4	915.0	25.40	455	921	664	4.69	2.94	0440	11.90	6.84	11.71	21.1	264.3	2522
		3.4	1295	1045	250	9.4	30.05	84	873	789	.0736	.79	.115	1211	65.2	28 2	938.5	22 50	422	961	654	3.91	2.45	0427	8 70	4 86	10.52	17.8	267.0	2080
		3.3	1305	1126	179	4 4	29 68	84	973	889	.0727	.29	068	1221	72 8	20.2	988.5	15.00	332	1042	621	2 31	1.45	.0400	4.25	2 22	7.39	10.6	271 6	1209
															BAR = 29.34" Hg															
	210	3.5	1099	950	149	4.1	29 64	84	821	737	0723	.30	.068	1015	72 6	17 6	912 5	12 45	278	866	517	2 33	1.46	0431	3.90	2.20	7.37	10.8	251 3	1317
		3.5	1110	886	224	10.4	30.11	85	740	655	.0734	.95	124	1025	63 9	26.5	872.5	20.05	370	801	556	4 22	2.64	0458	9 85	5.90	11.05	20.0	248.4	2411
		3.5	1104	865	239	12.4	30.25	85	716	631	0738	1.20	.140	1019	61 9	28 3	860 5	21.80	388	780	562	4.76	2.98	.0467	11.55	7.05	11.89	22.7	246.9	2739
	224	2.3	1600	1248	352	12 3	30 25	82	1040	958	0738	1 05	130	1518	63.1	25 1	1021 0	31.10	560	1166	830	4 46	2 80	.0392	11 80	6 05	11 47	19 1	291 6	2153
															BAR = 29.10" Hg															
4-26-52	280	3.5	1535	1235	300	12.4	30 01	77	1000	923	.0740	1.05	.131	1458	63.2	33 0	998.5	30.10	535	1158	810	4 42	2.77	.0397	11 90	6.35	11 38	19.2	288.0	2197

BAR = 29 535" Hg.

PERFORMANCE DATA FOR RADIATOR NO 2

Plain Fin - 15 Fins Per Inch
Face Area - 0.0469 Ft^2
Free Flow Area - 0.0283 Ft^2
Distance Between Fins - 0 00472 Ft

Date	Hours Total Time	1. Na Flow, GPM	2. Na Inlet Temp., °F	3. Na Outlet Temp, °F	4. Na Temp. Drop, °F	5. Orifice Air Press., Inches Hg. Abs.	6 Orifice Air Press., Inches Hg. Abs.	7 Air Inlet Temp., °F	8. Air Outlet Temp., °F	9. Air Temp Rise, °F	10 Air Density, lb/ft³	11. Orifice Diff. Press., Inches H_2O	12. Air Flow, lb/sec.	13 Max Temp Diff, °F	14 Cooling Effectiveness, %	15 Heat From Na, Btu/sec.	16 Mean Air Temp., °R	17 Heat to Air, Btu/sec.	18 Outlet Temp Diff. OTD, °F	19 Inlet Temp. Diff. ITD, °F	20 Log Mean Temp. Diff. LMTD, °F	21 Air Flow, lb/sec/ft² Free Flow Area	22. Air Flow, lbsec/ft² Face Area	23. Mean Air Density, lb/ft³	24. Press Drop Across Radiator, Inches H_2O	25. ΔP for Radiator, Inches H_2O	26 Over-all Heat Transfer Coefficient, U	27. Local Heat Transfer Coefficient, h, Btu/hr-ft²-°F	28 Viscosity of Air, lb/ft sec x 10^7	29. Free Stream Reynolds Number, R_e
6-9-52	40	2.7	960	860	100	4.0	29.57	88	826	738	.0716	15	.048	876	91 3	9.3	917.0	8.80	134	772	365	1 72	1.06	.0428	3.80	2.12	5 62	7 0	238.0	680
		3 0	960	832	128	6 2	29.74	89	774	685	.0712	31	.070	871	88 7	13 2	892 0	11.86	186	743	400	2 40	1 50	.0438	6.10	3.49	6.92	10 1	236.5	994
		3 0	965	811	154	8 0	30.34	90	754	664	0732	45	.084	875	75 9	16.0	882 0	13 71	211	721	415	2 96	1 78	0456	7.80	4.65	7.72	10 8	236 0	1187
		2.7	950	780	170	10.3	30.13	90	720	630	.0724	64	.101	860	73 3	16.6	865.0	15 65	230	690	418	3 57	2.16	0460	9.90	5.95	8 72	14.4	233.0	1446
		2.7	960	781	179	11.3	30 11	91	722	631	.0725	73	.108	869	72 7	17.6	867.0	16 86	238	690	424	3.84	2.34	.0461	10 90	6.56	9.27	15 7	233 5	1550
		2.7	966	774	192	12 1	30.17	92	711	619	.0725	80	.113	874	70 8	19.5	862.0	17 19	255	682	434	3 99	2.41	.0464	11.35	6.88	9.23	15 6	233 5	1613
		2 5	1105	895	210	12.1	30.11	91	818	727	.0725	74	.108	1014	71 6	19.8	915.0	19 40	187	804	422	3.82	2 31	.0437	11 60	6.62	10 70	19 0	248 0	1457
6-11-52	90	2.5	1100	945	155	4.2	29.56	88	937	849	.0715	14	044	1012	83 7	13.0	973.0	9 16	163	857	418	1 56	.94	.0403	4.20	2 21	5.10	6.1	251 5	584
		2.5	1104	920	184	6.2	29.71	88	885	797	0719	25	063	1016	78 6	15 6	947.0	12 06	219	832	458	2 22	1.34	.0416	6.00	3.26	6.15	8 2	250.0	840
		2.7	1095	900	195	7.4	29 81	87	852	765	.0724	.34	.074	1008	76 0	17 8	930 0	14.00	243	813	471	2 63	1.59	.0426	7.15	3 98	6 93	9.9	248.0	1002
		2.7	1100	871	229	10.4	30 05	88	819	731	.0725	.60	.098	1012	72.2	20 9	914.0	17.60	281	783	490	3.46	2.09	.0435	10.10	5.74	8 36	13 1	247 0	1323
		2.7	1105	864	241	12.2	30.18	88	801	713	.0731	73	.107	1017	70 0	22 0	905.0	18.75	304	776	505	3.78	2.28	.0443	11.80	6.83	8.65	13 8	246 5	1448
6-11-52	90	2.7	1300	1060	240	12.1	30.09	89	939	850	.0728	66	.102	1211	70 0	21 4	974.0	21.50	361	971	616	3 60	2.18	.0410	11.80	6.32	8.14	12.1	267 5	1272
		2.7	1300	1080	220	10.5	30.01	89	960	871	.0725	51	089	1211	71 9	19 6	985.0	19 30	340	991	609	3.14	1.90	.0404	10.20	5 38	7.40	10.6	269.0	1103
		2.7	1295	1100	195	8.4	29.86	89	985	896	0722	36	075	1206	74.2	17 4	997.0	16 75	310	1011	591	2.65	1.60	.0398	8.20	4.26	6 60	8.9	270.0	926
		2.7	1305	1130	175	6.6	29.76	89	1039	950	.0720	23	.061	1216	78 0	15 6	1024 0	14.50	266	1041	566	2.16	1 30	.0386	6 45	3.25	5.96	7.6	272.0	748
		2.7	1305	1170	135	4.6	29.58	89	1097	1008	.0714	12	.042	1216	92 0	12 0	1053.0	10.50	208	1081	529	1 48	.90	.0372	4.50	2.18	4.62	5.0	274 0	511
6-12-52	110	2.7	1500	1240	260	10.6	30.00	87	1050	963	.0726	43	.083	1413	68 2	22.0	1029.0	19.65	450	1153	748	2 93	1.77	.0386	10.40	5 24	6.12	7.7	286.0	968
		2.7	1510	1230	280	12.0	30.11	87	1098	1011	.0730	.58	.097	1423	71.2	23.6	1053 0	24.55	412	1143	717	3.43	2.07	0379	11.90	5.90	7.97	11.3	286.0	1131
		2.6	1590	1300	290	12.0	30.03	90	1171	1081	.0730	54	.093	1500	72 1	24 1	1091 0	24.80	419	1210	746	3 78	1 98	.0368	11.80	5.68	7.75	10.9	291.0	1066
6-13-52	135	2.7	1600	1310	290	12.2	30.24	85	1142	1057	.0735	.57	.096	1515	69 8	24 1	1074.0	25.30	458	1225	778	3.39	2.05	.0373	12.00	5.85	7.58	10 5	292.0	1096

PERFORMANCE DATA FOR RADIATOR NO 3

Interrupted Fin - 15 Fins Per Inch
Face Area - 0 0400 Ft^2
Free Flow Area - 0 0238 Ft^2
Distance Between Fins - 0 00472 Ft

Date	Hours Total Time	1 Ma Flow, GPM	2 Ma Inlet Temp., °F	3 Ma Outlet Temp, °F	4 Ma Temp Drop, °F	5 Orifice Air Press, Inches H_2O	6 Orifice Air Press, Inches Hg Abs	7 Air Inlet Temp, °F	8 Air Outlet Temp, °F	9 Air Temp Rise, °F	10 Air Density, lb/ft³	11 Orifice Diff Press, Inches H_2O	12. Air Flow, lb/sec	13 Max Temp Diff, °F	14 Cooling Effectiveness, %	15 Heat From Ma, Btu/sec	16 Mean Air Temp, °R	17 Heat to Air, Btu/sec	18 Outlet Temp Diff OTD, °F	19 Inlet Temp Diff ITD, °F	20 Log Mean Temp Diff LMTD, °F	21 Air Flow, lb/sec/ft² Free Flow Area	22 Air Flow, lb/sec/ft² Face Area	23 Mean Air Density, lb/ft³	24. Press Drop Across Radiator, Inches H_2O	25 ΔP for Radiator, Inches H_2O	26 Over-all Heat Transfer Coefficient, U	27 Local Heat Transfer Coefficient, h, Btu/hr-ft²-°F	28 Viscosity of Air, lb/ft sec x 10⁷	29 Free Stream Reynolds Number, R_e
9/3/52	3	2 2	890	785	105	3 7	29 67	80	816	736	0730	10	042	810	91 0	8 0	908 0	7 48	74	705	280	1 74	1 04	0434	3 50	1 99	6 75	9 8	180 0	914
	3	2.2	895	774	121	4 3	29 71	80	808	728	0730	14	048	815	89 1	9 4	904 0	8 55	87	694	292	2 02	1 20	0436	4 25	2 42	7 40	11 3	179 5	1062
	4	2.2	905	755	150	6 0	29 85	80	784	704	0740	24	062	825	85 3	11 6	892 0	10 75	121	675	322	2 62	1 56	0448	6 00	3.51	8 45	13 9	178 0	1392
	5	2.3	900	735	165	6 9	29.89	80	762	682	0740	31	071	820	83 2	13 2	881 0	11 85	138	655	332	2 98	1 78	0454	6 80	4 04	9 00	15.3	176 5	1595
	5	2.3	900	722	178	7 8	29 95	81	746	665	0740	36	076	819	81 3	14 4	873 5	12 45	154	641	341	3 21	1 91	0458	7 55	4 52	9 22	15 5	175 6	1728
	6	2 4	900	721	179	9 3	30 04	81	729	648	0740	44	085	819	79 0	15 0	865 0	13 45	171	640	355	3 57	2 12	0463	9 15	5 54	9 56	16 7	174.5	1932
	6	2 4	900	715	185	9 8	30 10	81	724	643	0740	52	092	819	78 5	15 6	862.5	14 40	176	634	359	3 84	2 28	0464	9 50	5 76	10 10	18 2	174 1	2084
	6	2.4	900	705	195	11.0	30 19	82	708	626	0740	62	101	818	76 6	16 4	855 0	15 45	192	623	366	4 24	2 52	0469	10 60	6 50	10 65	19 8	173 2	2312
	6	2.4	905	700	205	12 1	30 27	82	693	611	0740	70	107	823	74 3	17 2	847 5	16 00	212	618	380	4 50	2 68	0473	11 80	7 30	10 65	19 8	172 2	2464
9/4/52	26	2 4	700	625	75	2 1	29 65	78	643	565	0740	10	042	622	90 9	6 6	820 5	5 76	57	547	380	1 76	1 05	0485	2 00	1 26	6.76	10 1	168 7	987
	27	2 4	700	616	84	3 8	29 65	78	631	553	0740	14	049	622	88 9	7 4	814 5	6 58	69	538	228	2 06	1 22	0489	3 80	2 42	7 30	11 4	167 8	1158
	28	2 4	700	600	100	5.3	29 86	78	607	529	0740	24	063	622	85 0	8 8	802 5	8 10	93	522	248	2.64	1 58	0496	5 20	3 37	8 25	13 8	166 3	1502
	28	2 4	698	588	110	6 3	29 94	79	592	513	0740	31	071	619	83 0	9 6	795 5	8 85	106	509	259	2 98	1 78	0501	6 10	4 00	8 65	14 9	165 2	1704
	28	2 4	700	581	119	7 0	29.99	79	583	504	0740	36	077	621	81 1	10 4	791 0	9 41	117	502	264	3 24	1 92	0504	6 70	4 41	9 02	15 9	164 6	1855
	29	2 4	700	578	122	7 6	30 01	79	576	497	0740	43	084	621	80 0	10 7	787 5	10 30	124	499	270	3 52	2.10	0506	7 30	4 82	9 65	17 7	164 0	2031
	29	2 4	700	571	129	8 5	30 08	79	563	484	0740	50	091	621	78 0	11 3	781 0	10 70	137	492	288	3 82	2 28	0511	8 20	5 48	9 40	17 0	163 0	2214
	30	2.3	700	565	135	9.7	30 15	80	553	473	0740	.60	099	620	76 4	11 4	776 5	11 38	147	485	284	4 16	2 48	0515	9 40	6 32	10 10	19 1	162 2	2420
	30	2.3	702	560	142	11.0	30 25	80	539	459	0740	72	.108	622	73 7	12 0	769.5	12 08	163	480	294	4 54	2.70	0519	10 60	7 19	10 40	20 0	161 1	2658
	31	2 3	700	548	152	12 1	30.27	81	526	445	0740	84	117	619	72 0	13 6	763 5	12.65	174	467	298	4 92	2.92	0524	11 90	8 15	10 75	21 2	160 2	2896
9/5/52	50	2.4	1103	980	123	4 0	29 85	78	1013	935	0740	10	040	1025	91 1	10 2	1005 5	9 07	80	902	338	1 66	0 99	0396	4 00	2 07	6 80	9 6	192 7	813
	51	2 4	1100	960	140	4.8	29 89	79	999	920	0740	13	045	1021	90 0	11 6	999 0	10 40	101	881	359	1 95	1 16	0399	4 70	2 45	7 32	10 8	192 0	960
	52	2 4	1101	931	170	6 4	29 98	79	971	892	0740	20	058	1022	87 0	14 1	985 0	12 50	130	852	384	2 42	1.44	0405	6.30	3 34	8.23	12 8	190 1	2000
	52	2 4	1100	911	189	7 5	30 06	79	949	870	0740	26	066	1021	85 0	15 6	974 0	14 00	151	832	398	2 75	1 64	0410	7 30	3 91	8 90	14 4	188 6	1377
	52	2.4	1100	901	199	8 3	30 11	80	932	852	0740	32	073	1020	83 6	16 5	966 0	15 30	168	821	411	3 06	1 82	0414	8 10	4 38	9 40	15 6	187 6	1543
	53	2 4	1100	890	210	9 5	30 20	80	911	831	0740	40	081	1020	81 5	17 4	955 5	16 60	189	810	426	3 40	2 02	0418	9 30	5 08	9 85	16 7	186 2	1725
	53	2 4	1103	894	209	10 3	30 24	81	900	819	0740	46	088	1022	80 0	17 3	950 5	17 60	203	813	439	3 68	2 18	0421	10 10	5 56	10 10	17 4	185 6	1870
	54	2 4	1100	866	234	11 8	30 34	81	876	795	0740	58	097	1019	78 0	19 4	938 5	19 00	224	785	450	4 08	2 42	0427	11 50	6 42	10 10	19 0	184 0	2090
	55	2 4	1100	861	239	12 3	30 34	81	864	783	0740	61	099	1019	77 0	19 8	932 5	19 10	236	780	456	4 16	2 48	0429	12 10	6 78	10 60	18 8	183 2	2143
9/6/52	73	2 3	1300	1151	149	4 4	29 83	80	1187	1107	0740	08	037	1220	90 5	11 3	1093 5	10 20	113	1071	426	1 56	0 92	0365	4 35	2 08	6 05	7 7	204 2	718
	73	2 3	1301	1132	169	5 5	29 90	79	1180	1101	0740	12	042	1222	90 0	12 8	1089 5	11 60	120	1053	430	1 77	1 06	0366	5 30	2 54	6 81	9 3	203 6	822
	73	2 3	1307	1111	196	6 4	29 97	80	1167	1087	0740	16	052	1227	88 6	14 8	1083 5	14 00	140	1021	443	2 18	1 30	0369	6 35	3 06	7 97	11 8	202 9	1016
	73	2 3	1300	1083	217	7 6	30 06	80	1144	1064	0740	22	061	1220	87 0	16 5	1072 0	16 10	156	1003	447	2 56	1 52	0373	7 50	3 66	9 08	14 3	201 4	1201
	73	2 3	1300	1056	244	9 2	30 17	80	1107	1017	0745	33	074	1220	83 1	18 5	1048 5	18 55	193	976	483	3 08	1 84	0384	9 10	4 56	9 65	15 6	198 3	1470
	73	2 3	1302	1031	271	11 1	30 31	80	1073	993	0745	44	085	1212	82 0	20 6	1036 5	21 00	229	951	506	3 57	2 12	0391	11 00	5 62	10 50	17 7	196 7	1714
	73	2 3	1300	1013	287	12 4	30 39	80	1048	968	0750	52	093	1220	79 3	21 8	1024 0	22 40	252	923	516	3 90	2 32	0396	12.10	6 26	11 00	19.0	195 1	1890
9/8/52	126	2 3	1490	1242	248	7 6	30.04	87	1048	1234	0730	18	054	1403	87 9	18 6	1164 0	16 70	169	1155	513	8 23	1 35	0343	7 40	3 32	8 23	12 0	213 3	1044
	126	2 3	1494	1192	302	10 1	30 22	87	1273	1186	0735	31	071	1407	84 3	22 6	1110 0	21 00	221	1105	548	2 98	1 78	0362	10 00	4 73	9 68	15 2	206 3	1364
	126	2 3	1500	1163	337	12.2	30 36	87	1236	1149	0735	44	.085	1413	81 4	25 2	1091 5	24 40	264	1076	561	3 57	2 12	.0368	12 00	5 77	11 00	18 3	203 9	1653
	126	1.7	1480	1233	247	4 8	29 82	88	1331	1243	0720	08	038	1392	89 3	13 6	1169 5	12 50	149	1145	989	1 58	0.94	0337	4 60	2 02	6 45	8.4	214 0	695
	290	2.4	1500	1180	320	11 6	30 23	84	1134	1050	0739	47	086	1416	74 2	25 0	1069 0	22 50	366	1096	670	3 61	2 15	0377	11 50	5 66	8 46	12.4	201 0	1696
10/21/52	1030	2 0	1698	1248	450	12.0	30 25	83	1300	1217	0741	42	082	1615	75 4	30 7	1152 0	25 27	398	1165	714	3 45	2 05	0349	11.70	5 34	8 93	13 1	211 8	1536
	1200	2.0	1600	1225	375	12 3	30 70	74	1300	1226	0764	37	.079	1526	80 3	25.6	1147 0	24 50	300	1151	633	3 32	1 98	0356	12.20	5.68	9 77	14.7	211 1	1484

RADIATOR PERFORMANCE COMPUTATIONS

Data Sheet Column Number	Item	Source
1	Na flow, gpm	Electromagnetic flowmeter
2	Na inlet temperature, ^{o}F	Brown recorder
3	Na outlet temperature, ^{o}F	Brown recorder
4	Na temperature drop, ^{o}F	= Column 2 - Column 3
5	Orifice air pressure, in. H_2O	Water manometer
6	Orifice air pressure, in. Hg abs.	= Barometer reading + Column 5/ specific gravity of Hg
7	Air inlet temperature, ^{o}F	Room temperature at blower inlet
8	Air outlet temperature, ^{o}F	Average of six readings from temperature probes in a shielded duct 9 in. downstream from radiator outlet face
9	Air temperature rise, ^{o}F	= Column 8 - Column 7
10	Air density, lb/ft^3	$= .0765\ lb/ft^3 \times \frac{520^{o}R}{\text{Column 7} + 460} \times \frac{\text{Column 6}}{29.92}$
11	Orifice differential pressure, in. H_2O	Inclined manometer
12	Air flow, lb/sec	Orifice calibration curve
13	Max. temperature difference, ^{o}F	= Column 2 - Column 7
14	Cooling effectiveness, %	$= \frac{\text{Column 9}}{\text{Column 13}}$
15	Heat from Na, Btu/sec	$= w_n\ c_{p_n}\ \Delta T_n$ where w_n = weight flow of Na lb/sec; c_{p_n} = specific heat of Na (constant pressure); ΔT_n = Na temperature drop = Column 6
16	Mean air temperature, ^{o}R	= 1/2 Column 9 + Column 7 + 460

Data Sheet Column Number	Item	Source
17	Heat to air, Btu/sec = $W_a c_{p_a} \Delta T_a$	where W_a = weight flow of air lb/sec = Column 12 c_{p_a} = specific heat of air (constant pressure) at temperature in Column 16 ΔT_a = air temperature rise = Column 9
18	Outlet temperature difference OTD, ^oF	= Column 2 - Column 8
19	Inlet temperature difference ITD, ^oF	= Column 3 - Column 7
20	Log mean temperature difference LMTD, ^oF	$= \dfrac{\text{Column 19 - Column 18}}{\log_e \dfrac{\text{Column 19}}{\text{Column 18}}}$
21	Air flow, lb/sec/ft^2 free flow area	= Column 12 ÷ free flow area
22	Air flow, lb/sec/ft^2 face area	= Column 12 ÷ face area
23	Mean air density, lb/ft^3	$= \text{Column 10} \times \dfrac{\text{Column 7} + 460}{\text{Column 16}}$
24	Pressure drop across radiator, in. H_2O	- Water manometer
25	$\sigma\Delta P$ for radiator, inches H_2O	$= \dfrac{\text{Column 23} \times \text{Column 24}}{.0765}$
26	Over-all heat transfer coefficient, U, $\dfrac{\text{Btu}}{\text{Hr-ft}^2\text{-}^oF}$	$= \dfrac{Q}{A\Delta T}$ where Q = heat to air, Btu/hr = Column 17 x 3600 ΔT = log mean temperature difference = Column 20 A = heat transfer area of radiator (see Table III)
27	Local heat transfer coefficient, h, Btu/hr-ft^2-^oF	- read from Figure 20 using value of U in Column 26
28	Viscosity of air μ, lb/ft sec x 10^7	- See "Air Tables," Keenan and Kaye, p. 34, using temperature in Column 16
29	Free stream Reynolds number, R_e	$= \dfrac{\text{(Column 21)(twice distance between fins, ft)}}{\text{Column 28}}$

APPENDIX B

EXAMPLE OF THE USE OF FIGURE 19

(Logarithmic Mean Temperature Difference Against Cooling Effectiveness for Various Ratios of Primary Fluid Temperature Change to Inlet Temperature Difference)

Consider a counterflow heat exchanger shown below.

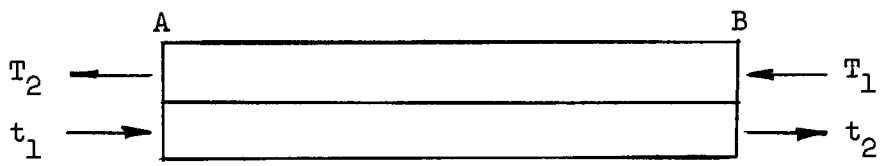

where T's refer to primary fluid temperatures
and t's refer to secondary fluid temperatures.

Heating effectiveness* is defined as

$$\eta = \frac{t_2 - t_1}{T_1 - t_1}$$

and calling $t_2 - t_1 = \Delta t$
and $T_1 - t_1$ = ITD (inlet temperature difference)

then $$\eta = \frac{\Delta t}{ITD}$$

and $$t_2 = t_1 + \Delta t = t_1 + \eta(ITD)$$

Logarithmic mean temperature difference is defined as:

$$LMTD = \frac{\Delta T_A - \Delta T_B}{\log_e\left(\frac{\Delta T_A}{\Delta T_B}\right)} = \frac{(T_2 - t_1) - (T_1 - t_2)}{\log_e\left(\frac{T_2 - t_1}{T_1 - t_2}\right)}$$

*Sometimes called cooling effectiveness.

$$\text{LMTD} = \frac{(t_2-t_1) - (T_1 - T_2)}{\log_e\left(\frac{T_2-t_1+T_1-T_1}{T_1-t_2+t_1-t_1}\right)} = \frac{(t_2-t_1) - (T_1-T_2)}{\log_e\left[\frac{(T_1-t_1) - (T_1-T_2)}{(T_1-t_1) - (t_2-t_1)}\right]}$$

Calling $T_1-T_2 = \Delta T$ and dividing both sides of the equation by ITD and the numerator and denominator of the log term by (T_1-t_1) there results

$$\frac{\text{LMTD}}{\text{ITD}} = \frac{1 - \frac{\Delta T}{\text{ITD}}}{\log_e\left(\frac{1 - \frac{\Delta T}{\text{ITD}}}{1 - \eta}\right)}$$

Referring to the diagram on page 90 let us assume that T_1 and t_1 are known or fixed. We then know the value of ITD since ITD = T_1-t_1. For any desired value of T_2 we must solve for t_2. Using the usual equations for heat transfer

$$Q_1 = wc_p(t_2-t_1)$$

$$Q_2 = UA(\text{LMTD})$$

we can assume a value for t_2, solve for LMTD and repeat this process until $Q_1 = Q_2$.

By means of Figure 19 this work is greatly simplified. Since $Q_1 = Q_2$ then

$$wc_p(t_2-t_1) = UA(\text{LMTD})$$

$$\text{LMTD} = \frac{wc_p}{UA}(t_2-t_1) = \frac{wc_p}{UA}\,\Delta t$$

Dividing both sides of the equation by ITD

$$\frac{\text{LMTD}}{\text{ITD}} = \frac{wc_p}{UA}\eta \qquad \text{since} \qquad \frac{\Delta t}{\text{ITD}} = \eta$$

$$\frac{\eta}{\frac{LMTD}{ITD}} = \frac{UA}{wc_p}$$

where U, A, w, and c_p are all known quantities. If we chose a value of T_2, we then know $T_1 - T_2 \equiv \Delta T$ and hence the value of $\frac{\Delta T}{ITD}$.

Since we now know the values of $\frac{\Delta T}{ITD}$ and $\frac{\eta}{\frac{LMTD}{ITD}}$, we determine their point of intersection on Figure 19. This then determines the value of η and $\frac{LMTD}{ITD}$ which allows us to solve for LMTD.

APPENDIX C

PUMP AND LINE WEIGHT STUDY
for
A FULL-SCALE TURBOJET NaK SYSTEM
(Sample Calculation)

Assumptions:

1. Coolant composition -- 54°/o Na - 46°/o K
2. NaK inlet temperature to radiator -- 1600°F
3. NaK outlet temperature from radiator -- 1100°F
4. Pump weight -- 2 lb/hp input
5. Pump efficiency -- 70°/o
6. NaK pressure drop through radiator -- 36 lb/in^2
7. NaK pressure drop through shield and intermediate heat exchanger -- 60 lb/in^2
8. Specific heat of NaK -- $c_p = 0.26 \frac{Btu}{lb\text{-}^oF}$
9. Radiator weight per engine -- 1580 lb(wet)
10. Distance from reactor to radiator -- 20 ft
11. Pipeline pressure drop -- 1 velocity head pressure drop per 50 pipe diameters of length
12. Pipeline material -- Type 316 stainless steel
13. Allowable steel stress -- 1,500 lb/in^2 at 1600°F
    11,000 lb/in^2 at 1100°F

    These figures were based on an allowable stress 20°/o of the ultimate tensile strength or 33°/o of the stress for rupture in 1000 hr, or the stress for 1°/o creep in 1000 hr, whichever was the lowest.
14. Heat flow -- 18,500 kw or $63 \times 10^6 \frac{Btu}{hr}$ per engine
15. Specific weight of NaK 1300°F -- $0.74 \frac{gm}{cc}$ or 46 lb/ft^3.

SCHEMATIC DRAWING FOR PUMP AND LINE WEIGHT STUDY

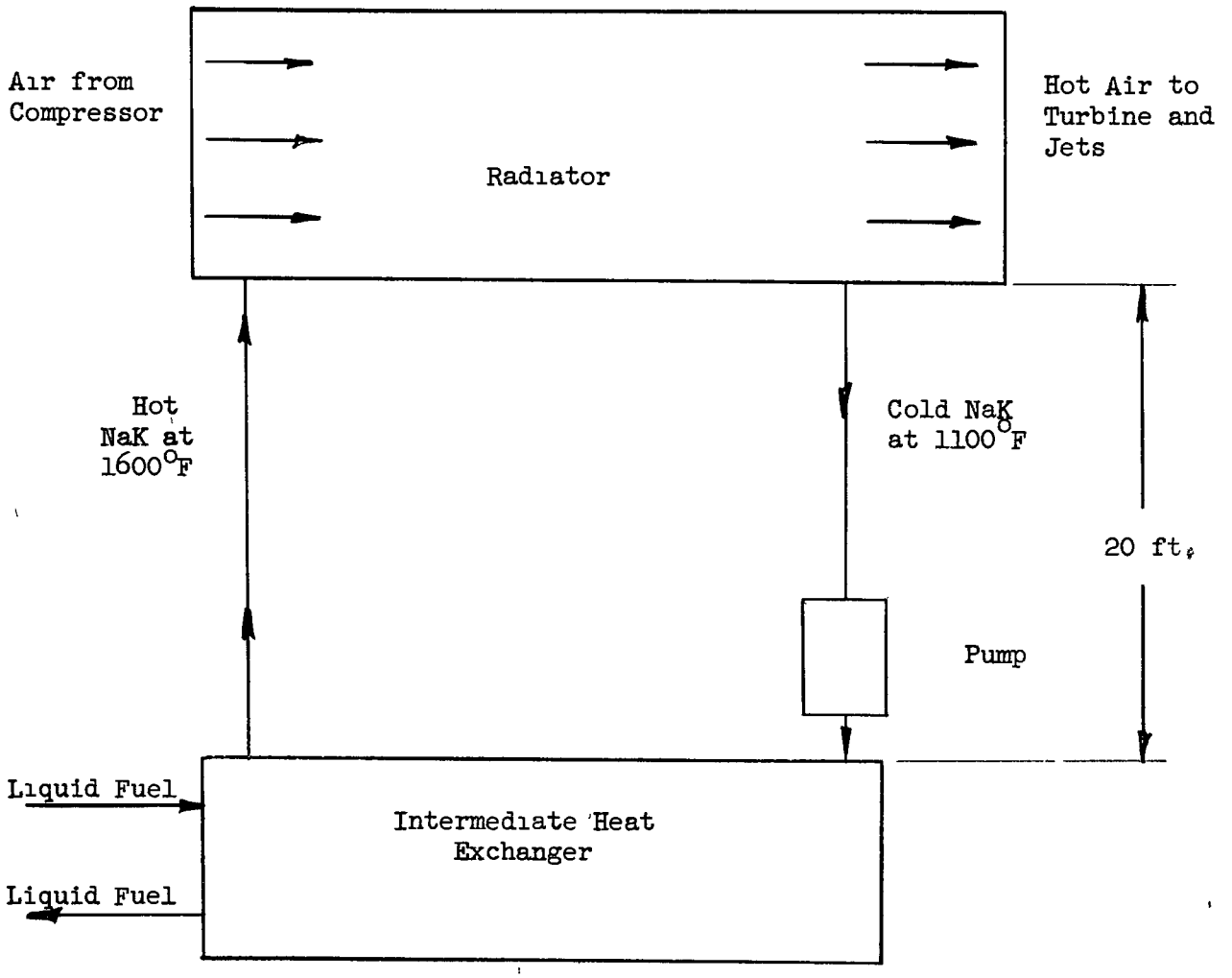

Sample Computations:

Assumed pipe data -- 3.500 in. schedule 40 Type 316 stainless steel pipe
Weight per ft = 9.2 lb.
I.D. = 3.548 in.
Wall thickness = 0.226 in.
Flow area = 0.06865 ft^2

$Q = c_p w \Delta T$ where Q = heat transferred in radiator = $63 \times 10^6 \frac{Btu}{Hr}$

c_p = specific heat of NaK = $0.26 \frac{Btu}{lb\text{-}^oF}$

$63 \times 10^6 = 0.26\ w\ (500)$ w = weight flow of NaK lb/hr

$w = 48.5 \times 10^4$ lb/hr ΔT = NaK temperature drop through radiator = 500^oF

Volume flow of NaK - V - $\frac{ft^3}{min}$

$V = 48.5 \times 10^4$ lb/hr = 176 ft^3/min

NaK pipe velocity - v - ft/sec

$v = 176\ ft^3/min \times 1\ min/60\ sec \times 1/0.0685\ ft^2 = 42.8$ ft/sec

Dynamic head - h - lb/in^2 of NaK for v = 42.8 ft/sec

$h = \rho v^2/2$ where ρ = density of sodium $\frac{46\ lb/ft^3}{g}$

$$h = \frac{46\ lb/ft^3}{32.2\ ft} \times \frac{(42.8\ ft/sec)^2}{2} \times 1\ ft^2/144\ in^2$$

$h = 9.09\ lb/in^2$

Pressure drop through piping - ΔP - lb/in^2

$$\Delta P = \frac{40\ ft \times 12\ in/ft \times 9.09\ lb/in^2}{3.548\ in \times 50}$$

$\Delta P = 24.60\ lb/in^2$

Total head to be developed by pump - H_T - lb/in^2

H_T = pressure drop through radiator + pressure drop through shield + pressure drop through pipe

$H_T = 36 + 60 + 24.60 = 120.60\ lb/in^2$

Pump power required - P_p - HP

P_p = total head x capacity = 120.60 x 176 x 144 x 1 hp/33,000 x 1/.7

P_p = 132 hp

Pump weight - w_p - lb

w_p = 132 hp x 2 lb/hp

w_p = 264 lb

Pipe weight - w_{pi} - lb

w_{pi} = 40 ft x 9.2 lb/ft

w_{pi} = 368 lb

Weight of NaK holdup in pipe - w_{NaK} - lb

w_{NaK} = 40 ft x 0.06865 ft^2 x 46 lb/ft^3

w_{NaK} = 126 lb

Total NaK system weight - w_T - lb

$w_T = w_p + w_{pi} + w_{NaK}$ + weight of radiator (wet)

w_T = 264 + 368 + 126 + 1580

w_T = 2338 lb

If we wish to design the pipe wall thickness on the basis of allowable wall stresses, we proceed as follows:

Assume a 5 lb/in^2 suction pressure

Pressure in pipe at 1100°F = 125.6 lb/in^2

Pressure in pipe at 1600°F = 65.6 lb/in^2 (60 lb/in^2 lost through shield)

$t = \frac{pD}{2s}$ where t = pipe thickness - in.

D = pipe diameter = 3.548 in.

p = pressure in pipe = 125.6 lb/in^2 at 1100°F

and 65.6 lb/in^2 at 1600°F

s = allowable wall stress in pipe = 11,000 lb/in^2 at 1100°F

and 1500 lb/in^2 at 1600°F

at 1100°F

$$t = \frac{125.6 \times 3.548}{2 \times 11{,}000} = 0.0203 \text{ in}$$

at 1600°F

$$t = \frac{65.6 \times 3.548}{2 \times 1500} = 0.0776 \text{ in}$$

weight per ft = 3.03 lb

weight of 40 ft = 121 lb

w_T = 2091 lb

APPENDIX D

PERFORMANCE CALCULATIONS FOR A MODIFIED SAPPHIRE TURBOJET ENGINE

Two tables are presented below giving the method of calculating the performance of a modified Sapphire turbojet engine. The first table outlines the procedure used when the radiator proportions are varied while the second table deals with the performance calculations of the Sapphire engine with a fixed radiator configuration for various altitudes and flight Mach number.

PERFORMANCE CALCULATIONS FOR A MODIFIED SAPPHIRE TURBOJET ENGINE FOR VARIOUS RADIATOR DEPTHS AND RADIATOR INLET FACE AREAS

Corrected compression ratio = 4.00:1
Engine weight = 2785 lb
Radiator weight = 90 lb/ft^3
Sea level air flow = 117 lb/sec

Radiator inlet face area = 10, 12, 15 ft^2
Engine diameter = 37.5 in.
Radiator depth = 12, 14, 16 in.

Method of Computation

Altitude, H - ft	Chosen arbitrarily
Mach number, M	Chosen arbitrarily
Radiator inlet face area, A_R - ft^2	Chosen as 10, 12, 15 ft^2
Air passage length, L_R - in.	Chosen as 12, 14, 16 in.
Air flow, F - lb/sec	$F = 117 \times \sigma \times Z_r \times \frac{T_o}{T_1}$ where 117 = sea level air flow lb/sec σ = altitude density ratio Z_r = ram compression ratio (see page 100) T_o = ambient air temperature - ^oR T_1 = compressor inlet temperature ^oR (see page100)

Method of Computation (continued)

Radiator air flow, G_R - lb/sec-ft^2 of radiator inlet area	$G_R = \frac{G}{A_R}$
Radiator inlet temperature, T_2 - ^oR	See page 100
Initial temperature difference, ITD - ^oR	ITD = 2060 - T_2 (2060^oR is Na inlet temp.)
Cooling effectiveness, η	Read from Fig. 22 using value of G_R and L_R
Turbine air inlet temperature, t_3 - ^oF	$t_3 = \left[T_2 - 460\right] + \left[\eta \, ITD\right]$
Specific thrust, I - lb/lb air/sec	From charts in ORNL Report ANP-57
Specific heat consumption, C_s - Btu/sec-lb thrust	From charts in ORNL Report ANP-57
Radiator weight per engine, W_R - lb	$W_R = 90 \text{ lb/ft}^3 \times A_R \times L_R/12$
Total thrust, τ - lb	$\tau = I \times G$
Engine weight per lb of thrust, W_e	$W_e = \frac{2785}{\tau}$
Radiator weight per lb of thrust, W_R	$W_R = \frac{W_{Re}}{\tau}$
Power consumption, C_T - kw	$C_T = 1.05479 \times \tau \times C_s$ $\left(1.05479 = \frac{3600 \text{ sec/hr}}{3413 \frac{\text{Btu}}{\text{kw - hr}}}\right)$
Pump and line weight per lb of thrust, W_p	$W_p = \frac{0.04 \, C_T}{\tau}$ (0.04 is an empirical factor from pump and line weight studies)
Total engine, radiator, pump and line weight, W_T - lb/lb thrust	$W_T = W_e + W_R + W_p$

PERFORMANCE CALCULATION METHODS FOR A MODIFIED SAPPHIRE TURBOJET ENGINE FOR A 12 INCH RADIATOR DEPTH AND A RADIATOR FRONTAL AREA OF 12 FT^2

Corrected compression ratio = 4.00:1
Engine weight = 2785 lb
Radiator weight = 1080 lb
Sea level air flow = 117 lb/sec

Radiator depth = 12 in
Radiator inlet face area = 12 ft^2
Engine diameter = 37.5 in.

Method of Computation

Altitude - H - ft	Chosen arbitrarily
Mach number - M	Chosen arbitrarily
Altitude density ratio - σ	Taken from tables of properties of standard air
Altitude pressure ratio - P_{ra}	Taken from tables of properties of standard air
Ambient air temperature - T_o - ^oR	Taken from tables of properties of standard air
Ram compression ratio - Z_r	$Z_r = 1 + e_r \left\{ \left[1 + \frac{\gamma-1}{2}(M^2) \right]^{\gamma/\gamma-1} - 1 \right\}$ where e_r = adiabatic efficiency of ram compression; M = Mach number; $\gamma = \frac{C_p}{C_v}$
Compressor inlet temperature - T_1 - ^oR	$T_1 = T_o \left[1 + \frac{\gamma-1}{2}(M^2) \right]$
Compressor outlet temperature - T_2 - ^oR	$T_2 = T_1 + 250$ (see note on page 102)
Corrected engine compression ratio - Z_e	$Z_e = \left[\frac{250}{T_o(1 + \frac{\gamma-1}{2}(M^2)} + 1 \right]^{\gamma/\gamma-1}$
Over-all compression ratio - Z_T	$Z_T = Z_r \times Z_e$
Air flow - G - lb/sec	$G = 117 \times \sigma \times Z_r \times \frac{T_o}{T_1}$
Ratio of compression inlet air density to sea level air density - σ_c	$\sigma_c = \sigma \times Z_r \times \frac{T_o}{T_1}$

Method of Computation (continued)

Ratio of radiator inlet air density to sea level air density - σ_r	$\sigma_r = \sigma \times Z_T \times \frac{T_o}{T_2}$
Compressor outlet pressure - P_2 - lb/ft^2	$P_2 = P_{ra} \times Z_T \times P_o$ where P_o = sea level atmospheric pressure in lb/ft^2
Radiator air flow - G_R - $lb/sec/ft^2$ of radiator inlet face area	$G_R = \frac{G}{12}$
Heating effectiveness - η	Read from Fig. 22 using value for G_R
Initial temperature difference - ITD ^oF	ITD = 2060 - T_2 (Na inlet temperature is assumed to be 2060 ^oR)
Turbine air inlet temperature - t_3 - ^oF	$t_3 = \left[T_2 - 460\right] + \left[\eta \cdot ITD\right]$
Pressure drop across radiator - ΔP_r - inches H_2O	Read from Fig. 16 using values for G_R and σ_r
Pressure drop across radiator - ΔP_R - lb/ft^2	$\Delta P_R = \frac{\Delta P_r}{12 \frac{in}{ft}} \times 62.4\ lb/ft^3 \times 1.1$ (1.1 is a calibration factor for manometer)
Pressure drop across radiator as % of radiator inlet pressure - % ΔP	$\% \Delta P = \frac{\Delta P_R}{P_2}$
Specific thrust - I - lb/lb air/sec	From charts in ORNL Report ANP-57
Total thrust - τ - lb	$\tau = I \times G$
Specific heat consumption - C_s - Btu/sec-lb thrust	From charts in ORNL Report ANP-57
Total heat consumption - C_T - kw	$C_T = 1.05479 \times C_s \times \tau$ $\left(1.05479 = \frac{3600\ sec/hr}{3413\ Btu/kw\text{-}hr}\right)$

Method of Computation (continued)

Lb engine weight per lb thrust - W_e	$W_e = \frac{2785}{\tau}$
Lb radiator weight per lb thrust - W_R	$W_R = \frac{1080}{\tau}$
Pump and line weight - W_p - lb/lb thrust	$W_p = 0.04 \times \frac{C_T}{\tau}$ (0.04 is an empirical factor from pump and line weight studies)
Total engine, radiator, pump and line weight - W_T - lb/lb thrust	$W_T = W_e + W_R + W_p$

The modified Sapphire engine was assumed to have a compression ratio of 4.00:1 at standard sea level conditions and M = 0.

Let T_1 = compressor inlet temperature °R

T_2 = compressor outlet temperature °R

ΔT = temperature rise through compressor = $T_2 - T_1$

$$\frac{T_2}{T_1} = \frac{T_1 + \Delta T}{T_1} = 1 + \frac{\Delta T}{T_1}$$

$$\frac{T_2}{T_1} = Z_e^{\frac{\gamma-1}{\gamma}}$$ where Z_e = sea level compression ratio of compressor

$$\gamma = \frac{C_p}{C_v}$$

$$\Delta T = T_1 \left[Z_e^{\frac{\gamma-1}{\gamma}} - 1 \right]$$

for $T_1 = 520°R$

$Z_e = 4$

$\gamma = 1.395$

$\Delta T = 250°F$

Since ΔT depends only on tip speed*, ΔT will be the same for all conditions since a constant compressor speed and efficiency is assumed.

---

*Reference 1, p. 30

ESTIMATED PERFORMANCE OF A MODIFIED WRIGHT TURBOJET ENGINE

Corrected Compression Ratio	4.00 1	Na ΔT Tarough Radiator	400°F
Engine Weight	3100 lb	Engine Diameter	44 5 in
Engine Length	140 in	S L Air Flow	220 lb/sec
Radiator Weight	1500 lb	Radiator Inlet Temperature	16 7 ft°
Radiator Depth	12 in		

Altitude, H - ft	Mach Number - M	Altitude Density Ratio - σ	Altitude Pressure Ratio - P_{ra}	Ambient Air Temperature, T_o - °R	Ram Compression Ratio, τ_r	Compressor Inlet Temperature, T_1 - °R	Compressor Outlet Temperature, T_2 - °R	Corrected Engine Compression Ratio - τ_e	Over-all Compression Ratio, τ_T	Air Flow, G - lb/sec	Ratio of Compression Inlet Air Density to Sea Level Air Density, σ_c	Ratio of Radiator Inlet Air Density to Sea Level Air Density - σ_r	Compression Outlet Pressure, P_2 - lb/ft²	Radiator Air Flow, G_R - lb/sec/ft² of Radiator Inlet Face Area	Heating Effectiveness - η	Initial Temperature Difference, ITD - °F	Turbine Air Inlet Temperature, t_3 - °F	Pressure Drop Across Radiator, ΔP_r - in H_2O	Pressure Drop Across Radiator, ΔP_R - lb/ft²	Pressure Drop Across Radiator as % of Radiator Inlet Pressure - $\%\Delta P$	Specific Thrust I - lb/lb air/sec	Total Thrust τ - lb	Specific Heat Consumption, C_s - Btu/sec-lb thrust	Total Heat Consumption C_T - kw	Lb Engine Weight per lb Thrust - W_e	Lb Radiator Weight per lb Thrust - W_R	Pump and Line Weight, W_p - lb/lb Thrust	Total Engine, Radiator, Pump and Line Weight, W_T - lb/lb Thrust
0	0	1.0000	1 0000	520	1 000	520	770	4 000	4 000	220	1 000	2 700	8464	13 20	540	1290	1007	26 0	148 72	1 76	47 2	10384	3 90	42716	0 2985	0 1445	0 1645	0 6075
0	3	1 0000	1 0000	520	1.055	529	779	3 930	4 146	228	1 037	2 770	8773	13 68	534	1281	1003	26 5	151 58	1 73	39 0	8892	5 10	47834	0 3486	0 1687	0 2152	0 7325
0	.6	1 0000	1 0000	520	1 250	559	809	3 700	4 625	256	1 163	2 970	9786	15 35	510	1251	987	28 5	163 02	1 67	31 3	8013	6 24	52741	0 3869	0 1872	0 2633	0 8374
0	9	1.0000	1.0000	520	1.595	605	855	3 400	5 423	302	1 371	3 300	11475	18 11	474	1205	966	30 5	174 46	1 52	24 5	7399	7 29	56894	0 4190	0 2027	0 3076	0.9293
15000	3	0.6291	0 5642	465	1 055	474	724	4 450	4 695	143	0 651	1 897	5605	8 58	615	1336	1086	20 2	115 54	2 06	42 5	6078	4 90	31414	0 5100	0 2468	0 2067	0.9635
15000	6	0.6291	0 5642	465	1 250	500	750	4 200	5 250	161	0 731	2 047	6268	9.66	591	1310	1064	22 4	128 13	2 04	34 5	5555	6 00	35156	0 5580	0 2700	0 2531	1 0811
15000	9	0 6291	0 5642	465	1 595	541	791	3 830	6 109	190	0 862	2 258	7293	11 40	562	1269	1044	26 0	148 72	2 04	27 5	5225	6 98	38469	0 5933	0 2871	0 2945	1 1749
35000	3	0.3098	0 2351	393	1 055	400	650	5 550	5 850	71	0 321	1 096	2910	4 26	725	1410	1212	13.8	78 94	2 71	47 7	3387	4 70	16791	0.9153	0.4429	0 1983	1 5565
35000	6	0 3098	0 2351	393	1 250	422	672	5 150	6 440	79	0 361	1.168	3204	4 74	706	1388	1192	15 1	86 37	2 70	39 6	3128	5 72	18872	0 9910	0 4795	0 2413	1 7118
35000	.9	0 3098	0 2351	393	1 595	457	707	4 650	7.420	93	0 425	1 277	3691	5 58	681	1353	1168	17 1	97 81	2 65	32 0	2976	6 68	20969	1 0417	0.5040	0 2818	1 8275
35000	1.2	0 3098	0 2351	393	2 240	506	756	4 130	9 250	119	0 539	1 490	4602	7.14	642	1304	1133	20.5	117 26	2 55	27 5	3273	7.71	26617	0 9471	0.4583	0 3253	1 7307
35000	1.5	0.3098	0 2351	393	3.290	570	820	3 620	11 900	155	0 703	1.769	5920	9 30	.598	1240	1102	24.7	141.28	2.39	22 7	3519	8 60	31922	0 8809	0 4263	0 3629	1 6701
45000	9	0.1926	0 1458	393	1 595	457	707	4 650	7 420	58	0.264	0.794	2289	3 48	751	1353	1263	14 8	84 66	3 70	35 8	2076	6.49	14211	1 4932	0.7225	0 2738	2 4895
45000	1.2	0.1926	0.1458	393	2.240	506	756	4 130	9 250	74	0.325	0 926	2854	4.44	716	1304	1230	17.5	100 10	3 51	30 6	2264	7.50	17910	1 3693	0.6625	0 3164	2 3482
45000	1.5	0.1926	0 1458	393	3 290	570	820	3 620	11 900	96	0.437	1.100	3671	5.76	676	1240	1198	20.5	117 26	3.19	26 0	2496	8 39	22089	1 2420	0 6010	0 3540	2 1970
55000	.9	0 1195	0.0905	393	1 595	457	707	4 650	7 420	36	0 164	0.493	1421	2 16	810	1353	1343	12.7	72 64	5.11	38 8	1397	6 38	9401	2 2190	1.0737	0 2692	3 5619
55000	1.2	0.1195	0 0905	393	2 240	506	756	4 130	9 250	46	0.208	0.575	1771	2 76	784	1304	1318	14 9	85 23	4 81	33 7	1550	7.32	11968	2 0000	0.9677	0 3089	3 2766
55000	1 5	0 1195	0.0905	393	3.290	570	820	3.620	11 900	60	0 271	0 682	2279	3 60	746	1240	1285	18.0	102 96	4.52	29 0	1740	8 20	15050	1.7816	0 8621	0 3460	2 9897

APPENDIX E

PERFORMANCE CALCULATIONS FOR A NUCLEAR POWERED RAM-JET ENGINE

The ram-jet engine may find future use as an auxiliary power plant at high altitudes and high air speeds or as a possible missile power plant. The first table presented below outlines the method used to compute the generalized ram-jet performance at altitudes greater than 35,000 ft. The second table outlines the method used to compute the performance of a nuclear powered ram-jet at 65,000 ft for various air speeds, radiator air flows, and radiator depths. The last table shows how the radiator size is affected by the number of ram-jet engines and flight Mach number.

METHOD OF COMPUTING GENERALIZED RAM-JET PERFORMANCE
(For Altitudes Greater Than 35,000 ft)

Altitude, H - 35,000 to 125,000 ft
Ambient air temperature, T_o - 393°R
Acoustic velocity, V - 974.5 ft/sec

Altitude density ratio σ - 0.07413
Ambient air pressure, P_o - 118.8 lb/ft^2
Enthalpy of ambient air, ϕ_o - 93.85 Btu/lb
Pressure ratio of ambient air,
P_{ro} = 0.4567

Method of Computation

Mach number, M	Chosen arbitrarily
Air speed, V - ft/sec	V = M x acoustic velocity = M x 974.5
Isentropic enthalpy rise of air in diffuser, $\Delta\phi_{is}$ - Btu/lb	$\Delta\phi_{is} = \frac{V^2}{2gJ}$ g = 32.17 ft/sec^2 J = 778.16 ft-lb/Btu
Enthalpy rise of air in diffuser used in computing ram compression ratio, $\Delta\phi$ - Btu/lb	$\Delta\phi = \Delta\phi_{is} \times \eta_D$ η_D = diffuser efficiency = 0.90 at M = 1.5 = 0.85 at M = 2.5 = 0.70 at M = 3.5
Radiator outlet temperature, T_2 - °R	Chosen arbitrarily as 1460, 1960, 2460, 2960°R
Pressure ratio at radiator outlet, P_{r_2}	Use "Gas Tables" by Keenan and Kaye, Table 1 and T_2
Enthalpy of air at radiator outlet, ϕ_2 - Btu/lb	Use "Gas Tables" by Keenan and Kaye, Table 1 and T_2

Method of Computation (continued)

Pressure ratio at compressor outlet, P_{r_1}	Use "Gas Tables by Keenan and Kaye, Table 1
Ram compression ratio, Z_r	$Z_r = \frac{P_{r_1}}{P_{r_o}} = \frac{P_{r_1}}{0.4567}$
Pressure drop across radiator as $^o/o$ of diffuser outlet pressure, $\Delta P_R {}^o/o$	Chosen arbitrarily as 0, 5, 10, 20, $30^o/o$
Pressure ratio at exhaust conditions, P_{r_3}	$P_{r_3} = \frac{P_{r_2}}{Z_r(1 - \frac{\Delta P_R}{100})}$
Enthalpy of air at exhaust conditions, ϕ_3 - Btu/lb	Use "Gas Tables" by Keenan and Kaye, Table 1 and P_{r_3}
Change in enthalpy of air during expansion, $\Delta \phi_e$ - Btu/lb	$\Delta \phi_e = \phi_2 - \phi_3$
Specific thrust, I - lb/lb air/sec	$I = \sqrt{2 \frac{J}{g} \times e_J \times (\Delta \phi_e + \Delta \phi)} - \frac{V}{g}$ where e_j = jet efficiency
Specific heat consumption, C_s - Btu/lb thrust-sec	$C_s = \frac{\phi_2 - \phi_1 - \Delta \phi}{I}$

COMPUTATION OF THE PERFORMANCE OF A NUCLEAR POWERED RAM-JET ENGINE

Total weight of missile - 100,000 lb
Reactor system - Circulating fluoride fuel with NaK secondary circuit
Reactor and intermediate heat exchanger weight (unshielded) - 12,500 lb
Radiator weight - 90 lb/ft^3
Duct weight - 7 lb/ft^2 duct surface area
Pump and line weight - .04 x kw/lb thrust
Lift to drag ratio - 4
Radiator airflow - G_R - 4, 6, 8, 12, 16 lb/sec-ft^2 radiator inlet area

Radiator depth - L_R - 3, 6, 9, 12 in
Altitude - H - 65,000 ft
Ambient air temperature - T_o - 393°R
Acoustic velocity - V - 974.5 ft/sec
Ambient air pressure - P_o - 118.8 lb/ft^2
Altitude density ratio - σ = 0.07413
Altitude pressure ratio - P_{ra} = 0.0561

Method of Computation

Mach number, M	Chosen arbitrarily
Radiator airflow, G_R - lb/sec-ft^2 radiator inlet area	Chosen arbitrarily as 4, 6, 8, 12, 16 lb/sec-ft^2 radiator inlet area
Radiator depth, L_R - in.	Chosen arbitrarily as 3, 6, 9, 12 in.
Ram compression ratio, Z_r	See page 105
Radiator inlet temperature, T_1 - ^{o}R	Use "Gas Tables" by Keenan and Kaye, Table 1 and ϕ_1 where $\phi_1 = \phi_o + \Delta\phi_{is} = 93.85 + \Delta\phi_{1s}$
Ratio of radiator inlet air density to sea level air density, σ_r	$\sigma_r = \sigma \times Z_r \times \frac{T_o}{T_1} = 0.07413 \times Z_r \times \frac{393}{T_1} = 29.133 \frac{Z_r}{T_1}$
Pressure drop across radiator, ΔP_r - in. H_2O	Read from Fig. 16 using values of G_R and σ_r
Pressure drop across radiator, ΔP_R - lb/ft^2	$\Delta P_R = \frac{\Delta P_r}{12 \text{ in/ft}} \times 62.4 \text{ lb/ft}^3 \times 1.1$ (1.1 is a calibration factor for manometer)

Method of Computation (continued)

Pressure at radiator inlet, P_1 - lb/ft^2	$P_1 = P_o \times Z_r = 118.8 \times Z_r$
Pressure drop across radiator as $^o/o$ of radiator inlet pressure, $\Delta P_r{}^o/o$	$\Delta P_r{}^o/o = \frac{\Delta P_R}{P_1} \times 100$
Heating effectiveness, η	Read from Fig. 22 using values for G_R and L_R
Initial temperature difference, ITD, ^oF	ITD = 2060 - T_1 (Na inlet temperature is assumed to be 2060°R)
Radiator outlet temperature, T_2 - ^oR	$T_2 = T_1 + \eta(\text{ITD})$
Specific thrust, I - lb/lb air/sec	See page 105
Net specific thrust, I_N - lb/lb air/sec	$I_N = I - I_D$ where I_D = specific drag due to nacelles lb/lb air/sec = 5 lb/lb air/sec at M = 2.5 = 3 lb/lb air/sec at M = 3.5 (see Reference 19)
Specific heat consumption, C_s - Btu/lb thrust-sec	See page 105
Lb thrust per ft^2 of radiator inlet area, τ_{RA} - lb/ft^2	$\tau_{RA} = I_N \times G_R$
Lb radiator per lb thrust, W_R - lb/lb thrust	$W_R = 90$ lb/ft^3 radiator x $\frac{L_R}{12 \text{ in/ft}} \times \frac{1}{T_{RA}} = \frac{7.5\, L_R}{T_{RA}}$

Method of Computation (continued)

Heat consumption per lb thrust, C_s - kw/lb thrust	$C_s = 1.05479\ C_S$ $\left(1.05479 = \frac{3600\ \text{sec/hr}}{3413\ \text{Btu/kw-hr}}\right)$
Pump and line weight plus reactor weight, $W_P + W_{Re}$ - lb/lb thrust	$W_P + W_{Rc} = 2 \times 0.04 \times C_s$ (0.04 is an empirical factor from pump and line weight studies)
Required ram-jet air flow, F_{rJ} - lb/sec	$F_{rJ} = \frac{25000}{I_n}$ (25000 = lb thrust required for 100,000 lb missile)
Required duct inlet area, A_d - ft^2	$A_d = \frac{F_{rJ}}{G_{rj}}$ where G_{rj} = air flow per ft^2 of duct area = 13 lb/sec-ft^2 at M = 2.5 = 18 lb/sec-ft^2 at M = 3.5
Required duct diameter, D_d - ft^2	$D_d = \sqrt{\frac{4\ A_d}{N\pi}}$ where N = number of ram-jet engines
Lb duct per lb thrust, W_d - lb/lb thrust	$W_d = \frac{7\pi D_d L_d}{25000/N}$ where 7 = lb per ft^2 of duct surface area
Total reactor, radiator, duct and pump and line weight, W_T - lb/lb thrust	$W_T = W_{R_e} + W_R + W_d + W_p$

EFFECT OF NUMBER OF RAM-JET ENGINES AND MACH NUMBER ON DUCT AND RADIATOR SIZE

Radiator Depth (Direction of Air Flow) (inches)	Radiator Air Flow $\frac{lb/sec}{ft^2}$	Number of Ram-Jet Engines	Air Required (lb/sec) M = 2.5	Air Required (lb/sec) M = 3.5	Air Velocity (ft/sec) M = 2.5	Air Velocity (ft/sec) M = 3.5	Duct Diameter (ft) M = 2.5	Duct Diameter (ft) M = 3.5	Radiator Frontal Area per Engine (ft^2) M = 2.5	Radiator Frontal Area per Engine (ft^2) M = 3.5	Radiator Height (nearest inch) M = 2.5	Radiator Height (nearest inch) M = 3.5	Radiator Length (in) (Axial) M = 2.5	Radiator Length (in) (Axial) M = 3.5	Total Weight (lb/lb thrust) M = 2.5	Total Weight (lb/lb thrust) M = 3.5	Required Duct Area per Engine (ft^2) M = 2.5	Required Duct Area per Engine (ft^2) M = 3.5	Ratio of Required Radiator Area to Required Duct Area M = 2.5	Ratio of Required Radiator Area to Required Duct Area M = 3.5
3	4	2	899	727	218	125	6.643	5.070	112.5	91.0	34	24	60	68	1.1046	0.9477	34.57	20.19	3.25	4.50
3	4	4	899	727	218	125	4.691	3.585	56.3	45.5	22	15	46	55	1.2250	1.0400	17.29	10.10	3.25	4.50
3	4	6	899	727	218	125	3.830	2.927	37.5	30.3	17	12	40	45	1.3177	1.1109	11.52	6.73	3.25	4.50
3	6	2	954	746	328	188	6.835	5.136	79.5	62.0	35	25	41	45	1.0458	0.8918	36.69	20.72	2.17	3.00
3	6	4	954	746	328	188	4.833	3.632	39.8	31.0	25	16	31	35	1.1705	0.9854	18.35	10.36	2.17	3.00
3	6	6	954	746	328	188	3.946	2.965	26.5	20.7	18	12	27	31	1.2658	1.0571	12.23	6.91	2.17	3.00
3	8	2	988	760	437	250	6.955	5.184	62.0	47.5	36	25	31	34	1.0141	0.8620	38.00	21.11	1.63	2.25
3	8	4	988	760	437	250	4.918	3.666	31.0	23.8	24	16	23	27	1.1408	0.9565	19.00	10.56	1.63	2.25
3	8	6	988	760	437	250	4.015	2.993	20.7	15.9	18	12	21	24	1.2379	1.0289	12.67	7.04	1.63	2.25
3	12	2	1041	779	655	376	7.140	5.248	43.5	32.5	37	25	21	23	0.9829	0.8305	40.00	21.64	1.09	1.51
3	12	4	1041	779	655	376	5.049	3.711	21.8	16.3	24	16	16	18	1.1129	0.9261	20.02	10.82	1.09	1.51
3	12	6	1041	779	655	376	4.122	3.030	14.5	10.9	19	12	14	16	1.2126	0.9994	13.34	7.21	1.09	1.51
3	16	2	1111	786	874	501	7.375	5.272	34.5	24.5	38	26	16	17	0.9750	0.8141	42.73	21.83	0.81	1.13
3	16	4	1111	786	874	501	5.215	3.728	17.3	12.3	25	16	12	14	1.1093	0.9101	21.37	10.92	0.81	1.13
3	16	6	1111	786	874	501	4.258	3.044	11.5	8.2	20	12	10	12	1.2124	0.9838	14.24	7.28	0.81	1.13
6	4	2	746	661	218	125	6.042	4.834	93.0	82.5	30	23	74	86	1.2597	1.0992	28.69	18.36	3.25	4.50
6	4	4	746	661	218	125	4.273	3.419	46.5	41.3	20	15	56	66	1.3699	1.1873	14.34	9.18	3.25	4.50
6	4	6	746	661	218	125	3.489	2.792	31.0	27.5	15	11	50	60	1.4543	1.2477	9.56	6.12	3.25	4.50
6	6	2	806	679	328	188	6.282	4.902	67.0	56.5	32	23	50	59	1.1616	1.0004	31.00	18.86	2.17	3.00
6	6	4	806	679	328	188	4.443	3.467	33.5	28.3	21	15	38	45	1.2761	1.0898	15.50	9.43	2.17	3.00
6	6	6	806	679	328	188	3.628	2.831	22.3	18.9	16	11	33	41	1.3639	1.1583	10.33	6.29	2.17	3.00
6	8	2	847	694	437	250	6.439	4.953	53.0	43.5	33	24	39	44	1.1153	0.9479	32.58	19.28	1.63	2.25
6	8	4	847	694	437	250	4.554	3.503	26.5	21.8	21	15	30	35	1.2327	1.0382	16.29	9.64	1.63	2.25
6	8	6	847	694	437	250	3.718	2.860	17.7	14.5	16	11	27	32	1.3226	1.1074	10.86	6.42	1.63	2.25
6	12	2	936	718	655	376	6.771	5.037	39.0	30.0	35	24	27	30	1.0690	0.8926	36.00	19.94	1.09	1.51
6	12	4	936	718	655	376	4.788	3.562	19.5	15.0	23	15	20	24	1.1924	0.9844	18.00	9.97	1.09	1.51
6	12	6	936	718	655	376	3.909	2.908	13.0	10.0	17	11	18	21	1.2864	1.0547	12.00	6.65	1.09	1.51
6	16	2	1087	735	874	501	7.294	5.010	34.0	23.0	38	24	21	23	1.0781	0.8629	41.80	20.42	0.81	1.13
6	16	4	1087	735	874	501	5.158	3.606	17.0	11.5	25	16	16	17	1.2110	0.9598	20.90	10.21	0.81	1.13
6	16	6	1087	735	874	501	4.211	2.944	11.3	7.7	19	12	14	15	1.3129	1.0310	13.93	6.80	0.81	1.13
9	4	2	681	620	218	125	5.773	4.682	85.0	77.5	29	22	106	127	1.4015	1.2372	26.19	17.22	3.25	4.50
9	4	4	681	620	218	125	4.083	3.311	42.5	38.8	18	14	85	100	1.5067	1.3225	13.10	8.61	3.25	4.50
9	4	6	681	620	218	125	3.334	2.703	28.3	25.9	14	10	73	93	1.5875	1.3879	8.73	5.74	3.25	4.50
9	6	2	729	639	328	188	5.974	4.754	61.0	53.0	30	23	73	83	1.2709	1.1002	28.04	17.75	2.17	3.00
9	6	4	729	639	328	188	4.225	3.362	30.5	26.5	19	14	58	68	1.3798	1.1868	14.02	8.88	2.17	3.00
9	6	6	729	639	328	188	3.450	2.745	20.3	17.7	15	10	49	64	1.4634	1.2532	9.34	5.92	2.17	3.00
9	8	2	781	656	437	250	6.183	4.816	49.0	41.0	31	23	57	64	1.2116	1.0282	30.04	18.22	1.63	2.25
9	8	4	781	656	437	250	4.375	3.406	24.5	20.5	20	14	44	53	1.3243	1.1260	15.02	9.11	1.63	2.25
9	8	6	781	656	437	250	3.571	2.781	16.3	13.7	15	11	39	45	1.4108	1.1833	10.01	6.07	1.63	2.25
9	12	2	877	679	655	376	6.553	4.902	36.5	28.5	33	23	40	45	1.1504	0.9537	33.73	18.86	1.09	1.51
9	12	4	877	679	655	376	4.634	3.466	18.3	14.3	22	15	30	34	1.2698	1.0430	16.86	9.43	1.09	1.51
9	12	6	877	679	655	376	3.784	2.830	12.2	9.5	17	11	26	31	1.3614	1.1115	11.24	6.29	1.09	1.51
9	16	2	1020	700	874	501	7.067	4.977	32.0	22.0	36	24	32	33	1.1539	0.9160	39.23	19.44	0.81	1.13
9	16	4	1020	700	874	501	4.997	3.519	16.0	11.0	24	15	24	26	1.2826	1.0066	19.62	9.72	0.81	1.13
9	16	6	1020	700	874	501	4.080	2.873	10.7	7.3	18	11	21	24	1.3814	1.0761	13.08	6.48	0.81	1.13
12	4	2	638	595	218	125	5.588	4.586	80.0	74.5	28	22	103	122	1.5295	1.3655	24.54	16.52	3.25	4.50
12	4	4	638	595	218	125	3.952	3.243	40.0	37.3	18	13	80	103	1.6313	1.4491	12.28	8.26	3.25	4.50
12	4	6	638	595	218	125	3.227	2.648	26.7	24.9	13	10	74	90	1.7094	1.5132	8.18	5.51	3.25	4.50
12	6	2	685	613	328	188	5.790	4.655	57.0	51.0	29	22	71	83	1.3686	1.1921	26.34	17.02	2.17	3.00
12	6	4	685	613	328	188	4.095	3.292	28.5	25.5	19	14	54	66	1.4742	1.2770	13.17	8.51	2.17	3.00
12	6	6	685	613	328	188	3.344	2.688	19.0	17.0	14	10	49	61	1.5552	1.3420	8.78	5.67	2.17	3.00
12	8	2	746	630	437	250	6.042	4.720	46.5	39.5	30	22	56	65	1.3061	1.1049	28.69	17.50	1.63	2.25
12	8	4	746	630	437	250	4.273	3.338	23.3	19.8	20	14	42	51	1.4163	1.1909	14.34	8.75	1.63	2.25
12	8	6	746	630	437	250	3.489	2.725	15.5	13.2	15	10	37	48	1.5007	1.2568	9.56	5.83	1.63	2.25
12	12	2	828	649	655	376	6.367	4.783	34.5	27.0	32	23	39	42	1.2245	1.0076	31.84	17.98	1.09	1.51
12	12	4	828	649	655	376	4.502	3.382	17.3	13.5	21	14	30	35	1.3405	1.0948	15.92	8.99	1.09	1.51
12	12	6	828	649	655	376	3.676	2.761	11.5	9.0	16	11	26	29	1.4295	1.1616	10.61	5.99	1.09	1.51
12	16	2	962	676	874	501	6.836	4.889	30.0	21.0	35	23	31	33	1.2164	0.9640	37.00	18.78	0.81	1.13
12	16	4	962	676	874	501	4.853	3.457	15.0	10.5	23	15	23	25	1.3415	1.0531	18.50	9.39	0.81	1.13
12	16	6	962	676	874	501	3.962	2.823	10.0	7.0	18	11	20	23	1.4373	1.1214	12.33	6.26	0.81	1.13

APPENDIX F

METALLOGRAPHIC EXAMINATION OF NICROBRAZED STAINLESS STEEL SODIUM-AIR HEAT EXCHANGERS FOLLOWING FAILURE DURING TEST

(By: E. E. Hoffman, ORNL Metallurgy Division)

Summary

It is concluded from the examination of these heat exchangers that the failures occurred at one of the brazed tube-to-header joints and that the leaking sodium accelerated the attack on the outer surface of the tube below the initial leak reducing the thickness of the tube and causing a larger secondary leak.

Test Data

The first heat exchanger was operated continuously for 330 hours. The average sodium "in" temperature for the test was 1200°F, while the average "out" temperature was 950°F. For 140 of the 330 hours the "in" temperature was 1500-1600°F, while the "out" temperature was 1200°F. The sodium flow rate was 3 gallons per minute which gave a flow velocity of approximately 2 feet per second in the tubes. The air entered the radiator fins at a temperature of 80°F. The average "out" temperature of the air was 850°F, while the maximum "out" temperature of the air was 1100°F. The maximum velocity of the air in the heat exchanger was 100 feet per second. The tubes were constructed of 304 stainless steel, the fins of 347 stainless steel and the headers of 316 stainless steel.

The second heat exchanger was operated continuously for 199 hours. The average sodium "in" temperature for the run was 1200°F and the "out" temperature was 1000°F. For 74 of the 199 hours the sodium "in" temperature was 1600°F while the "out" temprature was 1300°F. The sodium flow rate was 3 gallons per minute which gave a velocity of approximately 2 feet per second in the tubes. The air entered the radiator fins at a temperature of 80°F. The average "out" temperature of the air was 850°F, while the maximum "out" temperature was 1100°F. The maximum velocity of the air in the heat exchanger was 100 feet per second. The tubes were constructed of 304 stainless steel, the fins of 347 stainless steel and the headers and manifold of 316 stainless steel.

Discussion

Figures F-1 and F-2 show different views of half of the first heat exchanger following test. Fig. F-3 shows a portion of the radiator section above the inlet tanks where the leak occurred. The 347 stainless steel fin was heavily attacked by the leaking sodium. It is believed that the leak occurred on the bottom side of the center tube in the second row from the top (see Fig. F-3). This leak is thought to have occurred after the sodium leak in the nearby brazed tube-to-header joint. The wall thickness was greatly reduced in this area. Most of this reduction in thickness is believed to have taken place after the leak occurred, the tube and fins being attacked in a similar manner. Fig. F-4 shows an enlarged view of the tube which leaked during the test and an adjacent tube. Fig. F-5 shows a longitudinal view of these tubes at a still higher magnification. The thick sections are portions of the tank, while the thin sections in the center of the picture are portions of the tubes which projected up from the tank and entered the fins. The leak occurred in the tube and header section on the right in Fig. F-5. It may be easily seen that the braze material did not give a good joint especially in the top section. It is believed that at some section of this tube-to-header joint the sodium leak occurred and subsequent attack on the outside of the tube took place which thinned the tube down until a leak also occurred in the tube. It is improbable that the attack began on the inside of the tubes as no evidence of this was found on examining the tubes in areas where no leaks occurred.

The photomicrograph (Fig. F-6) of a braze made between the manifold and tank shows that the joint is sound. Figures F-7 and F-8 show two tube-to-header joints where the brazing alloy showed good flow properties, while Figures F-9 and F-10 show similar joints where flow was not sufficient to produce good joints. Although these joints can not be considered as desirable, they did not leak during the test.

Figures F-11, F-12, and F-13 show typical joints obtained by nicrobrazing the fins to the tubes. The curved portion in each case is the fin. All the brazed fin joints appeared to be adequate for strength and heat transfer.

The metallographic examination of the tubes did not reveal attack on the inner surface. However, there did seem to be a 2 to 3 mil oxide layer on the outer surface of the tubes as shown in Fig. F-14, which is a photomicrograph of the outer surface of adjacent tubes.

It can be seen in Fig. F-15 that the fins of the second heat exchanger were heavily attacked by the sodium after the leak developed. Fig. F-16 shows a close-up of the tube-to-header joint where the leak occurred. It is believed that this leak occurred in the tube-to-header joint despite the fact that a photomicrograph of a cross-section of this joint (Fig. F-17) appeared to be sound. Had the cross section been taken at a different position the leaking portion of the joint might have been detected. Following the small leak in the joint, the sodium rapidly attacked the tube and the large leak developed.

Of nine tube-to-header joints which were examined, one-third had voids present in the joints. Fig. F-18 shows one of the good joints, while Figures F-19 and F-20 show defective joints. These voids (Figures F-19 and F-20) extended over half way across the joints. There was no appreciable undercutting at any of the tube-to-header joints. It may be that following the revised nicrobrazing procedure in which nitrogen is carefully excluded from the system the formation of these voids may be reduced or prevented.

The 304 stainless steel tubes were examined at both the hot and cold end of the heat exchanger (Figures F-21 and F-22). The inner surfaces of both tubes were roughened. The surface of the tubes in the "hot" section was roughened slightly more than in the "cold" section. There seemed to be a layer of recrystallized grains on the surface of the "hot" tube. There appeared to be quite a bit of carbide precipitation in both the hot and cold section of the tubes. The inside surface of the manifold section (Fig. F-23) was etched slightly by the hot circulating sodium.

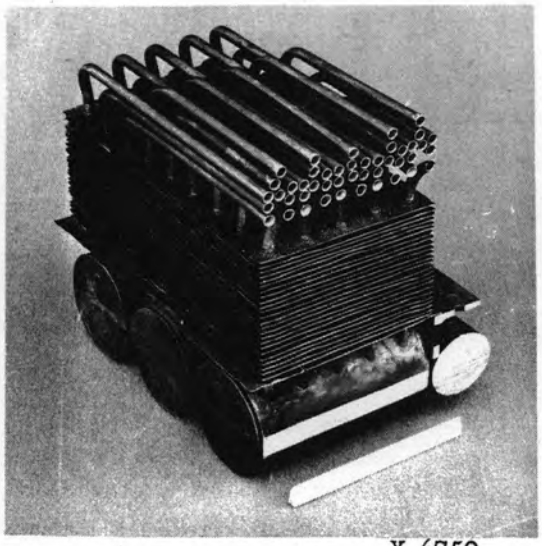

Y-6750

Fig. F1. Heat Exchanger.

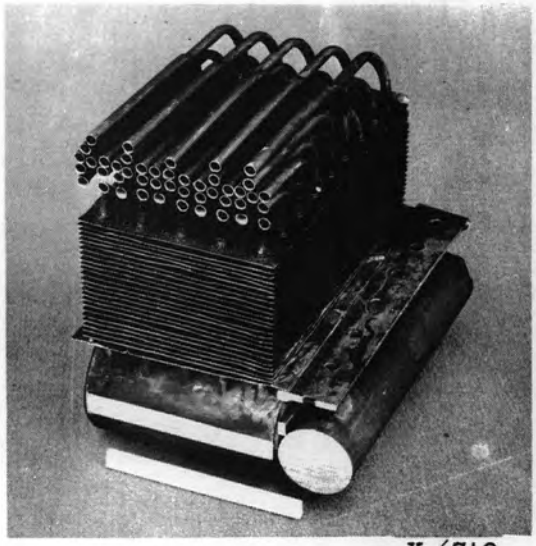

Y-6749

Fig. F2. Heat Exchanger.

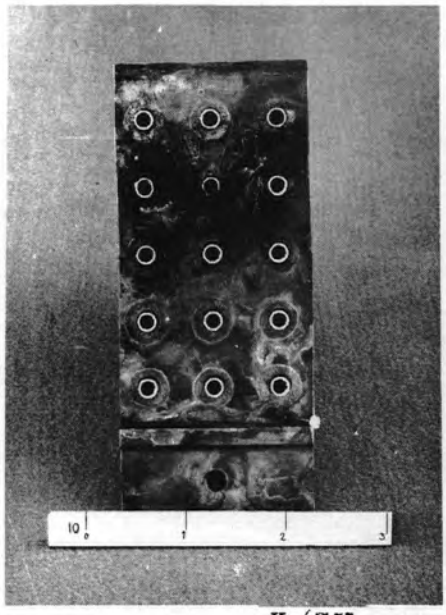

Y-6751

Fig. F3. Radiator Section (bottom view).

Unclassified

Y-6752

Fig. F4. Tube-to-header Section (tube on right leaked).

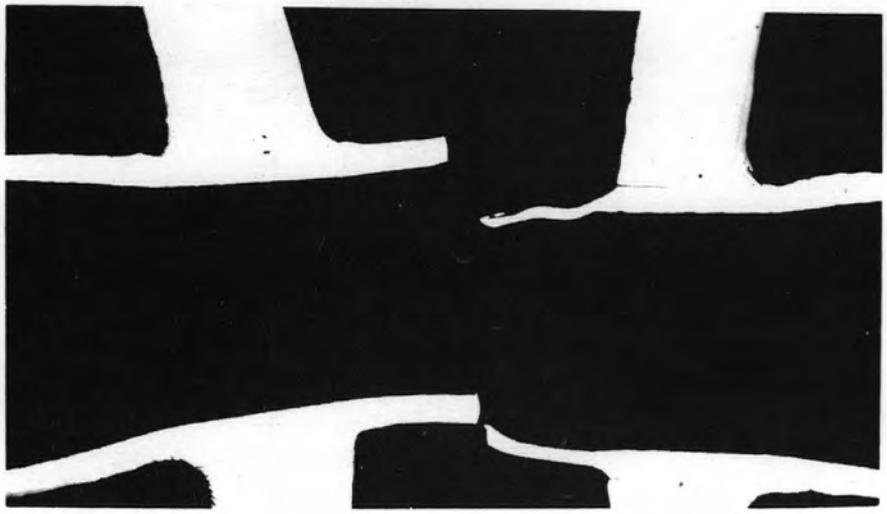

Y-7066

Fig. F5. Tube-to-header Section (Section on right leaked).

Unclassified

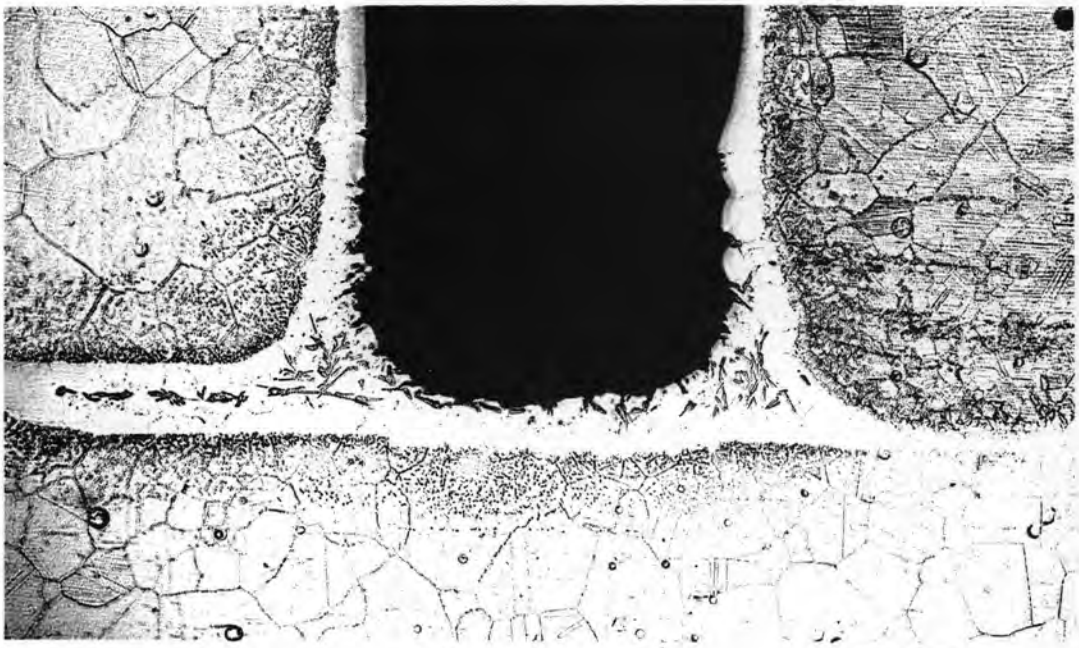

60 X Glyceria Regia Y-6998

Fig. F6. Manifold— Header Tank Braze.

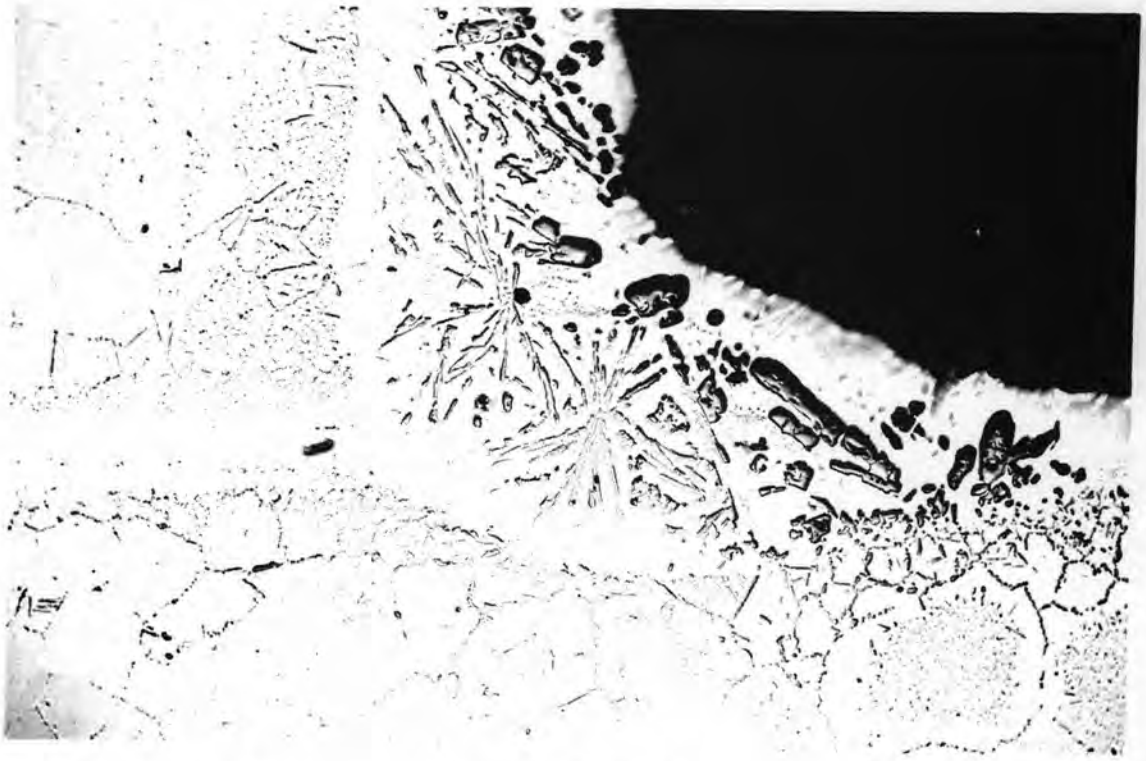

80 X Glyceria Regia Y-6999

Fig. F7. Tube-to-header Braze.

90 X Glyceria Regia Y-7032

Fig. F8. Tube-to-header Braze.

75 X Glyceria Regia Y-7030

Fig. F9. Tube-to-header Braze.

Unclassified

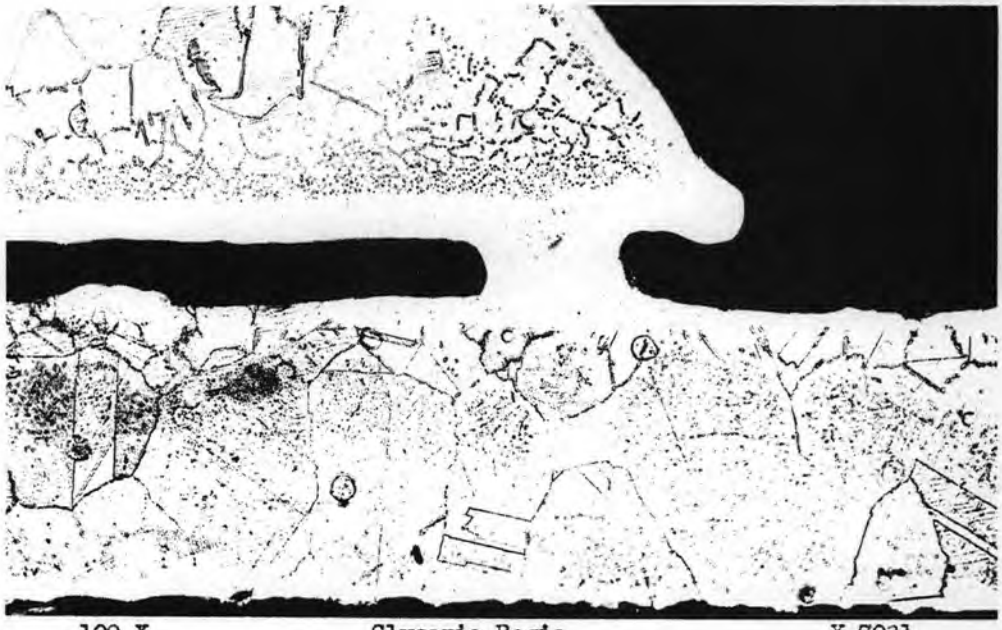

100 X Glyceria Regia Y-7031

Fig. F10. Tube-to-header Braze.

90 X Glyceria Regia Y-7172

Fig. F11. Tube-to-fin Braze.

90 X Glyceria Regia Y-7174

Fig. F12. Tube-to-fin Braze.

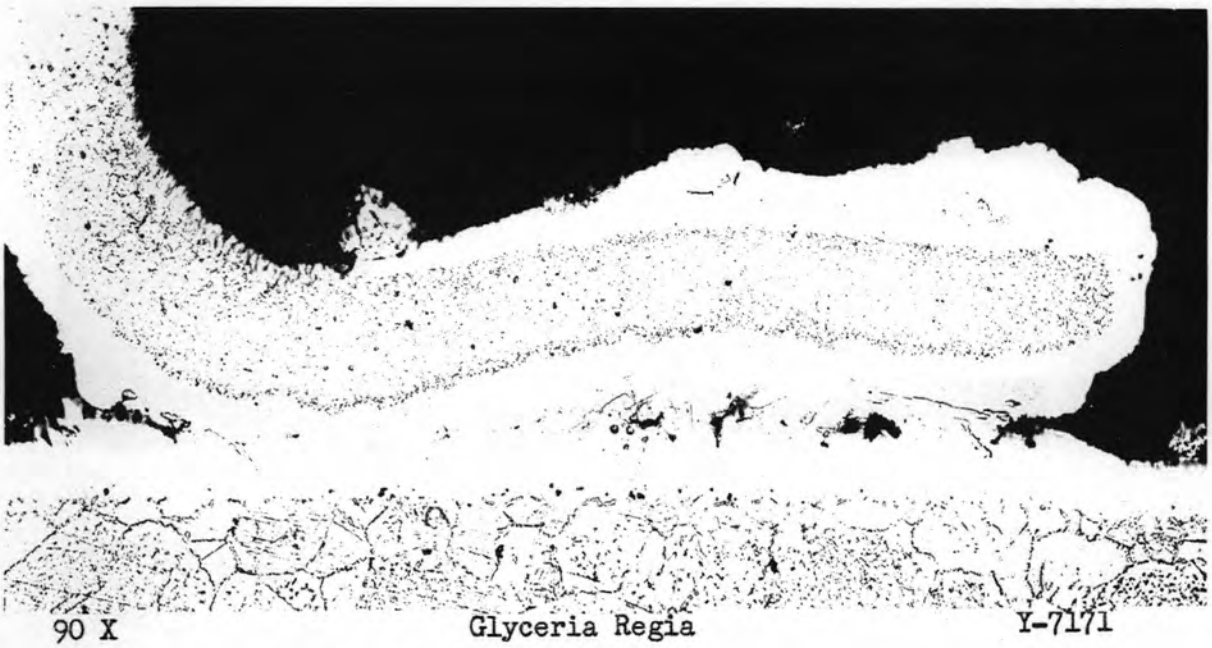

Fig. F13. Tube-to-fin Braze.

Fig. F14. Type 304 Stainless Steel Tubes (oxide scale on outer surfaces of adjacent tubes).

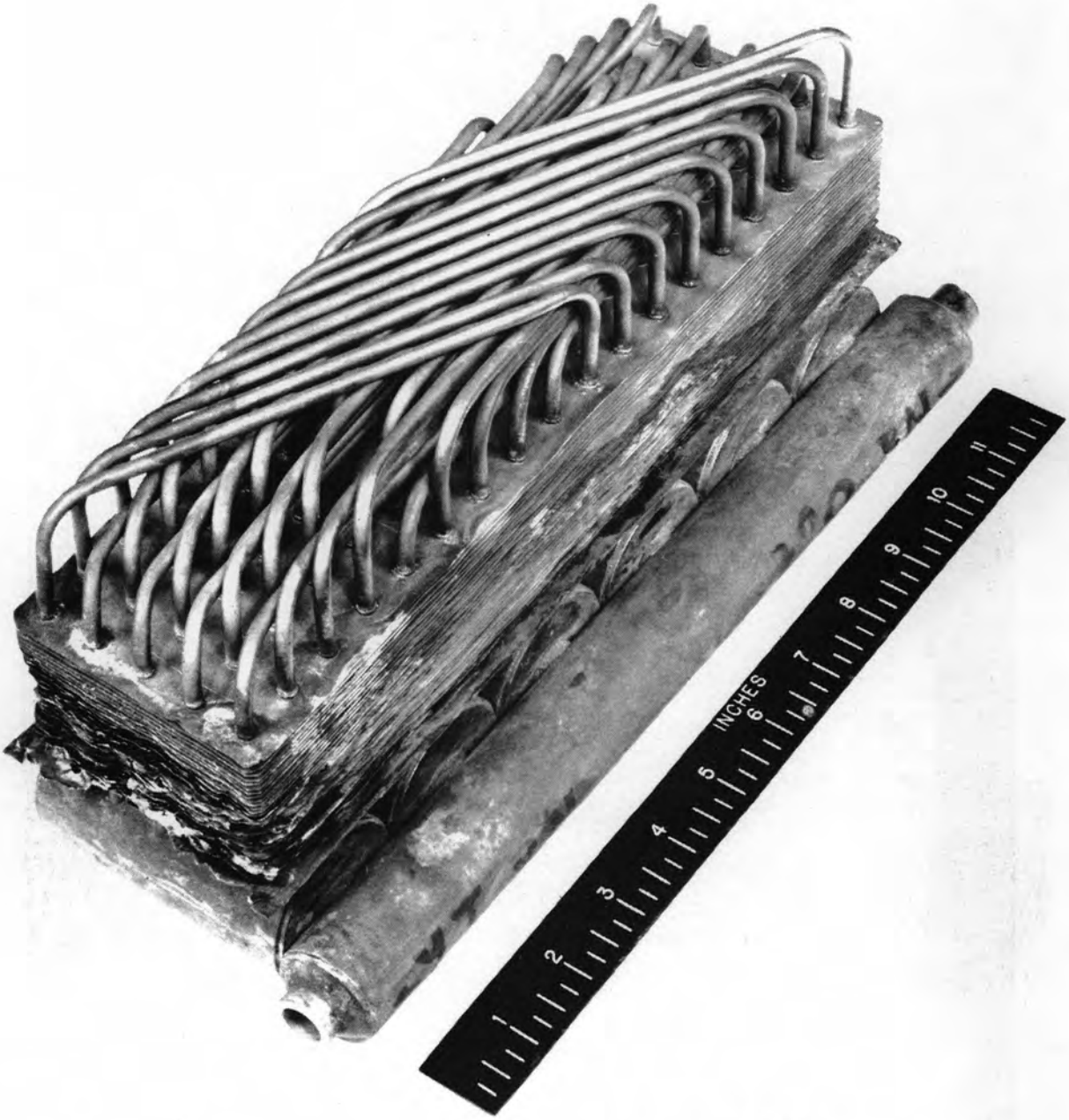

Y-7234

Fig. F15. Heat Exchanger Following Test.

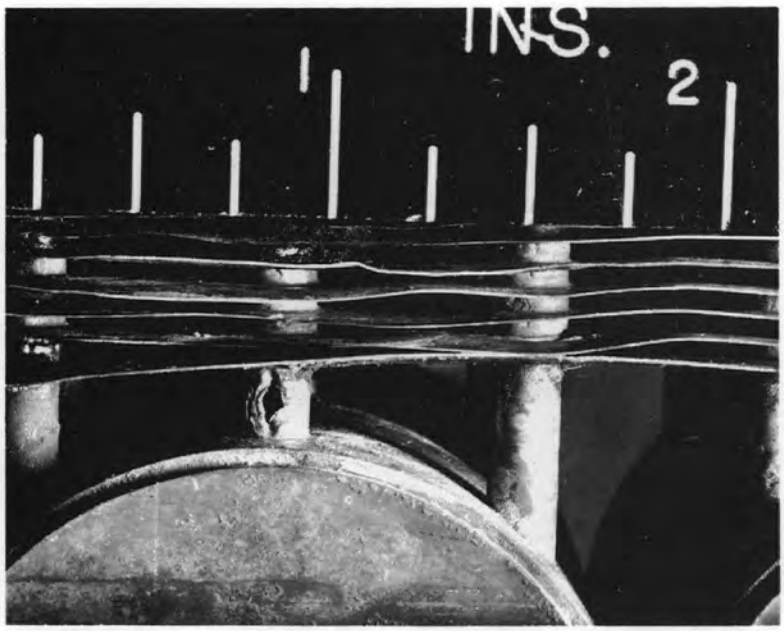

2 X Y-7235

Fig. F16. Leak in Tube.

60 X Glyceria Regia Y-7377

Fig. F17. Tube-to-header Braze Where Leak Occurred.

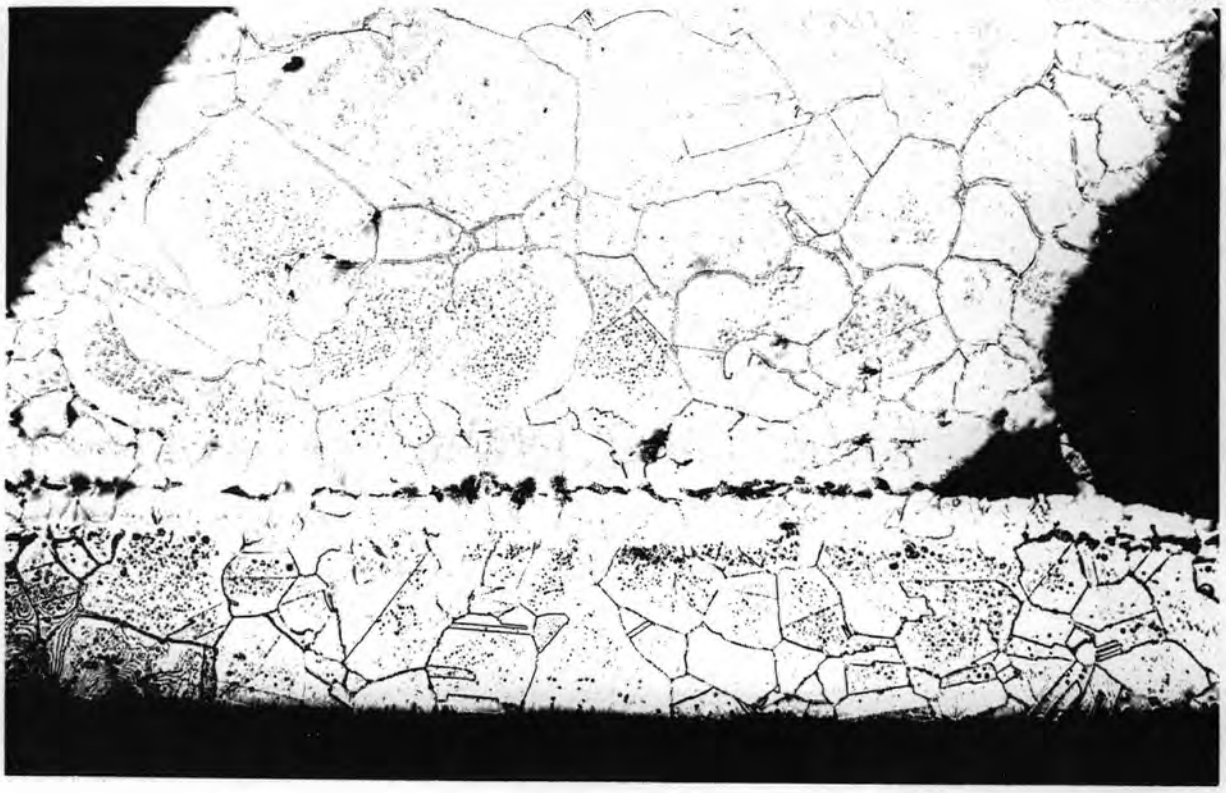

60 X Glyceria Regia Y-7375

Fig. F18. Nicrobrazed Tube-to-header.

60 X Glyceria Regia Y-7376

Fig. F19. Nicrobrazed Tube-to-header.

Unclassified

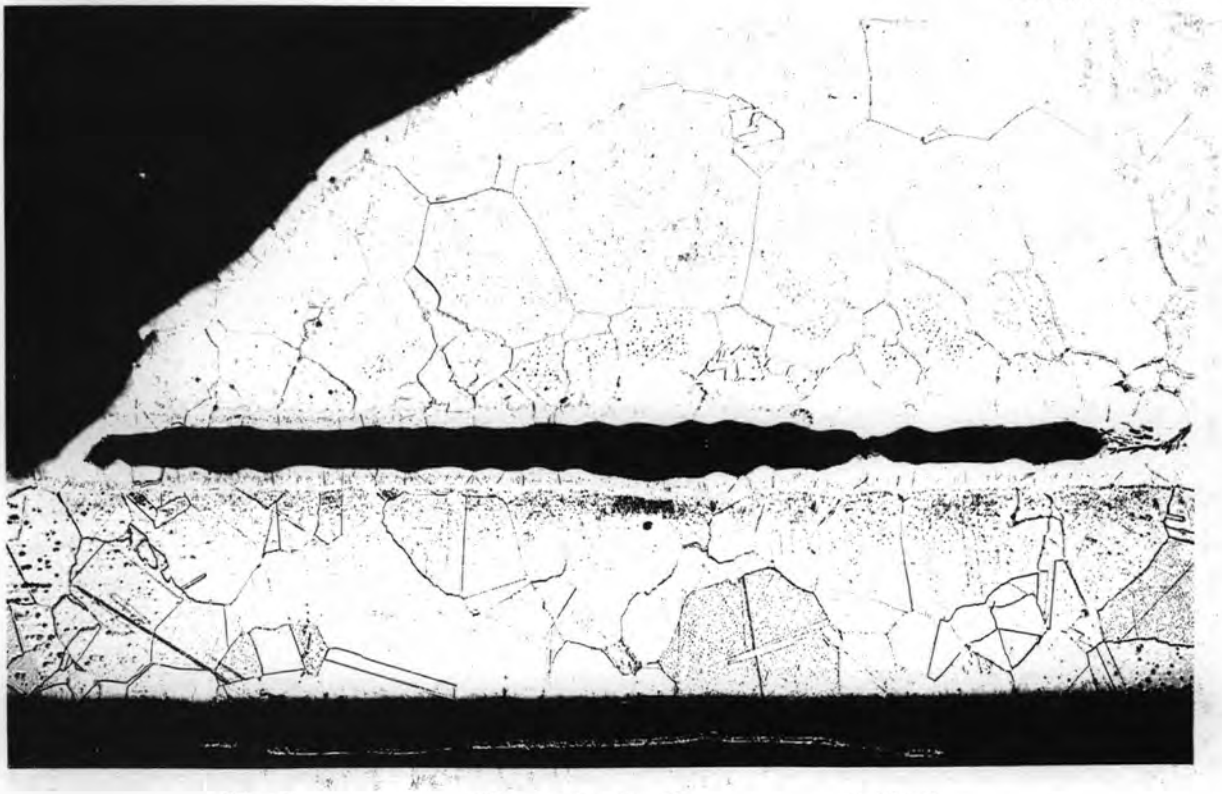

60 X Glyceria Regia Y-7378

Fig. F20. Nicrobrazed Tube-to-header.

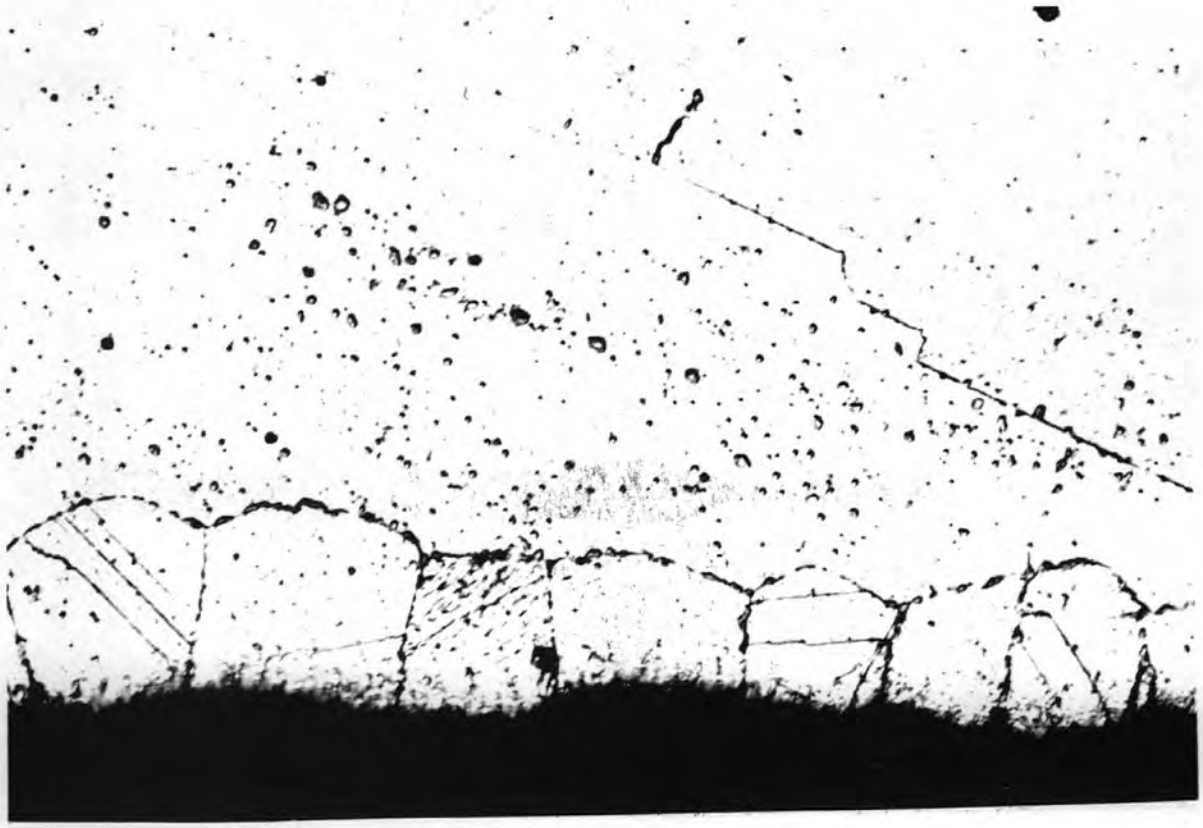

500 X Glyceria Regia Y-7380

Fig. F21. Inside Surface of Type 304 Stainless Tube from Hot Section.

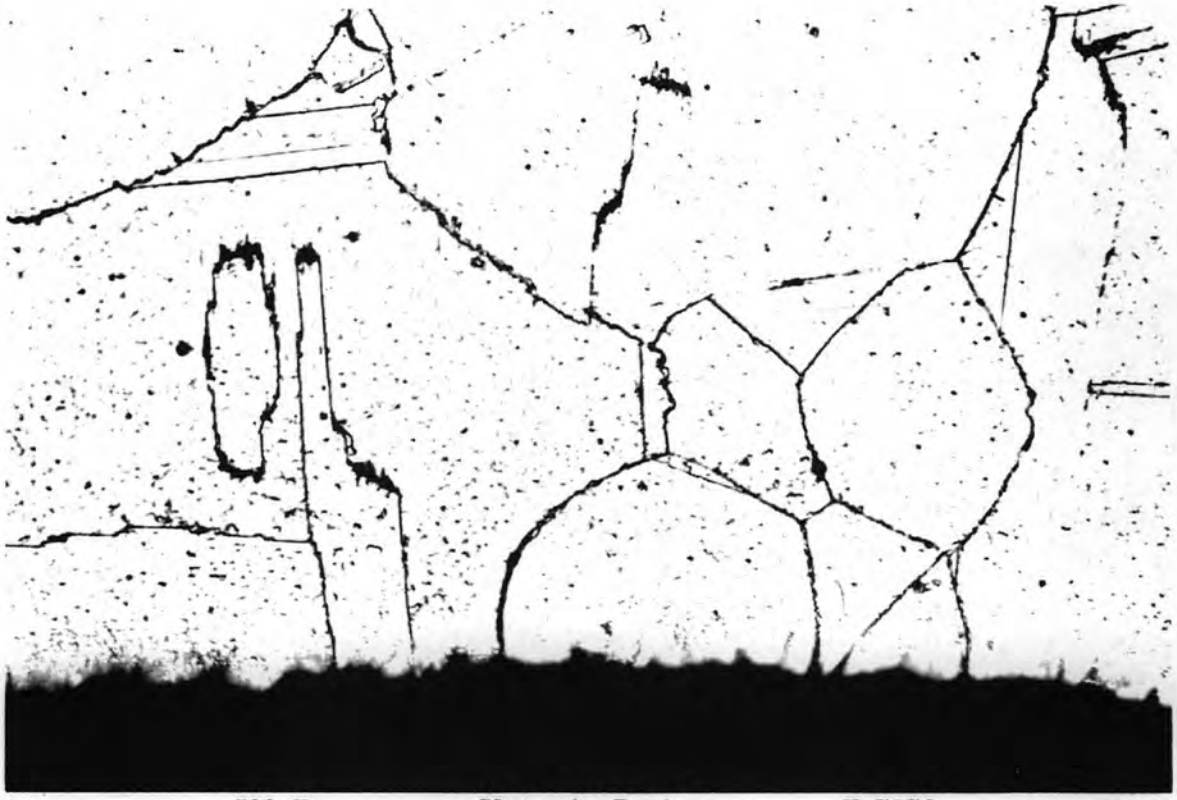

500 X Glyceria Regia Y-7379

Fig. F22. Inside Surface of Type 304 Stainless Tube from Cold Section.

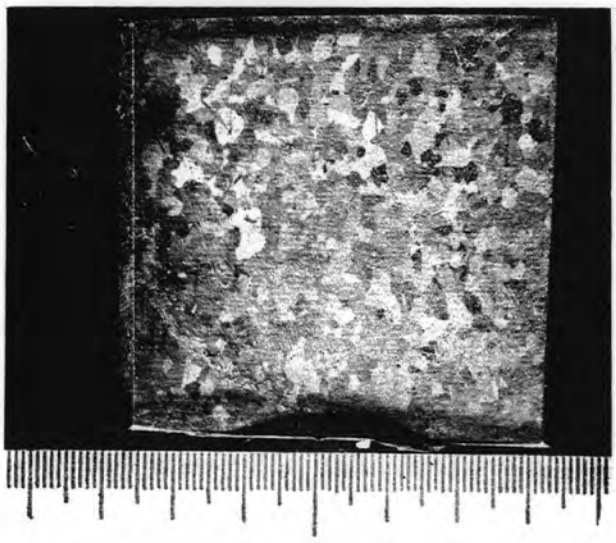

4 X Y-7240

Fig. F23. Inside Surface of Manifold (unetched).

REFERENCES

1 - Adams, H. T., Internal Combustion Turbine Theory University Press, Cambridge, 1949.

2 - Colburn, A. P., "A Method of Correlating Forced-Convection Heat-Transfer Data and A Comparison With Fluid Friction," Trans. AIChE, Vol 29, 1933.

3 - Cortright, E. M. and Connors, J. F., "Supersonic Inlets at High Mach Numbers," NACA Conference on Supersonic Missiles, March, 1952.

4 - Deissler, R. G., "Analytical Investigation of Fully Developed Laminar Flow in Tubes with Heat Transfer with Fluid Properties Variable Along the Radius," NACA TN 2410.

5 - Deissler, R. G., "Analytical Investigation of Turbulent Flow in Smooth Tubes with Heat Transfer with Variable Fluid Properties for Prandtl Number of 1," NACA TN 2242.

6 - Farmer, W. S., "Minimum Weight Analysis for an Air Radiator," CF 53-3-176.

7 - Fraas, A. P., "Effects of Major Parameters on the Performance of Turbojet Engines," ANP-57.

8 - Humble, L. V., Lowdermilk, W. H. and Desmon, L. G., "Measurements of Average Heat-Transfer and Friction Coefficients for Subsonic Flow of Air in Smooth Tubes at High Surface and Fluid Temperatures," NACA 1020.

9 - Johnson, D. L., Kays, W. M and London, A. L., "Heat Transfer and Flow Friction Characteristics of Some Compact Heat Exchanger Surfaces, Part 3 - Design Data for Five Surfaces," ASME Paper No. 1 51-A-129.

10 - Kays, W. M. and London, A. L., "Connective Heat Transfer and Flow Friction Behavior of Small Cylindrical Tubes - Circular and Rectangular Cross Sections," ASME Paper No. 51-A-130.

11 - Keenan, J. H. and Kaye, J., Gas Tables. John Wiley and Sons, New York, 1948.

12 - McAdams, W. H., Heat Transmission. McGraw-Hill, New York, 1942.

13 - Norris, R. H. and Spofford, W. A., "High Performance Fins for Heat Transfer," Trans. ASME, July, 1942.

14 - Norris, R. H., Streid, D. D., "Laminar-Flow Heat-Transfer Coefficients for Ducts," Trans. ASME, Aug., 1940.

15 - Peaslee, R. L. and Boam, W. M., "Design Properties of Brazed Joints for High-Temperature Applications," Welding Journal, August, 1952.

16 - Tate, G. E. and Cartinhour, J., "Disk Extended Surfaces for High Heat-Absorption Rates," Trans. ASME, 1945.

17 - Vennard, J. K., Elementary Fluid Mechanics, John Wiley and Son, New York, 1947.

18 - Whitman, G. D., "Performance and Endurance of a Nicrobrazed Stainless Steel Sodium-to-Air Radiator Core Element," Y-F17-19.

19 - Wright Aeronautical Division-Curtiss-Wright Corporation Nacelle Drag - 35,000 Feet Altitude, Dwg. No. SP 1292.

20 - Zucrow, M. J., Principles of Jet Propulsion and Gas Turbines, John Wiley and Sons, New York, 1948.